5-2018

Immunostimulatory Effects of Antigen-Conjugated InP/ZnS Quantum Dot Nanoparticles in an Avian Model

Christopher Lyle
University of Arkansas, Fayetteville

Immunostimulatory Effects of Antigen-Conjugated InP/ZnS Quantum Dot Nanoparticles in an Avian Model

A dissertation submitted in partial fulfillment
of the requirement for the degree of
Doctor of Philosophy in Poultry Science

by

Chris Lyle
University of Arkansas
Bachelor of Science in Animal Science, 1998
University of Arkansas at Little Rock
Master of Business Administration, 2004
University of Arkansas for Medical Sciences
Master of Science in Communication Disorders, 2008

May 2018
University of Arkansas

This dissertation is approved for recommendation to the Graduate Council

_____
Gisela F. Erf, PhD
Dissertation Director

_____
Walter G. Bottje, PhD
Committee Member

_____
Colin D. Heyes, PhD
Committee Member

Abstract

Due to their unique physicochemical and enhanced immunostimulatory properties, quantum dot (QD) nanoparticles have shown increasing promise in biomedical research applications including bioimaging, drug delivery, and as vaccine adjuvants. Toxicity, however, remains a concern for the use of QD in these applications and thus, there is an increased demand for effective in vitro and in vivo systems to measure the bioactivity of QD. In this study in vitro and in vivo chicken models were used to investigate the effects of QD on innate and adaptive immunity. Chicken macrophage cultures were treated in vitro with QD to measure macrophage activation and the effect of QD on cell viability. The chicken growing feather (GF) injection model was used as the cutaneous test-site to monitor leukocyte infiltration in response to intradermal injection of QD without and with conjugation to a protein antigen. Additionally, the humoral and cellular adaptive immune responses to protein antigen conjugated to QD were examined in chickens. In vitro results showed negligible macrophage activation in response to QD treatment; however, cell viability was negatively affected by QD in a dose-dependent manner. Leukocyte infiltration results of in vivo GF injections with QD revealed immunostimulatory activity of QD, independent of whether or not QD were conjugated to protein antigen. When used as a vaccine platform, immunization with QD conjugated with protein antigen generated a higher primary and secondary antibody response compared to antigen mixed with alum adjuvant. The adaptive cellular responses to protein antigen examined in GF of immunized chickens also support an important role of B cells in the local effector phases of the responses, while T cells appear to primarily help in B cell activation and differentiation, including antibody isotype switching from IgM to IgG. These results provide additional evidence that QD possess promising vaccine adjuvant properties while demonstrating the

viability and utility of the minimally invasive chicken GF cutaneous test-site to study the immunostimulatory effects of nanoparticles initiated in vivo. Further investigation of nanoparticles using the chicken GF injection model should provide additional valuable knowledge of the relative risks and rewards of using QD in biological applications.

Dedication

To my two remarkable daughters, Taylor and Grayson. You are the joy and color in my life and I hope that you will always know how much I love you. You truly can do anything that your heart desires – just find your passion and live it!

Acknowledgements

While there are many long hours spent working in the lab, reading, and writing in solitude, we cannot forget that so many have offered help and guidance and equip us with the tools we need to achieve our often lofty goals. There are so many thanks to spread to the wonderful people that have been there for me along the way -

First and foremost, I am most grateful to my wife, Ashley, for your patience and support through my many years of education and pursuit of this lifelong dream. This is just as much your accomplishment as it is mine. Thank you.

To Dr. Gisela F. Erf for taking a chance on me and pushing me to always have the highest standards. I am truly grateful for your example of work ethic, dedication and excellence. You embody to the true meaning of not only a scientist, but a friend.

To my committee, Dr. Walter Bottje and Dr. Colin Heyes, for your support and constructive criticism, asking the tough questions, and setting high standards. To you I am truly grateful for the time and energy you have dedicated in support of my project.

To the staff and fellow graduate students in Dr. Erf's lab. To Robert (Bob) L. Dienglewicz – little did I know when I joined Dr. Erf's lab that I would be working with you again after working together during my undergrad years nearly twenty years ago in the lab of Dr. Mark Parcells. You were equally instrumental then in helping me achieve my goal of graduation as you were this time around - always helping to maintain the macrophages while I juggled experiments, class and work. I hope you are enjoying every minute of your well-deserved retirement.

I could not have gotten through one of the toughest times during my project with the help and support of my fellow students Dr. Kristen A. Byrne, Daniel M. Falcon and lab mates,

Hyeonmin Jang and Carmen Boessen. I am so grateful for the wide-ranging help you provided from experimental setup to sample processing, especially when it was impossible to be two places at one time. You are all excellent scientists and role models and I am deeply grateful for all of your support.

To Dr. Zoraida P. Aguilar for the conjugation of quantum dot nanoparticles and ongoing technical guidance throughout this project. I look forward to continued work with you in the future to grow the presence of biotechnology in our region.

To many wonderful friends and mentors, especially Dr. Tim Chambers, Professor of Biochemistry at UAMS. You instilled in me confidence in my abilities and in my hands to pursue this dream. Without your support and mentorship, I wouldn't be where I am today.

And to my family at Pel-Freez Biologicals – I certainly could not have achieved this goal without your unwavering support. To Mr. David Dubbell, without your support this simply just wouldn't have been possible. To Dr. Gian Visentin for believing in me and setting the stage for me to begin this journey. To Mr. Jake Bushey for your patience, flexibility, and confidence in me to allow me the time that I needed during the times when there were so many pressing issues and for your encouragement to continue. You have my sincerest thanks and gratitude and I look forward to our continued success.

This work was supported by NIH-NIBIB R15 EB015187; G. F. Erf, PI.

Table of Contents

List of Figures **PAGE**

List of Tables **PAGE**

CHAPTER I

CHAPTER II

CHAPTER III

Introduction

A nanoparticle (NP) is defined by ASTM International as, "a sub-classification of ultrafine particle (UFP) with lengths in two or three dimensions greater than 0.001 μm (1 nm) and smaller than about 0.1 μm (100 nm) and which may or may not exhibit a size-related intensive property," (ASTM International E2456 – 06). While the size dimensions of UFP and NP are essentially identical, UFP are more typically described as potentially harmful environmental pollutants such as by-products of industrial processes, whereas the term "nanoparticle" is most often used to describe particles that are engineered for use for a particular purpose or application (Chang, 2010). In addition to commercial use of NP in consumer electronics and solar panels, much advancement has been made utilizing the unique properties of NP in biomedical applications such as biomedical imaging, drug delivery, and vaccine development (Xing and Rao, 2008; Zhang et al., 2014; Zhao et al., 2014).

While the repertoire of nanoparticle applications has grown quite dramatically, so has the concern that NP are toxic to living systems spawning the creation of a new scientific field known as "nanotoxicology" (Fischer and Chan, 2007). Much work has been conducted to determine the toxic effects of NP including both in vitro and in vivo studies; however, results have shown that these two model systems often show little correlation (Sayes et al., 2007). In vitro assays may be subject to interference due to the optical and catalytic properties of NP and may produce unreliable results (Dobrovolskaia et al., 2009). Since NP may be used to enhance stimulation of the immune system and direct drugs to specific targets in vivo, a thorough immunological evaluation of engineered nanoparticles designed for use in biomedical applications is needed (Dobrovolskaia and McNeil, 2007) including specifically, more in vivo immunological studies (Fischer and Chan, 2007; Smith et al., 2013).

Nanoparticles possess a number of unique properties that have the potential to interact with biological systems including size, chemical makeup, surface charge (zeta potential), and solubility (Chang, 2010; Dobrovolskaia et al., 2009; Nel et al., 2006); therefore, thorough biological study is needed to understand both the prospect of beneficial effects and the risks for harmful effects of NP secondary to NP exposure. Nanoparticle size and surface area possess an inverse relationship compared to bulk material. As the size of an NP decreases, the more atoms are displayed on the surface of the NP rather than on the inside of the particle and thus more reactive groups are available on the surface for interaction (Nel et al., 2006). Physicochemical characteristics of NP may be controlled by specific chemical synthesis methods resulting in variable particle size and function which can dictate the surface interactions that NP have with the surrounding environment. Nanoparticles may be coated with additional molecules to increase solubility or allow for the attachment of other molecules including hydrophobic or hydrophilic groups. These functionalized nanoparticles may now be targeted to specific locations in the body for cellular labeling or drug delivery or become sites for chemical reactions such as the loss or acceptance of electrons leading to the production of reactive oxygen species (ROS) (Xia et al., 2006; Nel et al., 2006). Functionalized NP may therefore be designed to intentionally stimulate the host immune system or to evade immune system recognition (Dobrovolskaia and McNeil, 2007).

Nanoparticles have the potential to interact with all aspects of the immune system, from innate to adaptive immunity including both humoral and cell-mediated responses (Ilinskaya and Dobrovolskaia, 2016). Nanoparticles are likely to make initial contact with the innate immune system, the body's first line of attack, comprised of the physical and chemical barriers that protect plants and animals from foreign materials, bacteria and viruses. The innate immune

system is essential for protection against these foreign invaders and for removing host cell debris (DNA, proteins, lipids) (Abbas et al., 2012; Ilinskaya and Dobrovolskaia, 2016). Both the innate and adaptive arms of the immune system include humoral and cell-mediated processes for immunological protection. Humoral responses are comprised of chemicals, proteins, antibodies in circulation in the blood and other body fluids that may come into contact with foreign material. Innate immunity's humoral component is known as the complement system which is a series of proteins that assist, or complement, the immune system by forming a biochemical cascade upon recognition of foreign material in the body leading to its destruction and removal. Antibodies secreted into the bloodstream by specialized B cells known as plasma cells are included in the humoral component of adaptive immunity. These antibodies have specificity for particular molecular signatures known as antigens on the surface of foreign materials (Abbas et al., 2012). The cell-mediated aspect of immunity includes various cells, collectively known as leukocytes that have specialized roles in immune defense. Cells of the innate immune system, including macrophages, neutrophils, and dendritic cells, recognize molecules expressed on the surface of bacteria and viruses known as pathogen associated molecular patterns (PAMPs). These innate leukocytes may either consume the invading pathogen directly by means of a process known as "phagocytosis" and eliminate them from the body or may digest the pathogen and subsequently present peptides from the pathogen to T cells (thymus-derived lymphocytes). The presentation of these molecules, or antigens, by these antigen presenting cells (APCs) in conjunction with special surface molecules on leukocytes known as the major histocompatibility complex proteins stimulate T helper cells that then proliferate and differentiate into effector cells that produce cytokines and express costimulatory molecules like CD40L. T helper cells help in the activation of B cells that have bound to the antigen with their antigen receptor and in the

initiation of adaptive immunity. With T cell help, activated antigen-specific B cells then proliferate in germinal centers of secondary lymphoid organs where they undergo isotype switching, affinity maturation, and differentiation into antibody-producing plasma cells. During these T-dependent primary immune responses, long-lived antigen-specific T and B cells will also be produced that are set aside in large numbers to quickly respond should the antigen be encountered again. Hence, during a repeat exposure to the same antigen, the response is faster, stronger (i.e., more antibody produced), and qualitatively better (e.g., different isotypes of antibodies, higher antigen affinity of antibodies) due to these large numbers of memory cells set aside during the primary response. This is the basis of protective immunity and constitutes the "memory" of the adaptive immune system.

In addition to the physical and chemical barriers and the humoral and cell-mediated processes of innate and adaptive immunity, cytokines are chemical messenger proteins secreted by leukocytes in response to various forms of immune stimulation. Cytokines act through receptors to modulate a variety of functions of innate and adaptive immunity including inflammation and actions involving other immune cells from recruitment to differentiation. Important cytokines that promote inflammation include interleukins 1, 6, 12, and 18 (IL-1, IL-6, IL-12, IL-18), tumor necrosis factor alpha (TNF-α), and interferon gamma (IFN-γ) while cytokines that act to reduce inflammation are interleukins 4 and 10 (IL-4, IL-10) (Abbas et al., 2012).

Numerous studies have been published investigating the interaction between nanoparticles and the immune system. Most of these studies focus on either the potential toxicity of NP or the potential beneficial effects NP may have when used in biomedical applications that exploit their unique properties to either evade the immune system or stimulate it in order to

achieve the desired response (Ilinskaya and Dobrovolskaia, 2016). Several types of nanoparticles have shown promise in a variety of biomedical applications including colloidal gold and silver, silicon and titanium dioxides, superparamagnetic iron oxide nanoparticles (IO) and quantum dots (QD) to name of few. Two of these, IO and QD, are utilized in the current study and will be discussed in further detail throughout this dissertation. Iron oxide NP have the advantage of being paramagnetic (weakly attracted by a magnet) allowing them to be separated from solution using a magnet in applications such as immunoprecipitation. As a contrast agent, these particles may be conjugated and directed toward particular tissues. Quantum dots are semiconductor fluorescent nanocrystals with unique spectral properties that offer advantages over traditional organic fluorophores used in biomedical imaging (Bruchez et al., 1998). Quantum dots may be functionalized with a variety of coating molecules that enable the conjugation of biomaterials such as peptides or proteins for a variety of possible applications. Functionalized QD have shown promise as optical probes for imaging live pancreatic cancer cells indicating the potential use for QD in the early detection of cancer (Yong et al., 2009).

Many additional biomedical applications for nanoparticles, including IO and QD, are being discovered at a seemingly record pace. Nanoparticles may be designed to evade the immune system while homing to specific sites in vivo, allowing the ability to deliver anti-cancer agents to tumor cells. Nanoparticles with optical properties such as fluorescence or physical properties such as gamma ray absorption may be used in biomedical imaging applications. Nanoparticles conjugated with protein antigens may stimulate the humoral arm of the adaptive immune system to produce antigen-specific antibodies. These applications are powerful and have the potential to save lives, however limitations remain regarding this relatively new technology. Dobrovolskaia and McNeil point out in their 2007 review of immunological

properties of nanoparticles some of the pitfalls facing biomedical nanoparticle studies: 1) lack of comprehensive physicochemical evaluation of the NP used in experiments and, thus, no consistency lot to lot or across manufacturers; 2) differences in surface coatings under physiological conditions; 3) lack of a thorough comparison of NP across various animal models; and 4) lack of a thorough immunological evaluation (Dobrovolskaia and McNeil, 2007).

Solid toxicity data are needed to ensure that NP used in applications such as these do not elicit reactions that produce harmful side-effects. A variety of NP including QD are currently being evaluated for use in vaccine development with the goal of improving immunogenicity through better antigen stability, targeting specificity, and sustained cargo release (Yang et al., 2016). Harnessing the inherent properties of NP, including their shape, size and surface properties offers a promising strategy to design more effective vaccines.

Although there have been many promising uses for QD and many in vitro studies performed investigating their toxicity (Soenen et al., 2011), there remains a great need for effective in vivo systems to measure toxicity and bioactivity of QD (Aguilar et al., 2012; Fischer and Chan, 2007;Hofmann-Amtenbrink et al., 2015; Nel et al, 2006). Recent studies in our lab have shown that the growing feather (GF) in chickens may be used as a dermal test tissue ("in vivo test tube") to monitor local cellular/tissue responses to a variety of test-materials including nanoparticles (Erf and Ramachandran, 2016). The GF consists of a column of pulp tissue, a complex tissue (8-10 mm height, 2 mm diameter) that is composed of the inner dermis which is enveloped by an epidermal layer and surrounded by an outer connective sheath (Erf, U.S. Patent No.: 8,216,551; Erf et al., 2007; Erf and Ramachandran, 2016). The dermis of multiple GF in an individual animal may be injected and collected over multiple time points post-injection enabling ex vivo monitoring of in vivo immune activities in response to the injected test materials. The

GF are easily accessible and injection and collection are minimally invasive compared to traditional tissue biopsies. This method allows for the temporal, qualitative, and quantitative assessment of cellular/tissue responses to a variety of injected materials, including InP/ZnS QD – an area for which now there is limited in vivo immunological data.

This dissertation project was designed to 1) investigate the effects of NP in vitro and to 2) characterize the immunological effects of antigen-conjugated NP in vivo, according to the three main objectives described below:

Objective 1: To measure 1) the in vitro response of MQ-NCSU chicken macrophages to IO and QD NP by nitric oxide production and cell viability; and 2) cellular entry of QD in MQ-NCSU macrophages with regard to time of entry and nanoparticle dose.

Objective 2: To measure infiltrating leukocytes using immunofluorescence-based flow cytometry during the innate immune response to QD alone and QD conjugated with protein antigen injected into complex dermal tissue using flow cytometry as an application of the chicken growing feather model.

Objective 3: To measure 1) infiltrating leukocytes during the primary and memory cell-mediated adaptive immune responses to intramuscular immunization with QD conjugated with protein antigen using immunofluorescence-based flow cytometry; and 2) the humoral adaptive immune response to the protein antigen with and without QD conjugation using the enzyme linked immunosorbent assay (ELISA) to quantify systemic IgM and IgG antibody production following primary and booster immunization as a platform for vaccine development.

REFERENCES

Abbas, A. K., A. H. Lichtman, and S. Pillai. 2012. Cellular and Molecular Immunology. 7th ed. Elsevier Saunders, Philadelphia, PA.

ASTM International E2456 – 06. Standard Terminology Relating to Nanotechnology. Copyright ASTM International, 100 Barr Harbor Drive, PO Box C700, West Conshohocken, PA 19428-2959.

Bruchez, M., M. Moronne, P. Gin, S. Weiss, and A. P. Alivisatos. 1998. Semiconductor nanocrystals as fluorescent biological labels. Science. 281:2013-2016.

Chang, C. The immune effects of naturally occurring and synthetic nanoparticles. 2010. J. Autoimmunity. 34:J234-J246.

Dobrovolskaia, M. A., D. R. Germolec, and J. L. Weaver. 2009. Evaluation of nanoparticle immunotoxicity. Nat. Nanotech. 4:411-414.

Dobrovolskaia, M. A, and S. E. McNeil. 2007. Immunological properties of engineered nanomaterials. Nat. Nanotech. 2:469-478.

Erf, G. F., Inventor. U.S. Patent No.: 8,216,551. Date of Patent: Jul. 10, 2012. In vivo system to monitor tissue responses in birds.

Erf, G. F., B. Lockhart, O. T. Bowen, K. Bateman, and R. Finley. 2007. Using the chicken feather as a window into cell-mediated tissue responses. J. Immunol. 178:99.12.

Erf, G. F., and I. R. Ramachandran. 2016. The growing feather as a dermal test site: comparison of leukocyte profiles during the response to Mycobacterium butyricum in growing feathers, wattles, and wing webs. Poult. Sci. 95:1–12.

Fischer, H. C., and W. C. W. Chan. 2007. Nanotoxicity: the growing need for in vivo study. Curr. Opin. Biotech. 18:656-571.

Nel, A., T. Xia, L. Madler, and N. Li. 2006. Toxic potential of materials at the nanolevel. Science. 311:622-627.

Sayes, C. M., K. L. Reed, and D. B. Warheit. 2007. Assessing toxicity of fine and nanoparticles: comparing in vitro measurements to in vivo pulmonary toxicity profiles. Toxicol. Sci. 97:163-180.

Smith, M. J., McLoughlin, C. E., White, K. L., and D. R. Germolec. 2013. Evaluating the adverse effects of nanomaterials on the immune system with animal models. In: Handbook of Immunological Properties of Engineered Nanomaterials. Ed. Dobrovolskaia, M. A., and McNeil, S. E. World Scientific Publishing Co. Pte. Ltd. Singapore.

Xia, T., M. Kovochich, J. Brant, M. Hotze, J. Sempf, T. Oberley, C. Sioutas, J. I. Yeh, M. R. Wiesner, and A. E. Nel. 2006. Comparison of the abilities of ambient and manufactured nanoparticles to induce cellular toxicity according to an oxidative stress paradigm. Nano Lett. 6:1794-1807.

Xing, Y, and J. Rao. 2008. Quantum dot bioconjugates for in vitro diagnostics & in vivo imaging. Cancer Biomarkers. 4:307-319.

Yang, L., W. Li, M. Kirberger, W. Liao, and J. Ren. 2016. Design of nanomaterial based systems for novel vaccine development. Biomater. Sci. 4:785-802.

Yong, K. T., H. Ding, I. Roy, W. C. Law, E. J. Bergey, A. Maitra, and P. N. Prasad. 2009. Imaging pancreatic cancer using bioconjugated InP quantum dots. ACS Nano. 3:502-510.

Zhang, C., D. Pan, K. Luo, W. She, C. Guo, Y. Yang, and Z. Gu. 2014. Peptide dendrimer–doxorubicin conjugate-based nanoparticles as an enzyme-responsive drug delivery system for cancer therapy. Adv. Healthcare Mater. 3:1299-1308.

Zhao, L., A. Seth, N. Wibowo, C. X. Zhao, N. Mitter, C. Yu, and A. P. J. Middelberg. 2014. Nanoparticle vaccines. Vaccine. 32:327-337.

Literature Review

According to one of the most prolific authors on the use of nanoparticles in medicine, Dr. Jorg Kreuter, in his historical perspective published in 2007 in the International Journal of Pharmaceutics, the concept of targeted drug delivery is credited to Dr. Paul Ehrlich's "Zauberkugeln" therapy, or in English, "Magic Bullets" (Kreuter, 2007). Building on Dr. Ehrlich's theory that aiming drugs at specific targets could greatly improve outcomes, Dr. Peter Speiser strategized in the 1960s and 1970s at the Swiss Federal Institute of Technology in Zurich, to develop targeted, controlled release therapies by encapsulating the drugs in polymerized micelles (Merkle and Speiser, 1973). Dr. Speiser and his team of graduate students, the third of which was Dr. Kreuter himself, began by applying their concept of controlled release to vaccinations. They focused on tetanus, diphtheria, and other diseases that required multiple injections to stimulate protective immunity with the idea that the controlled release of the immunostimulant using nano-encapusulation would mimic the multiple injections needed for protection. These were some of the first studies utilizing nanoparticles for the treatment or prevention of disease. These scientists went on to further develop novel methods for the chemical synthesis and administration of nanoparticle-based therapies, including using nanoparticles to carry drugs across the blood-brain barrier (Michaelis et al., 2006).

As nanoparticle (NP) technology has advanced since those early discoveries, exciting new industrial and biomedical applications have evolved to the point where applications of nanotechnology are seemingly limitless. To provide an idea as to the breadth of the field of NP in biology, a recent Pubmed search for the term "nanoparticles" returned over 140,000 articles dating back to those earliest studies by Dr. Kreuter in the 1970s, while a search for "nanoparticles and medicine" returned over 13,000 articles (https://www.ncbi.nlm.nih.gov/pubmed/, 16 June 2017). Underlying this promise for new

consumer products, specialized drug delivery vehicles, and better vaccines is the risk that nanoparticles are toxic to plants and animals. Nanoparticles are on the scale of cellular components and have the ability to enter cells, interact with mitochondria, and deposit in target organs (Nel et al., 2006). Therefore, there remains a great need for effective methods to study the toxic effects of NP (Fischer and Chan, 2007; Dobrovolskaia et al., 2009). In vitro models are quite prevalent, but are unable to mimic the interaction of NP with more complex living systems. Additionally, while in vitro results may generally support in vivo findings in NP experiments, often these results may not be strongly correlated due to possible interference of NP in in vitro assays (Sayes et al., 2007). More effective models are therefore needed to understand the biological effects particularly since many of the most promising biomedical applications of NP including cancer therapy, bio-imaging and vaccination may directly impact the immune system.

Nanoparticle Basics

While the purpose of the current study is to further characterize engineered NP in an avian model, a review of the literature would not be complete without first addressing the distinction between "ultrafine particles" (UFP) and "nanoparticles" (NP). While the most basic characteristic of these particles is essentially identical – particle size in the range of 1-100 nm – the origin of these particles and modes of human exposure are far different. A brief explanation of these differences between UFP and NP is warranted as much of what is known about the risks of NP toxicity is based on studies done on UFP.

"Ultrafine particle" is a term used to describe air pollutants, mineral dust and other ambient particles such as smoke, in the size range of 1-100 nm, that result as a by-product of human activity such as the operation of combustion engines or industrial manufacturing (Chang, 2010; Xia et al., 2006). These particles are inhaled by humans and have been shown to deposit

in human lungs in a size and dose dependent manner. Differences have been found in the types of UFP in the lungs of people from "low" versus "high" pollution cities. In "low" pollution areas, particles are found as singlet molecules composed mostly of metals, whereas the lungs of people from "high" pollution contain more chains of aggregated, carbonaceous UFP (Churg and Brauer, 2000). Particle size has been shown to determine the course of UFP in the body; larger particles (>10 μm) are unable to get past the nasal and airway ciliary mucosa and thus rarely get too deep into the respiratory tract, while smaller particles may get deeper due to Brownian motion and diffusion (Chang, 2010). Diesel exhaust particles (DEP) are a type of UFP air pollution generated by diesel combustion engines that are prevalent in high traffic areas. A sample of environmental air from one of these areas may contain a variety of particle sizes and chemistries and, due to the prevalence of DEP, they have become an important model to study immune effects of UFP (Chang, 2010). Ultrafine particles like DEP have been shown to induce reactive oxygen species (ROS), oxidative stress, and inflammation (Xia et al., 2006).

Like UFP, "nanoparticles" (NP) are typically in the 1-100 nm size range, though NP are distinct from UFP in that NP are typically engineered for a specific purpose or application commonly through a series of controlled chemical reactions resulting in a material that is much more homogenous in size and composition than UFP found in the environment. Chemical synthesis methods such as reaction time, temperature, and/or chemical composition may be intentionally manipulated to control particle size and surface chemistry to either promote evasion of the immune system, favorable in the application of NP as drug delivery vehicles, or as in the case of vaccine design, encourage uptake by immune cells in order to trigger a humoral immune response resulting in antibody production (Ali et al., 2016). During synthesis, inorganic NP meant for biological applications are typically coated with additional molecules to increase

solubility and with ligands that will allow for conjugation with protein antigens or other molecules which may target the particles to certain tissue or cell types within the body.

An extensive review of the physical chemistry and synthesis methods of NP is beyond the scope of the current study, however many in-depth reviews on this subject have been written including Henglein, 1989; Alivisatos, 1996; and Burda et al., 2005. A cursory look at the unique physicochemical properties of NP including particle size, shape, surface structure, solubility, and chemical composition is warranted since these properties account for their value in biomedical applications and directly impact their behavior in living systems (Nel et al., 2006). Size is perhaps the most important attribute of NP, not only distinguishing NP from their bulk counterparts in mere dimension, but as the particle size shrinks, particle behavior is altered. Nanoparticles are made up of a few hundred to several thousand atoms – as particle size is reduced, more atoms are contained on the outer surface of the particle versus the interior of the particle effectively increasing the surface area to size ratio and thereby increasing the number of reactive groups on the particle surface (Nel et al., 2006). Other size-related attributes such as the phenomenon of quantum confinement will be discussed in more detail below under the topic of quantum dot NP. Depending on chemical composition and reaction conditions, NP may form in a variety of shapes including nanorods, nanotubes, nanosheets, nanospheres, nanostars, and nanowires which may be utilized in a variety of imaging, therapeutic, and diagnostic applications due to optical properties, stability, superparamagnetism, and functionalization (Aguilar, 2012).

As there are many shapes that NP may take on, there are also many different possible types and chemical compositions including metal oxides, gold, quantum dots (QD) and carbon nanotubes (Aguilar, 2012). In the following section, potential toxicity and immunological

effects of several specific NP types used in biological applications will be discussed including the two NP utilized in the current study, iron oxide and QD.

Gold nanoparticles (AuNP) have achieved widespread use in a variety of biological applications and have thus been well-characterized. One study of AuNP that highlights the importance of the physical attribute of NP size was conducted by Pan et al. (2007). This study found that treatment of various cell cultures with AuNP with only minute size differences resulted in a variety of differential responses related to mitochondrial structure and function. One of the responses was the susceptibility to apoptosis whereby cells undergo an ordered series of events leading to cell death. These include increased membrane permeability followed by cytochrome c release from the mitochondrial lumen into the cystosol where a number caspases (cysteine-aspartate proteases) await activation leading to proteolytic cleavage of cellular proteins and nucleic acid. Pan et al. (2007) found that following treatment with 1.2 nm gold nanoclusters up to 24 hours, HeLa cervical carcinoma cells were very similar to untreated cells, 4.1% vs. 4.6% respectively, with regard to the level of apoptotic cells. Treating with 1.4 nm gold however, resulted in almost 3-fold increase in apoptotic cells, 13.6% in Au NP treated vs. 4.6% in control, despite a higher concentration used for the slightly larger AuNP, 140 μM versus 110 μM for the 1.2 nm and 1.4 nm AuNP respectively (Pan et al., 2007). At 1.4 nm in diameter, AuNP may have an optimal fit into the major groove of DNA thereby inducing DNA-damage mediated apoptosis, while slightly smaller particles may be more amenable to clearance by the kidneys. In a separate study, Du et al. (2012) found that AuNP stimulated production of nitric oxide in murine macrophage RAW 264.7 cell line as measured by the Griess method demonstrating that the measurement of nitric oxide can be used as a tool to determine toxicity of nanoparticles in in vitro cell culture assays (Du et al., 2012).

Like gold nanoparticles, iron oxide nanoparticles (IO) have found a wide variety of applications including iron replacement therapies (Danielson, 2004), MRI contrast agents (Wang et al., 2001), and vaccine adjuvants (Pusic et al., 2013). Of these, the application of IO as a vaccine adjuvant is most relevant to the current study. In the 2013 study by Pusic et al., adjuvant properties of recombinant blood-stage human malaria vaccine antigen-conjugated IO NP (<20 nm) were compared to antigen emulsified in traditional vaccine adjuvants including incomplete Freund's adjuvant (IFA), complete Freund's adjuvant (CFA), Montanide ISA51. Advantages of IO NP as a vaccine adjuvant include their safety profile, low cost of production compared to other inorganic NP, and their ability to elicit antibody responses greater than that of the toxic adjuvants such as CFA. Results of the Pusic IO NP study found that not only were higher antibody titers elicited independent of the delivery route, the antibodies produced were functionally better at causing inhibition of parasite proliferation in both mice and non-human primates (Pusic et al., 2013).

Quantum Dot Nanoparticles

As the investigation of immunostimulatory effects of quantum dot nanoparticles (QD) is the primary goal of the current study, the following discussion will focus on the biomedical uses, toxicity and immune effects of QD, with additional information included for other NP when applicable. Quantum dots are semiconductor nanocrystals possessing a number of unique physical and optical properties (Alivisatos, 1996). These NP have found many uses in biological applications from imaging to new cancer diagnostic and treatment tools to drug and vaccine delivery (Rosenthal et al. 2011). Properties including size, chemical composition and surface coating(s) have the greatest influence on how QD are used and how they interact with biological systems (Alivisatos, 1996).

Quantum dots are typically under 10 nm is size, putting them on the scale of biological macromolecules with properties between that of single atoms and their bulk material counterparts. Particle size, and thus fluorescence, may be "tuned" by manipulating the QD chemical synthesis methods used, such as the elemental makeup and reaction time and temperature (Alivisatos, 1996). Generally QD are composed of a combination of elements from groups II and VI of the periodic table, such as CdSe and CdTe, or from groups III and V, such as InP and InAs (Chan et al., 2002). Following initial synthesis, QD are functionalized by adding a "cap," or shell as it is commonly referred, such as ZnS that is compatible chemically with the QD core. The shell material has a larger bandgap than the core resulting in the semiconductor properties and multiple energy states that contribute significantly to the fluorescent properties of QD (Chan et al., 2002). The shell typically also allows for solubility in aqueous environments and further enables bio-functionalization via the binding of additional molecules to the QD surface such as proteins, DNA, sugars, etc., without adversely affected stability (Chan and Nie, 1998). When QD are excited with light energy that exceeds the bandgap of the core material, electrons are promoted from the valence band to the conductance band leaving holes. When electrons recombine with electron holes, light is emitted. The extent of the quantum confinement in QD, which is directly related to particle size, dictates the emission wavelength. The smaller the size of the QD particle, the greater the degree of quantum confinement, thus the shorter the distance the electrons are moving and the shorter the wavelength of light that is emitted (Alivisatos, 1996). As the size of the QD core increases, so does the wavelength of the light that is emitted. Quantum dots have narrow emission wavelengths (20 to 30 nm) in the visible spectrum ranging from 400 nm to 2 μm (Bruchez et al., 1998) depending on their chemical makeup.

The unique optical properties of QD offer several advantages in biological applications over more traditional organic dyes such as fluorescein, rhodamine, phycoerythrin, etc., (Chan et al, 2002; Resch-Genger et al., 2008). Organic dyes are subject to photo-bleaching where prolonged exposure to high-energy UV and laser light sources such as those used in fluorescence microscopy results in the breakdown of covalent bonds in the dye molecules and an irreversible loss of color (Rosenthal et al., 2011; Bruchez et al., 1998). In flow cytometry spectral overlap of the emission wavelengths as determined by the Stokes shifts of common organic dyes necessitates the need for digital compensation by instrument software (Njemini et al., 2013). As the larger bandgap of the shell confines emission to the core, photo-bleaching is eliminated and very narrow emission wavelengths are possible (Chan et al., 2002) enabling much better color resolution in any application where the simultaneous distinction of two or more labeled molecules is desired. Quantum dots have another unique property related to their core-shell structure – blinking – a property that may be undesirable in certain applications. Omogo et al. has shown that blinking may be reduced by carefully controlling the thickness of ZnS shells in multi-shelled QD while maintaining their small size and biocompatibility (Omogo et al., 2016).

Toxicity

As nanotechnology & chemical synthesis methods have evolved, so has the study of "nanotoxicology." As new applications of NP are being discovered for use in medicine, toxicological techniques utilizing in vitro and in vivo systems are being used in order to learn more about how NP may positively or negatively impact living systems. Metals are common active ingredients in UFP and engineered NP and have been shown to penetrate the linings of internal organs such as the respiratory and GI tracts, eyes, nasal passages, etc. (Chang, 2010). The concerns for toxicity of engineered NP are due in large part to the risk for potential loss of

their shell coating and subsequent deposition in tissues and organs (Nel et al., 2006). Long term physiological effects of metal exposure may be profound leading to respiratory illness and inflammation (Chang, 2010) thus much attention has been directed toward determining the various mechanisms of NP toxicity.

Many studies have shown that the toxic effects of NP are based on their interactions with the cellular environment. Nanoparticles may enter endothelial and epithelial cells and macrophages through a variety of processes including clathrin-mediated endocytosis, caveolae-dependent endocytosis, pinocytosis, and phagocytosis (Zhang and Monteiro-Riviere, 2009; Zhao et al., 2011). One of the most commonly observed mechanisms of NP toxicity is the production of ROS due to the presence of highly reactive NP surface molecules that promote the generation of oxygen rich intermediates via the Fenton reaction ($Fe^{++} + H_2O_2 \rightarrow Fe^{+++} + OH^{\bullet} + OH^{-}$) (Chang, 2010). In this reaction a transition metal catalyzes a redox reaction in the endoplasmic reticulum or the mitochondria leading to ROS production from hydrogen peroxide. The reactive species that are produced have the ability to cause DNA damage. Chang (2010) describes a second mechanism of NP toxicity involving the production of intracellular superoxides by enzymes in bronchial epithelial cells utilizing polycyclic aromatic hydrocarbons and a cytochrome P450 pathway to donate electrons to oxygen (Chang, 2010). Activation of mitochondrial enzymes such as NADPH oxidase also leads to the generation of large quantities of $O_2^{\bullet-}$ which is a part of the mechanism phagocytes use to initiate intracellular killing of pathogens (Abbas et al., 2012). Among the various physiological effects of ROS, Bottje et al. described reduced feed efficiency in male broiler chickens with reduced mitochondrial function as measured by increased ROS as a result of the breakdown in the electron transport chain (Bottje et al., 2002). Xia et al. outlined a 3-tiered system to describe the extent of ROS to create

cellular injury coupled with human body's ability to cope. First, exposure to ROS leads to activation of normal protective mechanisms available to living cells. The second step is activation of transcription factors that trigger inflammation when the body's protective mechanism is overwhelmed by the extent of oxidative injury. The final step is cytotoxicity at the cellular level (Xia et al., 2006).

Quantum dots specifically have been shown to have detrimental effects on cellular mitochondria including increasing levels of ROS, altering mitochondria morphology, and mitochondria-mediated apoptosis (Ali et al., 2016; Andon and Fadeel, 2013; Hauck et al., 2010; Soenen et al., 2011). Zhang et al. investigated oxidative stress in vitro (murine liver) and in vivo (mice) following CdTe QD treatment. Superoxide dismutase (SOD, antioxidant), catalase (CAT, H_2O_2 reducer), and malondialdehyde (MDA, marker for oxidative stress) were measured in liver homogenates using low, medium, and high doses of CdTe QD. SOD and CAT increased in the low-treatment group while MDA increased in the high-treatment group (Zhang et al., 2015). ROS were also found to rise in response to QD in a dose dependent manner. The antioxidant tBHQ lowered ROS in the high-treatment group significantly but ROS was still higher than the mid-treatment group. Apoptosis induction was evident as shown via flow cytometry and by upregulation of pro-apoptotic p53 and Bax mRNA expression and down-regulation of anti-apoptotic Bcl-2 mRNA expression. tBHQ pre-treatment in the high-treatment group overcame oxidative stress to return Bax and p53 expression to baseline levels while Bcl-2 mRNA did not return to control levels, but was equivalent to the level of the mid-treatment group (Zhang et al., 2015).

In 2015, Nguyen et al. looked specifically at mitochondrial toxicity in mammalian hepatocytes in response CdTe QD (Nguyen et al., 2015). Noted are a few interesting findings in

their study with relation to mitochondria and evidence of cadmium toxicity, the first being mitochondrial swelling and loss of cristae, however transmission electron microscopy (TEM) did not show QD in the cell or in the mitochondria. Nguyen et al. also looked at localization of QD in the mitochondria by isolating mitochondria and measuring fluorescence at 540 nm emission. They found 2.5 to 3-fold higher fluorescence intensity in QD-treated cells. Finally, they investigated electron transport chain component (ETC) levels and activity at 24 hours post treatment and found decreases in complexes II, III, and IV, with an increase in complex V suggesting that the impairment of the ETC may be leading to the induction of ROS generation (Nguyen et al., 2015).

While CdSe-based QD were shown to have toxic effects in vivo, recent studies have shown that InP-based QD offer a safer alternative (Brunetti et al., 2013). In one of the few studies comparing the effects of cadmium-based and indium-based QD, Brunetti et al. found that indium-based QD were safer both in vitro and in vivo using *Drosophila* as an animal model. Their findings were based on exposure to cadmium (Cd^{2+}) and indium (In(III)) ions, both of which were found to have leached from their respective QD. In vitro results showed a greater decrease in cell viability and membrane damage in addition to upregulation of antioxidant and detoxifying enzyme expression levels in human lung carcinoma and human neuroblastoma cell lines when treated with cadmium-based QD compared to indium-based QD. In vivo gene expression results showed upregulation of genes involved with stress response, DNA damage, and ROS production. Apoptosis was implicated as the mechanism of cell death with a higher level of apoptosis in CdSe/ZnS vs. InP/ZnS treated QD (Brunetti et al., 2013).

Immunology

While ROS generation and subsequent mitochondria-mediated pathways of toxicity are prevalent in response to NP, additional mechanisms of toxicity including protein denaturation, DNA damage and inflammation have been shown, although with limited experimental evidence (Nel et al., 2006). While the general mechanisms of toxicity have been elucidated, the immunological aspects of NP exposure have not been well established due to the current lack of in vivo studies. In vitro studies provide insight into how a particular cell type may respond to NP treatment; however, interplay between all of the various aspects of the immune system including signaling between innate and adaptive immune cells, circulation of blood and lymph, antigen presentation, etc., simply cannot be recreated in a dish (Dobrovolskaia et al., 2009; Fischer and Chan, 2007). In vivo studies are necessary to begin to understand toxicity and immune activity in response to NP and these studies may be designed to answer many yet unanswered questions such as the differential effects of multiple NP formulations, safety profiling for clinical use of NP, standardization of commercial NP preparations, and many more (Hofmann-Amtenbrink et al., 2015).

While much work is left to be done in the NP field, many studies related to the use of NP in medicine have been completed over the past 20 years. Over the past 10 years, more and more studies and reviews have been published describing NP with respect to the immune system, immunotoxicity, and the potential uses of NP in immunotherapy. Many studies have shown that NP may be phagocytosed by tissue macrophages and have described their effects on cell viability, induction of apoptosis, etc. Additional studies have begun to look at both in vitro and in vivo effects of NP in tandem. In one of the first studies published to evaluate in vitro and in vivo effects of QD in mice, Wang et al. (2016) assessed cell uptake, cell viability, apoptosis and

ROS in response to CdSe/ZnS QD. This group compared macrophages and lymphocytes and found macrophages took up QD followed by a decrease in cell viability while lymphocytes did not take up QD but did undergo expansion. The authors attributed this increase in lymphocytes to immune stimulation followed by transformation of "immature mother cells" to dividing lymphocytes leading to increased cell density (Wang et al., 2016). Macrophages also showed an increase in ROS followed by induction of apoptosis. In their in vivo studies, Wang et al. (2016) found that due to QD size at 6.5 nm, the NP accumulated in the body whereas previous studies had shown that QD <5.5 nm could be cleared. The study's authors concluded that in vitro cytotoxicity measurements should be combined with in vivo immunotoxicity testing so that a better understanding of molecular mechanisms of nanotoxicity to QD could be realized because evidence gained from in vivo animal studies is more relevant to humans (Wang et al., 2016).

Indium-based QD are presumed to be safer than cadmium-based QD due to more covalent bonding between group III-V elements versus group II-VI elements resulting in more resistance to degradation, however few studies have been published investigating the in vivo effects of InP/ZnS QD. Lin et al. (2015) published one of the first studies looking at the in vivo effects of the InP/ZnS QD using BALB/c mice. This group found accumulation of InP/ZnS QD in the spleen and liver and elemental indium in major organs after 84 days. However, the authors observed neither weight changes nor any adverse hematological or biochemical changes compared to PBS (Lin et al., 2015). While InP/ZnS QD produced no acute toxic effects, this study failed to compare InP/ZnS to cadmium-based QD in their model. Without direct comparisons, the question remains whether any significant differences would be uncovered between the two treatments.

These studies, while important in investigating the incremental effects of a type of NP on one model system or another, either in vitro or in vivo or both, are lacking the additional measurements of direct immune system effects. In vivo studies are able to take advantage of the entire living system that the in vitro studies cannot replicate. For NP such as QD to become widely accepted and approved for use as treatment or diagnostics agents, more immunological study is necessary.

As described earlier NP enter a variety of cell types and interact with the immune system. Animals have a variety of defense mechanisms that protect them from harmful effects of pathogens such as bacteria and viruses including the innate and adaptive immune systems (Abbas, 2012). While many bacteria are able to colonize various organ systems of animals without doing harm, e.g., commensal bacteria in the gut that aid digestion, many other types of bacteria and other pathogens may harm the host, and are targets of the immune system. Animals have physical defenses such as the skin and mucosal epithelial cells that keep unwanted organisms from gaining entry into the body. Should an organism cross these barriers, resident tissue macrophages and dendritic cells, epithelial cells with ciliary bodies lining the respiratory tract, and cellular tight junctions offer additional lines of defense to deter further entry of pathogens into the body (Abbas et al., 2012). There are also biochemical barriers such as tears and saliva which contain an antimicrobial chemical known as lysozyme that will destroy pathogenic organisms should they come in contact with the eyes or mouth. The complement system and antigen presentation to B cells and T cells are additional functions of the innate and adaptive immune systems that work in coordination to destroy foreign materials and create immunologic memory (Albiger et al., 2007; Abbas et al., 2012).

The innate immune system includes the body's physical barriers, the complement system and immune cells that deter entry, remove, or further process foreign materials and invading pathogenic organisms. Macrophages and dendritic cells recognize and remove damaged and/or dead host cells as well as non-cellular particulate material or other substances that should not be present in healthy tissue (Abbas et al., 2012) moreover, dendritic cells and may further stimulate the adaptive immune system. The innate immune system recognizes pathogen associated molecular patterns (PAMPs) and damage associated molecular patterns (DAMPs) which are specific for microbes and dying cells, respectively, leading to inflammation. Pattern recognition receptors (PRRs) on the outer membranes and the membranes of intracellular structures of macrophages, neutrophils, dendritic cells and barrier epithelial cells recognize PAMPs and DAMPs. Upon binding of PAMPs or DAMPs with a PRR, signal transduction events take place that initiate the inflammatory response either directly via cell membrane bound receptors or through the cytoplasm. Cell membrane bound receptors, such as the toll-like receptors (TLRs), stimulate nuclear factor kappa-B (NFk-B) and activator protein-1 (AP-1) interferon response factors that encode many of the signaling molecules known as cytokines involved in inflammation. Cytoplasmic signals are relayed by nucleotide-binding oligomerization domain-like receptors (NLRs) and retinoic acid-inducible gene I (RIG)-like receptors (RLRs) leading to Type 1 interferon production promoting macrophage activation. Macrophages have two primary functions 1) internalize and destroy microbes and 2) produce cytokines that allow communication with other cells of the immune system to increase the level of attack at the site of inflammation (Abbas et al., 2012). The recruitment of additional leukocytes to the site of inflammation is a key hallmark of innate immunity.

While innate immunity provides broad, non-specific protection from birth against a wide-variety of foreign materials that may enter the vertebrate body, the adaptive immune system builds pathogen-specific immunity over the lifetime of the organism. Adaptive immunity includes both humoral and cell-mediated responses, utilizing primarily B and T lymphocytes, respectively. B lymphocytes get their name from their origin of discovery, the bursa of Fabricius in birds. In mammals, as there is no equivalent organ to the bursa, B lymphocytes were discovered to mature in the bone-marrow, thus B lymphocytes are bursa-, or bone-marrow derived leukocytes (Abbas et al., 2012). B cells are involved in both the humoral arm of adaptive immunity through the production of antigen-specific antibodies and cell-mediated adaptive immunity through their role as antigen presenting cells. Antibodies are produced by B cells through a process of genetic recombination that results in regions in the antibody protein that recognize specific antigens. Through their function as the B cell surface receptor (BCR), when membrane-bound BCR binds pathogens and facilitate internalization of the pathogen by the B cell for antigen presentation to T helper cells, with the help of T helper cells, B cells may further mature into plasma cells that secrete antibodies, a soluble form of BCR. Antibodies are able to neutralize pathogens by binding directly to them. Secreted antibodies also play a role in the complement system, binding to surfaces of microbes and facilitating binding of complement protein C1q leading to microbe destruction via the classical complement pathway. Antibodies are most effective opsonins, marking microbes for Fc receptor-mediated phagocytosis.

Thymus-derived T lymphocytes recognize antigens presented with major histocompatibility complex (MHC) proteins on the surface of antigen presenting cells such as dendritic cells, macrophages, and B lymphocytes. Antigen presentation allows antigen-specific T cells to bind antigen-peptide-MHC complexes with their T cell receptor (TCR). This results in

lymphocyte proliferation, greatly increasing their numbers to combat rapidly replicating pathogens (Abbas et al., 2012). The work of helper (CD4+, T_H), cytotoxic (CTL, CD8+), and regulatory (T_{reg}) T lymphocytes is largely directed by the various signaling molecules called cytokines that are produced by the various cells of the immune system during the course of the immune response. Depending on the type of infection and the cytokines produced, T_H cells may be directed to carry out either the adaptive immune response towards cell-mediated or humoral immunity. Especially for humoral immunity, T_H cells are particularly important for B cells to undergo isotype switching and affinity maturation which improves antibody effectiveness and memory development.

Nanoparticles in Biological Applications

Nanoparticles either evade the immune system or stimulate the immune system depending on their properties; therefore, NP have been designed for use in many biomedical applications including imaging, drug delivery, and vaccine development (Ilinskaya and Dobrovolskaia, 2016). Compared to traditional organic fluorophores used for labeling such as phycoerythrin (PE) or fluorescein isothiocyanate (FITC), QD possess long-term photostability and superior brightness making them appealing for live animal targeting and imaging (Xing et al., 2008). Optical probes are created through functionalization of QD via conjugation of multiple copies of various biomolecules, such as proteins, peptides, DNA, and small molecules (Rosenthal et al., 2011). Probes of this type have shown promise for imaging live pancreatic cancer cells, highlighting their potential use in the early detection of cancer (Yong et al., 2009) as well as whole animal imaging (Bruchez et al., 1998; Gao et al., 2012). Regarding the use of NP as drug delivery agents, cancer treatment has been a major area of research, leading to the establishment of the Nanotechnology Characterization Laboratory to promote the use of

nanomaterials to combat cancer (www.ncl.cancer.gov) and many published studies and reviews on the topic. Prophylactic and therapeutic immunotherapies use nanoparticles to encapsulate anti-cancer compounds or to carry anti-cancer peptides and molecules as a means of cancer immunization (Singh and Bhaskar, 2014). Li et al. (2014) demonstrated the ability to deliver the potent chemotherapy agent doxorubicin to the cell nucleus by stimulating cellular enzymatic cleavage of peptides bound to the QD outer coating. As in cancer immunotherapy, a variety of nanoparticles including QD are currently being evaluated for use in pathogenic vaccines with the goal of improving immunogenicity through better antigen stability, targeting specificity, and sustained cargo release (Zhao et al., 2014; Yang et al., 2016). Since not all foreign particles that enter the body are immunogenic, meaning they do not trigger a cellular and humoral immune, additional substances known as adjuvants are combined with the foreign material to mount an immune response by activating TLRs and inflammatory cytokine receptors (Reddy et al., 2007). Boosting protective immunity to malaria with NP vaccine technology has been the focus of several recent studies. As the malarial parasite transitions between extracellular and intracellular states during infection, NP including lipid vesicles, iron oxide and QD have been employed as adjuvants eliciting strong T helper cell-dependent immune responses critical for protection (Moon et al., 2012; Little, 2012; Pusic et al., 2011; Pusic et al., 2013). In these studies when antigen was conjugated to NP, more robust protective antibody titers were elicited with lower doses of antigen given (Moon et al., 2012, Pusic et al., 2011; Pusic et al., 2013), better stimulation of the production of active areas of B cell proliferation known as germinal centers (Moon et al., 2012), and heightened production of pro-inflammatory cytokines (Moon et al., 2012, Pusic et al., 2011; Pusic et al., 2013) compared to controls, demonstrating the effectiveness of NP as novel vaccine adjuvants.

Application of the Avian "In Vivo Test Tube" to the Study of Nanoparticles

Nonclinical studies in animals are essential to the drug and vaccine development life cycle. Animal studies enable proof-of-concept of new technologies and provide valuable safety and efficacy data necessary prior to moving into human clinical studies (WHO, 2005). As there have been many promising uses for NP developed and many studies performed investigating their toxicity, there remains a great need for effective in vivo systems to measure toxicity and immunological effects of NP, including QD (Nel et al., 2006; Aguilar, 2012; Hofmann-Amtenbrink et al., 2015). In vitro models are useful to an extent; however, in vivo data is necessary to understand the distribution and clearance by the complex living organism (Fischer and Chan, 2007).

The chicken has a long history as a platform for major contributions to the field of immunology. Studies in chickens have resulting in many groundbreaking discoveries which have helped to shape our current knowledge of key aspects of immunology including the work of Glick et al. and the discovery of the bursa of Fabricius as the site of antibody production (Glick et al., 1955; Davison et al., 2014). Avian models have been used to study a variety of diseases including autoimmune vitiligo, thyroiditis, and systemic sclerosis (Davison et al., 2014). A recent study highlighted the benefits of an avian model to investigate the early development of human epithelial ovarian cancer. De Melo Bernardo et al. (2015) outlined prolific ovulation and similar metastatic progression of the hen as advantageous traits benefitting the study of this disease (De Melo Bernardo et al., 2015). As avian models become more prolific, so too should the availability of laboratory tools and reagents for avian model research.

The growing feather (GF) in chickens has been used as a dermal test tissue ("in vivo test tube") to monitor local cellular/tissue responses to a variety of test-materials (Erf, U.S. Patent

No.: 8,216,551; Erf et al., 2007, Erf et al., 2016). The GF consists of a column of complex tissue (8-10 mm height, 2 mm diameter) composed of the inner pulp (dermis) which is enveloped by an epidermal layer and surrounded by an outer connective sheath (Erf, U.S. Patent No.: 8,216,551; Erf et al., 2007). Multiple feathers in an individual animal may be injected with test material and collected over multiple time points post-injection enabling monitoring of immune activities in response to the injected test-materials. Growing feathers are easily accessible and injection and collection are minimally invasive compared to traditional tissue biopsies. This method allows for repeated immunological monitoring of immune responses to a variety of injected materials over time, including QD – an area for which now there is limited in vivo immunological data, and provides a unique model for further study of the immunology of dermal injections (Erf and Ramachandran, 2016, Erf et al., 2017). Major disadvantages of the majority of mammalian models currently available are the inability to repeatedly sample individuals and inherent biological variability between individuals necessitates large numbers of animals needed to increase the statistical power of animal studies.

REFERENCES

Abbas, A. K., A. H. Lichtman, and S. Pillai. 2012. Cellular and Molecular Immunology. 7th ed. Elsevier Saunders, Philadelphia, PA.

Aguilar, Z. P. 2012. Nanomaterials for Medical Applications. Elsevier, Boston.

Ali A., M. Suhail, S. Mathew, M. A. Shah, S. M. Harakeh, S. Ahmad, Z. Kazmi, M. A. R. Alhamdan, A. Chaudhary, G. A. Damanhouri, and I. Qadri. 2016. Nanomaterial induced immune responses and cytotoxicity. 16:40-57.

Alivisatos, A. P. 1996. Semiconductor clusters, nanocrystals, and quantum dots. Science. 217:933-937.

Alivisatos, A. P. 1996. Perspectives on the physical chemistry of semiconductor nanocrystals. J. Phys. Chem. 100:13226-13239.

Andon, F. T. and B. Fadeel. 2013. Programmed cell death: molecular mechanisms and implications for safety assessment of nanomaterials. Accounts Chem. Res. 46:733-742.

Bottje, W., Z. X. Tang, M. Iqbal, D. Cawthon, R. Okimoto, T. Wing, and M. Cooper. 2002. Association of mitochondrial function with feed efficiency within a single genetic line of male broilers. Poultry Sci. 81:546-555.

Bruchez, M., M. Moronne, P. Gin, S. Weiss, and A. P. Alivisatos. 1998. Semiconductor nanocrystals as fluorescent biological labels. Science. 281:2013-2016.

Brunetti, V., H. Chibli, R. Fiammengo, A. Galeone, M. A. Malvindi, G. Vecchio, R. Cingolani, J. L. Nadeau, and P. P. Pompa. 2013. InP/ZnS as a safter alternative to CdSe/ZnS core/shell quantum dots: in vitro and in vivo toxicity assessment. Nanoscale. 5:307-317.

Burda, C., X. Chen, R. Narayanan, and M. A. El-Sayed. 2005. Chemistry and properties of nanocrystals of different shapes. Chem. Rev. 105:1025-1102.

Chan, W. C. W., D. J. Maxwell, X. Gao, R. E. Bailey, M. Han, and S. Nie. 2002. Luminescent quantum dots for multiplexed biological detection and imaging. Curr. Opin. Biotechnol. 13:40-46.

Chan, W. C. W., and S. Nie. 1998. Quantum dot bioconjugates for ultrasensitive nonisotopic detection. Science. 281:2016-2018.

Chang, C. The immune effects of naturally occurring and synthetic nanoparticles. 2010. J. Autoimmunity. 34:J234-J246.

Churg, A., and M. Brauer. 2000. Ambient atmospheric particles in the airways of human lungs. Ultrastruct. Pathol. 24:353-361.

Danielson, B. G. 2004. Structure, chemistry, and pharmacokinetics of intravenous iron agents. J. Am. Soc. Nephrol. 15(suppl 2):S93-S98.

Davison, F., B. Kaspers, and K. A. Schat. 2014. Avian Immunology. 2nd ed. Elsevier, San Diego, CA.

De Melo Bernardo, A., S. Thorsteinsdottir, and C. L. Mummery. 2015. Advantages of the avian model for human ovarian cancer. Mol. Clin. Oncology. 3:1191-1198.

Dobrovolskaia, M. A., D. R. Germolec, and J. L. Weaver. 2009. Evaluation of nanoparticle immunotoxicity. Nat. Nanotech. 4:411-414.

Du, L., X. Miao, H. Jia, Y. Gao, K. Liu, X. Zhang, and Y. Liu. 2012. Detection of nitric oxide in macrophage cells for the assessment of the cytotoxicity of gold nanoparticles. Talanta. 101:11-16.

Erf, G. F., Inventor. U.S. Patent No.: 8,216,551. Date of Patent: Jul. 10, 2012. In vivo system to monitor tissue responses in birds.

Erf, G. F., D. M. Falcon, K. S. Sullivan, and S. E. Bourdo. 2017. T lymphocytes dominate local leukocyte infiltration in response to intradermal injection of functionalized graphene-based nanomaterial. J. Appl. Toxicol. 37:1317-1324.

Erf, G. F., B. Lockhart, O. T. Bowen, K. Bateman, R. Finley. 2007. Using the chicken feather as a window into cell-mediated tissue responses. J. Immunol. 178:99.12.

Erf, G. F., and I. R. Ramachandran. 2016. The growing feather as a dermal test site: comparison of leukocyte profiles during the response to Mycobacterium butyricum in growing feathers, wattles, and wing webs. Poult. Sci. 95:1–12.

Fischer, H. C., and W. C. W. Chan. 2007. Nanotoxicity: the growing need for in vivo study. Curr. Opin. Biotech. 18:656-571.

Gao, J., K. Chen, R. Luong, D. M. Bouley, H. Mao, T. Qiao, S. S. Gambhir, and Z. Cheng. 2012. A novel clinically translatable fluorescent nanoparticle for targeted molecular imaging of tumors in living subjects. Nano Lett. 12:281-286.

Glick, B., T. S. Chang, and R. G. Jaap. 1955. The bursa of Fabricius and antibody production. Poultry Sci. 35:224-225.

Hauck, T. S., R. E. Anderson, H. C. Fischer, S. Newbigging, and W. C. W. Chan. 2010. In vivo quantum dot toxicity assessment. Small. 6:138-144.

Henglein, A. 1989. Small-particle research: physicochemical properties of extremely small colloidal metal and semiconductor particles. Chem. Rev. 89:1891-1873.

Hofmann-Amtenbrink, M., D. W. Grainger, and H. Hofmann. 2015. Nanoparticles in medicine: current challenges facing inorganic nanoparticle toxicity assessments and standardizations. Nanomed.: Nanotech. Biol. Med. 11:1689-1694.

Ilinskaya, A. N., and M. A. Dobrovolskaia. 2016. Understanding the immunogenicity and antigenicity of nanomaterials: past, present and future. Tox. Appl. Pharmacol. 299:70-77.

Kreuter, J. 2007. Nanoparticles – a historical perspective. Int. J. Pharmaceutics. 331:1-10.

Lin, G., Q. Ouyang, R. Hu, Z. Ding, J. Tian, F. Yin, G. Xu, Q. Chen, X. Wang, and K. T. Yong. 2015. In vivo toxicity assessment of non-cadmium quantum dots in BALB/c mice. Nanomedicine: NBM. 5:341-350.

Little, S. R. 2012. Reorienting our view of particle-based adjuvants for subunit vaccines. Proc. Natl. Acad. Sci. USA. 109:999-1000.

Merkle, H. P., and P. Speiser. 1973. Preparation and in vitro evaluation of cellulose acetate phthalate coacervate microcapsules. J. Pharm. Sci. 62:1444-1448.

Michaelis, K., M. M. Hoffmann, S. Dreis, E. Herbert, R. N. Alyautdin, M. Michaelis, J. Kreuter, and K. Langer. 2006. Covalent linkage of apolipoprotein E to albumin nanoparticles strongly enhances drug transport into the brain. J. Pharmacol. Exp. Ther. 317:1246-1253.

Moon, J. L., H. Suh, A. V. Li, C. F. Ockenhouse, A. Yadava, and D. J. Irvine. 2012. Enhancing humoral reponses to a malaria antigen with nanoparticle vaccines that expand T_{fh} cells and promote germinal center induction. Proc. Natl. Acad. Sci. USA. 109:1080-1085.

Nel, A., T. Xia, L. Madler, and N. Li. 2006. Toxic potential of materials at the nanolevel. Science. 311:622-627.

Nguyen, K., P. Rippstein, A. F. Tayabali, and W. G. Willmore. 2015. Mitochondrial toxicity of cadmium telluride quantum dot nanoparticles in mammalian hepatocytes. Toxicol. Sci. 146:31-42.

Njemini, R., O. O. Onyema, W. Renmans, I. Bautmans, M. De Waele, and T. Mets. 2013. Shortcomings in the application of multicolor flow cytometry in lymphocyte subsets enumeration. Scand. J. Immunol. 79:75-89.

Omogo, B., F. Gao, P. Bajwa, M. Kaneko, and C. D. Heyes. 2016. Reducing blinking in small core-multishell quantum dots by carefully balancing confinement potential and induced lattice strain: the “Goldilocks” effect. ACS Nano. 10:4072-4082.

Pan, Y., S. Neuss, A. Leifert, M. Fischler, F. Wen, U. Simon, G. Schmid, W. Brandau, and W. Jahnen-Dechent. 2007. Size-dependent cytotoxicity of gold nanoparticles. Small. 3:1941-1949.

Pusic, K., H. Xu, A. Stridiron, Z. Aguilar, A. Wang, and G. Hui. 2011. Blood stage merozoite surface protein conjugated to nanoparticles induce potent parasite inhibitory antibodies. Vaccine. 29:8898-8908.

Pusic, K., Z. Aguilar, J. McLoughlin, S. Kobuch, H. Xu, M. Tsang, A. Wang, and G. Hui. 2013. Iron oxide nanoparticles as a clinically acceptable delivery platform for a recombinant blood-stage human malaria vaccine. FASEB J. 27:1153-1166.

Reddy, S. T., A. J. van der Vlies, E. Simeoni, V. Angeli, G. J. Randolph, C. P. O'Neil, L. K. Lee, M. A. Swartz, and J. A. Hubbell. 2007. Exploiting lymphatic transport and complement activation in nanoparticle vaccines. Nat. Biotechnol. 25:1159-1164.

Resch-Genger, U., M. Grabolle, S. Cavaliere-Jaricot, R. Nitschke, and T. Nann. 2008. Quantum dots versus organic dyes as fluorescent labels. Nat. Meth. 5:763-775.

Rosenthal, S. J., J. C. Chang, O. Kovtun, J. R. McBride, and I. D. Tomlinson. 2011. Biocompatible quantum dots for biological applications. Chemistry & Biology. 18:10-24.

Sayes, C. M., K. L. Reed, and D. B. Warheit. 2007. Assessing toxicity of fine and nanoparticles: comparing in vitro measurements to in vivo pulmonary toxicity profiles. Toxicol. Sci. 97:163-180.

Shi, F., and G. F. Erf. 2012. IFN-γ, IL-21, and IL-10 co-expression in evolving autoimmune vitiligo lesions of Smyth line chickens. J. Invest. Derm. 132:642-649.

Singh, M. S., and S. Bhaskar. 2014. Nanocarrier-based immunotherapy in cancer management and research. ImmunoTargets and Therapy. 3:121-134.

Soenen, S. J., P. Rivera-Gil, J.-M. Montenegrob, W. J. Parak, S. C. De Smedt, and K. Braeckmans. 2011. Cellular toxicity of inorganic nanoparticles: common aspects and guidelines for improved nanotoxicity evaluation. Nano Today. 6:446-465.

Wang, Y. X. J., S. M. Hussain, and G. P. Krestin. 2001. Superparamagnetic iron oxide contrast agents: physicochemical characteristics and applications in MR imaging. Eur. Radiol. 11:2319-2331.

Wang, X., J. Tian, K. T. Yong, X. Zhu, M. C. M. Lin, W. Jang, J. Li, Q. Huang, and G. Lin. 2016. Immunotoxicity assessment of CdSe/ZnS quantum dots in macrophages, lymphocytes and BALB/c mice. J. Nanobiotechnol. 14:10.

World Health Organization. 2005. WHO guidelines on nonclinical evaluation of vaccines. WHO Technical Report Series. No. 927.

Xia, T., M. Kovochich, J. Brant, M. Hotze, J. Sempf, T. Oberley, C. Sioutas, J. I. Yeh, M. R. Wiesner, and A. E. Nel. 2006. Comparison of the abilities of ambient and manufactured

nanoparticles to induce cellular toxicity according to an oxidative stress paradigm. Nano Lett. 6:1794-1807.

Xing, Y, and J. Rao. 2008. Quantum dot bioconjugates for in vitro diagnostics & in vivo imaging. Cancer Biomarkers. 4:307-319.

Yang, L., W. Li, M. Kirberger, W. Liao, and J. Ren. 2016. Design of nanomaterial based systems for novel vaccine development. Biomater. Sci. 4:785-802.

Yong, K. T., H. Ding, I. Roy, W. C. Law, E. J. Bergey, A. Maitra, and P. N. Prasad. 2009. Imaging pancreatic cancer using bioconjugated InP quantum dots. ACS Nano. 3:502-510.

Zhang, L. W., and N. A. Monteiro-Riviere. 2009. Mechanisms of quantum dot nanoparticle cellular uptake. Tox. Sci. 110:138-155.

Zhang, T., Y. Hu, M. Tang, L. Kong, J. Ying, T. Wu, Y. Xue, and Y. Pu. 2015. Liver toxicity of cadmium telluride quantum dots (CdTe QD) due to oxidative stress in vitro and in vivo. Int. J. Mol. Sci. 16:23279-23299.

Zhao, F., Y. Zhao, Y. Liu, X. Chang, C. Chen, and Y. Zhao. Cellular uptake, intracellular trafficking, and cytotoxicity of nanomaterials. 2011. Small. 7: 1322-1337.

Zhao, L., A. Seth, N. Wibowo, C. X. Zhao, N. Mitter, C. Yu, and A. P. J. Middelberg. 2014. Nanoparticle vaccines. Vaccine. 32:327-337.

CHAPTER I

In vitro responses of chicken macrophages to iron oxide and quantum dot nanoparticles

Introduction

Since the turn of the twentieth century, cell culture and other tissue models have been utilized to investigate the effects of diagnostic and therapeutic agents when testing in living subjects was either prohibited or otherwise not feasible. Despite the ubiquity of these "in vitro" models in the researchers' toolkit, "in vivo" testing data is essential to achieve scientific validity and to the pursuit of regulatory approval. This challenge is faced by all developers of promising new treatments or technologies that have great potential for biological applications, especially nanoparticle (NP) technology that has shown so much promise in biomedical applications (Rosenthal et al. 2011; Aguilar, 2012).

Scientists have discovered many unique physicochemical properties of nanomaterials that may be harnessed for the development of new, more effective strategies for drug delivery, biomedical imaging, and vaccine adjuvants (Bruchez et al., 1998; Chang 2010; Rosenthal et al., 2011; Zhao et al., 2014). Iron oxide nanoparticles have been used in a variety of applications from magnetic resonance contrast agents (Wang et al., 2001) to vaccine adjuvants for malaria subunit vaccines (Pusic et al., 2013). Similarly, NP such as superconductor quantum dots have found application in bio-imaging due to their unique optical properties, and in cancer diagnostic and therapeutic applications when functionalized with a variety of surface molecules, including nucleic acids, proteins, lipids and carbohydrates (Rosenthal et al., 2011; Bilan et al., 2016). Other NP technologies include colloidal gold, metal oxides such as titanium and zinc oxide, and organic NP like carbon nanotubes and liposomes.

While the potential uses of NP in biological applications are quite promising, many NP studies indicate that great risks remain for toxic side effects. Current nanoparticle toxicity research commonly utilizes cell cultures to determine NP toxicity and possible

immunostimulatory effects (Zhang et al., 2015; Choi et al., 2007). Reactive oxygen species, upregulation of stress response genes, and induction of apoptosis have been established as common mechanisms of toxicity in response to NP exposure (Lovric et al., 2005; Nguyen et al., 2015) in a variety of cell culture systems. Nitric oxide production by macrophages and cell viability assays are also frequently used as indicators of immunomodulation and toxicity in response to in vitro treatments. Nitric oxide is produced in cells upon the conversion of L-arginine and oxygen into L-citrulline and nitric oxide (NO) in an oxidoreductase reaction catalyzed by nitric oxide synthase 2 (NOS2) (Hibbs et al., 1987; Bogdan, 2015). Nitric oxide generation can indirectly be measured in the form of its stable conversion products nitrite and nitrate in the cell culture medium using Griess reagent (Griess, 1879; Stuehr and Marletta, 1985). Several recent studies have investigated NO production in macrophages in response to NP treatments. Du et al. (2012) found that murine macrophages produced increasing levels of NO in response to increasing concentrations of citrate-coated gold NP, but NO levels were relatively unchanged compared to those in untreated cultures when murine macrophages were treated with gold NP coated with thiolated polyethylene glycol.

Effects of NP on cell viability in in vitro cell culture models can be addressed by MTT assay. In this assay, actively metabolizing cells take up 3-[4,5-dimethylthiazol-2-yl]-2,5 diphenyl tetrazolium bromide (MTT), converting the compound to blue-purple formazan crystals that are then dissolved in a solvent such as dimethyl sulfoxide (DMSO). The absorbance of the resulting color is read spectrophotometrically at 540 nm using a microplate spectrophotometer. The relative absorbance is positively correlated to the number of viable, or actively metabolizing, cells (Clift et al., 2010; Nguyen et al., 2015).

With the overall goal to develop the avian system as a model to determine bioactivities of NP in vitro and in vivo, the objective of this study was to examine possible immunostimulatory and toxic effects of NP on avian macrophages. Specifically, macrophages from the MQ-NCSU chicken macrophage cell line were exposed in culture to lipopolysaccharide (LPS), mouse IgG protein antigen, iron oxide (IO) NP, or water soluble indium phosphide zinc sulfide quantum dot (QD) NP. Nitric oxide generation was examined by Griess reaction and cell viability by MTT assay. Utilizing the unique fluorescent properties of the QD, the dynamics of QD-macrophage interactions were observed using fluorescence microscopy. The results from these in vitro studies were also used to determine the optimal QD dose for subsequent in vivo QD studies.

This work was supported by NIH-NIBIB R15 EB015187; G. F. Erf, PI.

MATERIALS AND METHODS

Reagents Lipopolysaccharide (LPS, stock concentration 2 mg/mL) from *Salmonella typhimurium* was purchased from Sigma (St. Louis, MO). Mouse IgG (mIgG, stock concentration 10 mg/mL) was used as the test antigen and was purchased from Rockland Immunochemicals Inc. (Limerick, PA). Two formulations of commercial iron oxide nanoparticles were purchased from Ocean NanoTech (San Diego, CA), one marketed as "endotoxin-free" (EF-IO, catalog number SXP-10-01, stock concentration 1 mg/mL) and the other absent the "endotoxin-free" claim (IO, catalog number SHP-10-25, stock concentration 5 mg/mL). Both formulations contain 10 nm iron oxide (Fe_2O_3) nanoparticles with carboxylic acid functional groups. Indium phosphide zinc sulfide (InP/ZnS, 7 nm, stock concentration 5 mg/mL) quantum dots (QD) were from Mesolight, Inc., (Little Rock, AR)

Cell Culture Macrophages from the MQ-NCSU chicken mononuclear phagocyte cell line were maintained in T-25 culture flasks (Corning, Corning, NY) at 40.5°C supplemented with 5%

CO_2 in LM Hahn medium as described by Qureshi et al. (1990). Cells were passaged every 2-3 days by scraping the cells into the medium and transferring a portion of the cell suspension into a new T-25 flask with fresh culture medium. Results of preliminary experiments established NP treatment parameters including cell seeding density and NP preparation. For each experiment, unless otherwise noted, cells were grown to approximately 80% confluence, scraped, and centrifuged at 250 x *g* for 5 minutes at room temperature. Following centrifugation, the supernatant medium was discarded and the cell pellet was re-suspended thoroughly in phenol-red-free RPMI 1640 medium supplemented with 10% heat-inactivated fetal bovine serum, antibiotic/antimycotic solution and 2 mM L-glutamine (RPMI 1640 cell culture medium). Cell concentration was adjusted to 1 x 10^6/mL viable cells in RPMI 1640 cell culture medium, then 100 µL of the macrophage cell suspension was added to wells of a flat bottom 96-well tissue culture plate for a final cell density of 1 x 10^5 macrophages/well. Cells were allowed to adhere for 1 hour prior to treatment, unless otherwise noted.

Lipopolysaccharide, mIgG, and NP treatments were diluted in complete RPMI 1640 cell culture medium at two times the treatment concentration, mixed thoroughly by vortexing at high speed and 100 µL added to each well in triplicate per treatment concentration for a final volume of 200 µL per well. Final treatment concentrations were 0.000005, 0.00005, 0.0005, 0.005, 0.05, 0.5, 5 µg/mL for LPS; 0.5, 1, 2.5, 5, 10, and 20 µg/mL for EF-IO, IO, and mIgG; and 0.015, 0.031, 0.062, 0.125, 0.25, and 0.5 µM for QD. Untreated macrophages served as the negative assay control, while LPS treatment served as the positive assay control. Macrophages were cultured for 24 hours at 40.5°C and 5% CO_2 in a humidified cell culture incubator (Thermo Fisher Scientific, Marietta, OH).

Nitric Oxide Assay Macrophage synthesis of nitric oxide (NO) in response to LPS, mIgG and NP treatment was quantified by measuring total nitrite in the culture medium using the Griess reagent as described by Hussain and Qureshi (1997). Griess reagent was prepared by mixing 1% sulfanilamide (Sigma; 1 g in 100 mL 5% H_3PO_4) 1:1 with 0.1% N-(1-naphthyl) ethylenediamine dihydrochloride (NED; Sigma; 100 mg NED in 100 mL ultrapure water) immediately before use. Sodium nitrite standards ($NaNO_2$; Sigma) were prepared by dissolving 0.069 g $NaNO_2$ in 100 mL ultrapure water to make a 10 mM $NaNO_2$ stock solution then diluting 10 mM $NaNO_2$ in ultrapure water to 1.25, 2.5, 5, 10, 20, 30, 40, 50, 60, 70, 80, and 90 µM.

Following the 24 hour incubation of macrophage cultures, the 96-well tissue culture plates were then centrifuged at 250 x *g* for 5 minutes at room temperature. Following centrifugation, 100 µL of supernatant medium from each well was carefully transferred to a second, flat-bottom 96-well plate (NO assay plate), taking care to retain sample replicate positions and to avoid disrupting the tissue monolayer. The microplate with the cell cultures was returned to the incubator for subsequent measurement of cell viability using the MTT assay.

Griess reagent, 100 µL/well, was added to each well of the NO assay plate and the plate incubated with shaking for 8 minutes at room temperature for red color development. The optical absorbance at 540 nm was read using a Bio-Tek ELx800 (Bio-Tek Instruments, Winooski, VT) microplate reader. The intensity of the red color as measured by the optical absorbance at 540 nm is directly proportional to presence of nitrite ions ($NaNO_2$) in the solution. To determine the relationship between concentration of $NaNO_2$ and optical absorbance measurements, a range of known concentrations of $NaNO_2$ (1.25, 2.5, 5, 10, 20, 30, 40, 50, 60, 70, 80, and 90 µM $NaNO_2$) were included in duplicate on each NO assay plate. A linear standard curve was then generated using the best-fit standard curve equation by linear regression (a.u. on

the y-axis and nitrite concentration on the x-axis) and used to convert optical absorbance measurements obtained for the macrophage culture medium supernates to $NaNO_2$, and hence NO, concentrations (µM). This standard curve was used to determine NO generation by macrophages treated with LPS, mIgG, and IO. These treatments were not associated with endogenous color generation that contributed to optical absorbance readings at 540 nm. For the QD treatment, however, due to the inherent red color of the QD, a "spiked" standard curve was prepared adding 0.125 µM QD to each of the nitrite standards (1.25, 2.5, 5, 10, 20, 30, 40, 50, 60, 70, 80, and 90 µM $NaNO_2$; QD-standard curve). The concentration 0.125 µM QD was chosen for the QD-standard curve because it was in the middle of the range of the QD treatment concentrations tested. Additionally, to better control for the color-contribution of QD to the assessment of NO generation by macrophages cultured in the presence of the various QD dosages, culture plates were set up adding 100 µL QD (0, 0.015, 0.031, 0.062, 0.125, 0.25, and 0.5 µM) to wells containing 100 µL of macrophages or 100 µL of culture medium alone (no macrophages) and incubated as described above. After 24 hours of incubation, culture medium was collected and subjected to NO assay. Optical absorbance measurements for the QD cultures were converted to NO concentration (µM) using both of the standard curves (QD spiked and normal).

Cell Viability Assay Following centrifugation of the 96-well culture plate and partial removal of cell culture medium for the NO assay, remaining actively metabolizing viable cells were quantified using the 3-[4,5-dimethylthiazol-2-yl]-2,5 diphenyl tetrazolium bromide (MTT; Sigma) assay. Viable cells remaining after LPS, mIgG, or NP treatment will metabolize MTT in the culture medium converting MTT to formazan crystals. Following sufficient crystal development, formazan crystals are dissolved in a solvent such as DMSO, resulting in a purple solution. The intensity of the purple color is directly proportional to the number of viable cells

and the color may be measured by optical absorbance at 540 nm. To prepare the MTT solution, 8 mg MTT was dissolved in 2 mL DPBS then filtered with a 0.45 μm syringe filter, resulting in a 4 mg/mL stock solution. The 4 mg/mL MTT stock solution was diluted 1:10 in RPMI 1640 culture medium to produce a 2X concentrated solution of which 100 μL was added to the remaining culture medium in each well of the plate for a final concentration of 0.2 mg/mL MTT and a final volume of 200 μL per well. The plate was returned to the 40.5°C humidified incubator and cultures incubated for approximately 2 hours to allow MTT metabolism by remaining viable cells. Following incubation, culture medium was removed from each well with care taken not to disrupt the tissue monolayer. Next, to dissolve the formazan crystals 150 μL DMSO (Sigma) was added per well and the plate put on a microplate shaker for 5-10 minutes. Once the formazan crystals were fully dissolved, the optical absorbance of the resulting purple solution was measured at 540 nm using the microplate reader. The percentage of viable untreated cells was set at 100%. For treated cells, the percentages of viable cells were determined as a percentage of viable cells that did not receive treatment; i.e. the mean absorbance of the treated cells was divided by the mean absorbance of the untreated cells and the fraction multiplied by 100.

Microscopic Observation of QD Entry into MQ-NCSU Macrophages Chicken macrophages (MQ-NCSU) were seeded in 500 μL RPMI 1640 medium at a density of 2 x 10^5/well on autoclaved glass coverslips in a 24-well plate (Corning) and grown to approximately 60% confluence overnight in a 40.5°C humidified incubator supplemented with 5% CO_2. Quantum dots (InP/ZnS, 10 μM) were diluted directly in the cell culture medium to final concentrations of 0.0625, 0.01250, 0.025, 0.05, and 0.1 μM. The cultures were then incubated in a 40.5°C humidified incubator supplemented with 5% CO_2 for 5, 24, and 48 h. Endotoxin-free

water added to the cell culture medium instead of QD served as the untreated negative control. Following QD treatment, cells were washed twice with PBS then fixed in 2% paraforamaldehyde, pH 7.45, for 15 minutes at room temperature. The cover slips with adherent macrophages were then inverted on glass slides containing approximately 20 µL Vectashield mounting medium with DAPI nuclear stain (Vector Laboratories, Burlingame, CA). An Olympus BX50F microscope with an ultraviolet light source and fluorescent filter "WU" consisting of a 400 nm dichroic mirror, 330-385 nm bandpass excitation filter and a 420 nm barrier filter was used to visualize simultaneous fluorescence of DAPI and QD. Images were captured using a CoolSNAP-Pro color CCD camera and Image-Pro 6.2 software.

Statistical Analysis Sigma Plot 13 Statistical Software (Systat Software, Inc., San Jose, CA) was used to determine significant effects of LPS, mIgG, and NP treatments on NO production and cell viability. Main treatment effects, main treatment concentration effects, and treatment by treatment concentration interactions were determine using one-way repeated measure analysis of variance (ANOVA). Following ANOVA, Fisher's least square difference (LSD) was used for multiple means comparisons. Nitric oxide and cell viability assays were repeated a minimum of three different times. For all analyses, differences were considered significant at $P \leq 0.05$.

RESULTS

The standard curves describing the relationship between optical absorbance (y-axis) and nitrite (NO) concentration (µM; x-axis) for each NO assay were linear and highly repeatable from plate to plate. Addition of a medium dose of QD to the nitrite standards resulted in a reduction in the slope of the QD-standard curve [e.g., the linear equation for the normal standard curve was $y = 0.0107x + 0.0404$; $R^2 = 0.998$ versus $y = 0.0094x + 0.0991$; $R^2 = 0.998$ for the

QD-standard curve], but otherwise did not interfere with the linear, positive relationship between optical absorbance and known nitrite concentrations.

Nitric oxide production in LPS, mIgG and NP-treated MQ-NSCU macrophages

Lipopolysaccharide

The LPS dose response curves were highly reproducible following LPS treatment, indicating the utility of LPS as a positive control for nitric oxide production by chicken macrophages. No effect of LPS concentration on nitric oxide generation was found following treatment with 0.000005, 0.00005, 0.0005, or 0.005 μg/mL. However, nitric oxide concentrations rose sharply ($P < 0.05$) at 0.05 μg/mL LPS to 44.9 ± 2.0 μM and then plateaued at 54.1 ± 3.1 μM when stimulated with LPS at 0.5 μg/mL and above (Figure 1, Table 1a).

Mouse IgG Protein Antigen

No significant increase in nitric oxide was observed following treatment with mouse IgG protein antigen alone (Figure 1, Table 1a).

Iron Oxide Nanoparticles

Treatment and treatment concentration interactions were observed following IO and EF-IO treatments. Using multiple means comparisons at each treatment concentration, nitric oxide levels rose steeply at 5 μg/mL IO ($P < 0.05$) from 6.9 ± 1.7 μM to 39.2 μM (± 0.7) at 20 μg/mL IO. Nitric oxide production was unchanged following EF-IO treatment at each concentration tested (Figure 1, Table 1a). It should be noted that subsequent cultures using a new and different lot of IO-NP did not stimulate NO production at the same dosages as the IO used in this study and results were not different from those obtained when IO-EF NP were used (data not shown).

Quantum Dot Nanoparticles

NO-assay conducted with samples from the culture medium containing the various doses of QD tested but no cells, and the culture medium containing the various doses of QD tested and macrophages, revealed QD dose-dependent increases in color independent of whether or not macrophages were present in the 24 hour cultures. When optical density values were converted to nitrite concentrations (µM) using the normal- and QD-standard curves, the dose response curves obtained were parallel, but nitric oxide estimates were somewhat lower when based on the QD-standard curve. (Figure 2, Table 2a). Independent of which standard curve was used to obtain estimates for nitric oxide production, these assays revealed that the QD presence in the culture medium did not stimulate detectable NO production by the macrophages except with the highest dosage of 0.5 µM QD tested. At the 0.5 µM QD dose, the NO production estimates for the QD treated macrophage cultures were 28.3 ± 0.7 and 26.0 ± 0.8 based on the normal and QD-standard curves, respectively; whereas for the QD treated culture medium without cells the respective NO estimates were 17.6 ± 1.0 and 13.8 ± 1.1 µM. Taking this background contribution of the QD into account, an average of 10.7 µM ($P < 0.05$) NO was generated by the macrophages in the presence of 0.5 µM QD (Figure 2, Table 2a).

MQ-NSCU chicken macrophage viability following LPS, mIgG and NP treatment

The viability of MQ-NSCU chicken macrophages following 24 h treatment with LPS, mIgG and NP was measured using the MTT assay. A steady decrease (treatment concentration main effect $P < 0.001$) in cell viability occurred with increasing LPS concentration including a 30.4 ± 3.6% decrease at 0.05 µg/mL, an additional 22.1 ± 4.1% decrease at 0.5 µg/mL, and an additional 12.7 ± 4.7% decrease at 5.0 µg/mL, though no effect was observed following treatment with 0.0005 and 0.005 µg/mL LPS (Figure 1, Table 1b). No significant decrease in

cell viability was observed following mIgG treatment (Figure 1, Table 1b). Treatment by treatment concentration interaction was observed following macrophage treatment with IO. Multiple means comparison for IO treatment indicated 90.0 ± 3.7% and 82.5 ± 4.3% remaining viable cells following macrophage treatment with 10 µg/mL and 20 µg/mL IO, respectively, compared to untreated control ($P = 0.016$). No significant decrease was observed in cell viability following EF-IO treatment (Figure 1, Table 1b). QD treatment resulted in a significant reduction in cell viability (treatment concentration main effect $P < 0.001$). Cell viability sharply declined at the lowest concentrations of QD, with 45.8 ± 8.7% viable cells remaining following macrophage treatment with 0.062 µM QD. Macrophage viability continued to decline as QD concentration increased, but at a reduced rate. Following treatment with the highest concentration of QD, 0.5 µM, 13.6 ± 1.3 % macrophages were viable (Figure 2, Table 2b).

Microscopic observation of QD entry into MQ-NCSU macrophages

MQ-NCSU chicken macrophages took up QD in a time and dose dependent manner as observed using fluorescence microscopy. DAPI staining identified the macrophage nucleus with blue color. The area surrounding the nucleus and extending to the cell membrane had punctated red area within 5 h following treatment with 0.1 uM QD. By 24 h post QD-treatment, QD were no longer observed as individual red dots, rather, with the exception of the nucleus, the entire inside of the cell appeared to be saturated with red color (Figure 3).

DISCUSSION

In this study we investigated activation and cell viability of macrophages from the MQ-NCSU chicken macrophage cell line following treatment with increasing concentrations of iron oxide, mouse IgG protein antigen, and quantum dot (QD) nanoparticles in culture. Following 24 h incubation with treatments, the cell culture medium was analyzed for the presence of nitrite as

a sign of macrophage activation via the inducible nitric oxide (NO) synthase mechanism. Following removal of cell growth medium for nitrite measurement, the viability of the same macrophage cultures was assessed using the MTT cell viability assay. Fluorescence microscopy was also used to visualize QD entry in MQ-NCSU macrophages.

Lipopolysaccharide (LPS), also referred to as endotoxin, treatment proved to be a valuable positive control for macrophage activation as the mechanism of LPS binding toll-like receptor 4 (TLR-4) on the surface of chicken macrophages and induction of nitric oxide synthesis is well known (Bowen, 2006). Nanoparticle preparation involves various chemicals, solvents, etc. (Alivisatos, 1996), and controlling for endotoxin contamination during manufacturing requires costly control measures. As NP often interfere with endotoxin measurement assays, it is difficult to know however whether an immune response is truly triggered by the NP or by a contaminant. Endotoxin testing is an important requirement as regulatory guidelines dictate thresholds for endotoxin contamination for pharmaceutical preparations and medical devices to ensure patient safety.

As these results show, possible endotoxin contamination in nanoparticle preparations may lead to macrophage activation as evidenced by total nitrite measurement. There is a great need for simpler analysis systems and controls to assist the researcher in determining whether an NP effect is real. Controls used in in vitro studies with and without cells are important to include in these in vitro experiments (Dobrovolskaia et al., 2009). Companies producing NP often include electron micrographs depicting size and dispersion, but these specifications may vary from lot to lot. Molecular weight of NP is another important factor to consider when designing NP experiments. Since NP may differ so widely in their physicochemical characteristics, the

concentration of nanoparticles may also vary widely, increasing the importance of proper characterization.

In addition to assay interference caused by possible endotoxin contamination, optical absorbance of NP preparations is also important to consider with regard to in vitro assays measuring the effects of NP on a colorogenic response. Based on the results shown in Figure 2, the accurate measurement of NO following QD treatment is complicated by the QD solution's optical absorbance, which results in dose-dependent increase in optical absorbance and high background color in the absence of NO generating macrophages. In fact, the NO-dose response curves generated in this study appear to be due to optical absorbance by the increasing levels (0, 0.015, 0.031, 0.062, 0.125, 0.25, and 0.5 µM) of QD present in the culture medium. However, background NO production estimate and optical density contribution by QD, and hence background NO production estimates, plateaued near 18 µM NO for the three highest QD dosages tested (0.125, 0.25, and 0.5 µM). The divergent NO estimates observed with the 0.5 µM QD dose in the absence (approx. 16 µM NO) and presence of macrophages in the cultures (approx. 27 µM NO) revealed that QD can stimulate chicken macrophages to generate NO production and that with the appropriate controls (i.e. no cells, culture medium plus range of QD dosages tested) this NO production can be detected even in the presence of the high optical absorbance background contribution of the QD in this colorogenic assay.

Cell viability decreased with increasing doses of LPS, though was relatively unchanged versus untreated control for mIgG and IO treatments. The observed reduction in cell viability in the presence of increasing doses of QD added to the MQ-NCSU macrophage cultures is in line with reports by others. Clift et al. (2010) found significant cytotoxicity via the MTT assay in J774.A1 murine macrophages following 48 h treatment with 80 nM hydrophobic cadmium core

QD (Clift et al., 2010). Despite claims that InP/ZnS quantum dots are safer than cadmium-based QD, our results showed cell viability decreased in a dose response manner, with approximately 45% viable cells following treatment with 0.062 µM QD and approximately 15% viable cells following treatment with 0.5 µM QD. Interestingly, while macrophage viability dropped to 20% with 0.5 µM QD, this dosage of QD was the only one tested that stimulated NO generation by the macrophages. The NO detected likely accumulated in the culture medium as stable nitrite early during the 24 hour incubation and was generated by QD stimulated macrophages before the dramatic reduction in cell viability occurred. Inclusion of earlier time-points to assess the effects of QD on chicken macrophages in these assays would help address this phenomenon of QD macrophage activation and cell death.

Brunetti et al. (2013) directly compared indium- and cadmium-based QD in vitro and found increased expression of antioxidant and detoxifying enzymes following cadmium QD treatment versus indium QD treatment in both human lung carcinoma and human neuroblastoma cells. They reported a decrease in intracellular release of metal ions over extended time (96 h) for indium versus cadmium QD, supporting the logic that indium has a stronger bond relative to cadmium and is more resistant to hydrolysis (Brunetti et al., 2013).

Microscopy studies indicated QD gained entry into MQ-NCSU chicken macrophages within 45 minutes appearing first as define red dots both near the cell membrane and surrounding the nucleus. As treatment time increased, QD fluorescence was less localized in red punctuations and more evenly dispersed inside the cell and around the nucleus. QD entered cells more quickly at higher doses compared to lower doses. Clift et al. (2010) also found QD to be present in murine macrophages using microscopy at 2 h of co-culture. Additional studies are needed to further characterize the dynamics of entry of QD in MQ-NCSU chicken macrophages.

The results of this study illustrate the utility of in vitro chicken cell culture model in the investigation of the potential immunostimulatory and toxic effects of nanoparticles. The cell culture approach is often preferred by investigators due to the relative ease of accessibility of in vitro cell culture and its' relatively low cost compared to in vivo studies. While in vitro studies are useful for the study of NP, the optical properties of NP have the potential to cause interference with assay readouts (Dobrovolskaia et al., 2009). In addition, as the results of these NO assays demonstrated, variability in commercial NP preparations is possible. As we have shown, LPS is a potent stimulator of NO production. LPS, also known as endotoxin, contamination in NP preparations, rather than the NP themselves, may be the cause of immune system stimulation. The results of this study illustrate the need for standardization of NP preparations both within and across manufacturers, as these products are still relatively new to the market. As NP are highly sophisticated materials with a variety of unique physicochemical properties, sophisticated instruments such as electron microscopes, zeta sizers, etc., are needed to characterize them. By nature of QD chemical synthesis methods, QD size is variable and thus any given sample may vary from lot to lot. Even the slightest variability in NP size could make a significant difference in the biological response to NP. As Pan et al. (2007) demonstrated, a difference of even 0.2 nm in gold NP size could affect the particles' ability to fit into the structure of DNA, for example. Therefore, additional methods are needed to demonstrate the biological effects of NP. Du et al. (2012) have developed an electrochemical sensor for nitric oxide that is claimed to be a more sensitive and specific real-time assay for NO assessment. Measuring in vitro response to NP treatment using chicken macrophages as in the current study, may offer an additional method that is more sensitive to differences in NP treatment and concentration.

As NP including IO and QD offer much promise for biological applications, additional studies are needed to quantify the endotoxin contamination in NP. Perhaps in combination with LPS, a viable control system for researchers working with NP in biomedical applications could be developed to validate that the observed effects are due to NP as the active ingredient rather than endotoxin. Due to the high costs of NP production and the lack of regulation and standardized NP manufacturing methods, manufacturing controls and validated testing models are critical to the success of NP in biomedical applications (Charitidis et al., 2014). Cadmium-based QD have been shown to stimulate ROS and expression of pro-apoptotic genes *p53* and *Bcl*-2 with decreased expression of the *Bax* anti-apoptotic gene (Zhang et al., 2015) further suggesting cell death follows a mitochondria-mediated pathway. Additional studies focusing on various NP cap and ligand chemistries optimized to facilitate quick cell entry, but compatible with requirements of imaging studies with regard to reducing the negative effects of QD treatment would contribute to the growing body of NP toxicity and biomedical application literature.

While these in vitro studies were important to establish the chicken model as a viable NP test system, these studies were also important in establishing optimal concentrations to use in subsequent in vivo studies with live chickens. As our results indicate, these in vitro studies were successful in establishing optimal mIgG and NP concentrations for use in in vivo studies.

REFERENCES

Aguilar, Z. P. 2012. Nanomaterials for Medical Applications. Elsevier, Boston.

Bilan, R., A. Sukhanova, and I. Nabiev. 2016. Quantum dot-based nanotools for bioimaging, diagnostics, and drug delivery. ChemBioChem. 10.1002/cbic.201600357.

Bogdan, C. 2015. Nitric oxide synthase in innate and adaptive immunity: an update. Trends Immunol. 36:161-178.

Bowen, O. T., R. F. Wideman, N. B. Anthony, and G. F. Erf. 2006. Variation in the pulmonary hypertensive responsiveness of broilers to lipopolysaccharide and innate variation in nitric oxide production by mononuclear cells. Poult. Sci. 85:1349-1363.

Bruchez, M., M. Moronne, P. Gin, S. Weiss, and A. P. Alivisatos. 1998. Semiconductor nanocrystals as fluorescent biological labels. Science. 281:2013-2016.

Brunetti, V., H. Chibli, R. Fiammengo, A. Galeone, M. A. Malvindi, G. Vecchio, R. Cingolani, J. L. Nadeau, and P. P. Pompa. 2013. InP/ZnS as a safter alternative to CdSe/ZnS core/shell quantum dots: in vitro and in vivo toxicity assessment. Nanoscale. 5:307-317.

Chang, C. The immune effects of naturally occurring and synthetic nanoparticles. 2010. J. Autoimmunity. 34:J234-J246.

Charitidis, C. A., P. Georgiou, M. K. Koklioti, A. F. Trompeta, and V. Markakis. 2014. Manufacturing nanomaterials: from research to industry. Manufacturing Rev. 1:11

Choi, H. S., W. Liu, P. Misra, E. Tanaka, J. P. Zimmer, B. I. Ipe, M. G. Bawendi, and J. V. Frangioni. 2007. Renal clearance of nanoparticles. Nat. Biotechnol. 25:1165-1170.

Clift, M. J., M. S. Boyles, D. M. Brown, and V. Stone. 2010. An investigation into the potential for different surface-coated quantum dots to cause oxidative stress and affect macrophage cell signaling in vitro. Nanotoxicology. 4:139-149.

Dobrovolskaia, M. A., D. R. Germolec, and J. L. Weaver. 2009. Evaluation of nanoparticle immunotoxicity. Nat. Nanotech. 4:411-414.

Du, L., X. Miao, H. Jia, Y. Gao, K. Liu, X. Zhang, and Y. Liu. 2012. Detection of nitric oxide in macrophage cells for the assessment of the cytotoxicity of gold nanoparticles. Talanta. 101:11-16.

Griess, P. 1879. Bemerkungen zu der Abhandlung der H.H. Weselsky und Benedikt “Ueber einige Azoverbindungen.” Chem. Ber. 12, 426–8.

Hibbs, J. B., R. R. Taintor, and Z. Vavrin. 1987. Macrophage cytotoxicity: role for l-arginine deiminase and imino nitrogen oxidation to nitrite. Science. 235:473-476.

Hussain, I., and M. A. Qureshi. 1997. Nitric oxide synthase activity and mRNA expression in chicken macrophages. Poult Sci. 76:1524-1530.

Lovric, J., S. J. Cho, F. M. Winnik, and D. Maysinger. 2005. Unmodified cadmium telluride quantum dots induce reactive oxygen species formation leading to multiple organelle damage and cell death. Chemistry & Biology. 12:1227-1234.

Nguyen, K., P. Rippstein, A. F. Tayabali, and W. G. Willmore. 2015. Mitochondrial toxicity of cadmium telluride quantum dot nanoparticles in mammalian hepatocytes. Toxicol. Sci. 146:31-42.

Pusic, K., Z. Aguilar, J. McLoughlin, S. Kobuch, H. Xu, M. Tsang, A. Wang, and G. Hui. 2013. Iron oxide nanoparticles as a clinically acceptable delivery platform for a recombinant blood-stage human malaria vaccine. FASEB J. 27:1153-1166.

Qureshi, M. A., Miller, L., Lillehoj, H. S., and Ficken, M. D. 1990. Establishment and characterization of a chicken mononuclear cell line. Vet. Immun. Immunopath. 26:237-250.

Rosenthal, S. J., J. C. Chang, O. Kovtun, J. R. McBride, and I. D. Tomlinson. 2011. Biocompatible quantum dots for biological applications. Chemistry & Biology. 18:10-24.

Stuehr, D. J., and M. A. Marletta. 1985. Mammalian nitrate biosynthesis: mouse macrophages produce nitrite and nitrate in response to Escherichia coli lipopolysaccharide. Proc. Natl. Acad. Sci. USA. 82:7738-7742.

Wang, Y. X. J., S. M. Hussain, and G. P. Krestin. 2001. Superparamagnetic iron oxide contrast agents: physicochemical characteristics and applications in MR imaging. Eur. Radiol. 11:2319-2331.

Zhang, T., Y. Hu, M. Tang, L. Kong, J. Ying, T. Wu, Y. Xue, and Y. Pu. 2015. Liver toxicity of cadmium telluride quantum dots (CdTe QD) due to oxidative stress in vitro and in vivo. Int. J. Mol. Sci. 16:23279-23299.

Zhao, L., A. Seth, N. Wibowo, C. X. Zhao, N. Mitter, C. Yu, and A. P. J. Middelberg. 2014. Nanoparticle vaccines. Vaccine. 32:327-337.

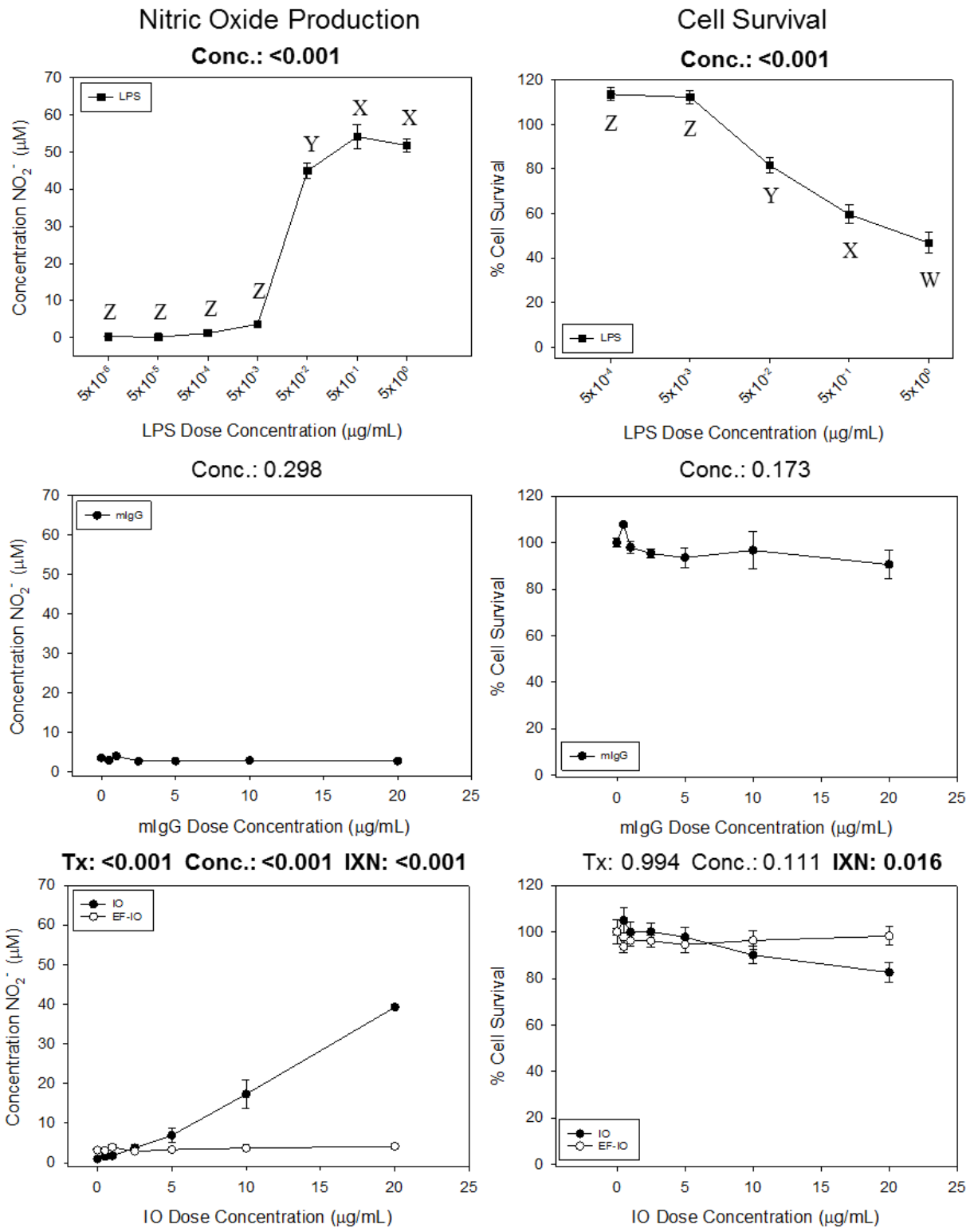
Nitric Oxide Production
Conc.: <0.001
LPS
Concentration NO_2^- (µM)
Z Z Z Z Y X X
5x10⁻⁶ 5x10⁻⁵ 5x10⁻⁴ 5x10⁻³ 5x10⁻² 5x10⁻¹ 5x10⁰
LPS Dose Concentration (µg/mL)
Cell Survival
Conc.: <0.001
% Cell Survival
Z Z Y X W
LPS
5x10⁻⁴ 5x10⁻³ 5x10⁻² 5x10⁻¹ 5x10⁰
LPS Dose Concentration (µg/mL)
Conc.: 0.298
mIgG
Concentration NO_2^- (µM)
mIgG Dose Concentration (µg/mL)
Conc.: 0.173
% Cell Survival
mIgG
mIgG Dose Concentration (µg/mL)
Tx: <0.001 Conc.: <0.001 IXN: <0.001
IO
EF-IO
Concentration NO_2^- (µM)
IO Dose Concentration (µg/mL)
Tx: 0.994 Conc.: 0.111 IXN: 0.016
% Cell Survival
IO
EF-IO
IO Dose Concentration (µg/mL)

Figure 1. Nitric oxide production and cell viability in response to lipopolysaccharide (LPS), protein antigen (mIgG) and iron oxide nanoparticle treatment. Chicken macrophages (MQ-NCSU) were treated for 24 h with lipopolysaccharide (LPS), mouse IgG (mIgG) and iron oxide nanoparticles (IO; and IO sold as endotoxin free, IO-EF). The left panel shows total nitric oxide production and the right panel shows cell viability at the conclusion of treatment. Following the 24 h incubation, cell culture medium was mixed with Griess reagent and the absorbance of the resulting solution was measured at 540 nm to determine total nitrite concentration. Known concentrations of nitrite were used to establish a standard curve describing the relationship between optical absorbance and nitrite (and indirectly nitric oxide) concentration. Lipopolysaccharide treatment served as a positive macrophage stimulation control. Cell viability was determined using the MTT assay where viable cells metabolize MTT to form insoluble formazan crystals that, upon dissolution in DMSO, produce purple color that is spectrophotometrically determined at 540 nm. The amount of purple color is directly proportional to the number of viable cells remaining following treatment. Results based on 1-way ANOVA (LPS and mIgG treatments) or 2-way ANOVA (IO and IO-EF treatments) are indicated above each graph; Tx = P value for treatment effect; Conc. = P value for concentration effect; IXN = P value for treatment by concentration interaction. For multiple means comparison and additional statistical data, see Tables 1a (NO assay) and 1b (MTT assay) for additional statistical analysis. Data shown are mean ± SEM; $n \geq 3$ per treatment group and treatment concentration.

A

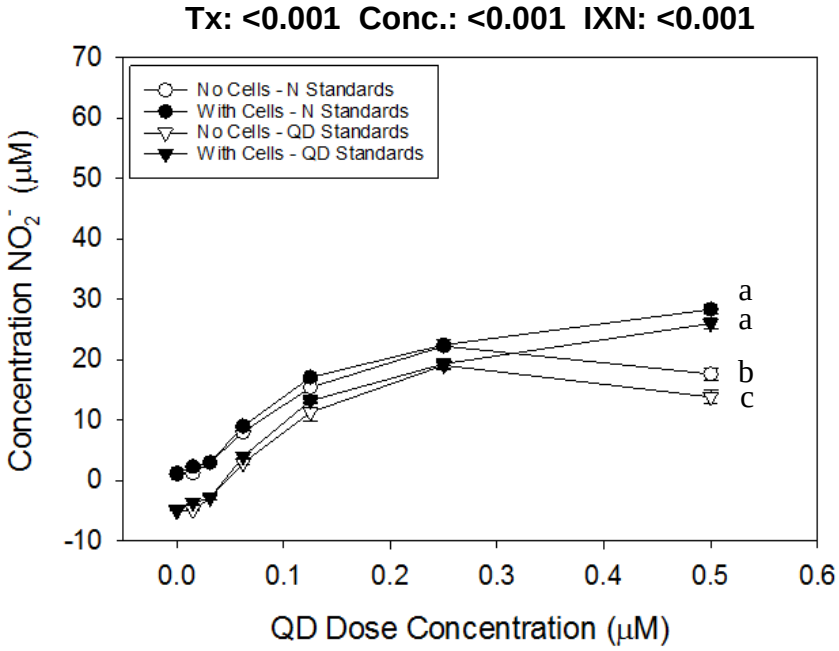
Tx: <0.001 Conc.: <0.001 IXN: <0.001
No Cells - N Standards
With Cells - N Standards
No Cells - QD Standards
With Cells - QD Standards
Concentration NO_2^- (μM)
QD Dose Concentration (μM)
a
a
b
c

B

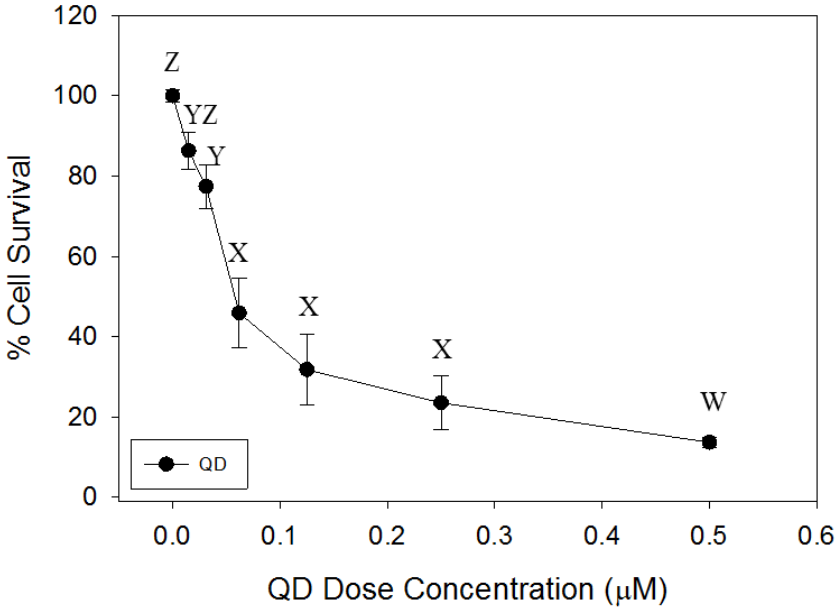
Conc.: <0.001
% Cell Survival
QD Dose Concentration (μM)
QD
Z
YZ
Y
X
X
X
W

Figure 2. Nitric oxide production and cell viability in chicken macrophages cultured in the presence of quantum dot nanoparticles (QD). A) Due to the deep red color of the QD solution and potential of QD to contribute to optical absorbance background, 24 h cultures were set up incubating 0, 0.015, 0.031, 0.062, 0.125, 0.25, and 0.5 µM QD in culture medium with and without macrophages from the MQ-NCSU chicken macrophage cell-line. Following the 24 h incubation, cell culture medium was mixed with Griess reagent and the absorbance of the resulting solution was measured at 540 nm. Known concentrations of nitrite (1.25, 2.5, 5, 10, 20, 30, 40, 50, 60, 70, 80, and 90 µM $NaNO_2$) were used to establish a standard curve describing the relationship between optical absorbance and nitrite and, indirectly, nitric oxide (NO) concentrations. To determine whether QD affected the accuracy of $NaNO_2$ standards, two sets of standards were prepared for the NO assay, one with and one without 0.125 µM QD added to each standard (QD-Std curve and Normal Std Curve, respectively). Both standard curves were used to convert optical absorbance for the various culture medium samples to NO concentrations. B) Cell viability was determined using the MTT assay, where viable cells metabolize MTT to form insoluble formazan crystals that, upon dissolution in DMSO, produce purple color that is read spectrophotometrically at 540 nm. The amount of purple color is directly proportional to the number of viable cells remaining following treatment. Results based on 2-way ANOVA (NO assay) or 1-way ANOVA (MTT assay) are indicated above each graph; Tx = P value for treatment effect; Conc. = P value for concentration effect; IXN = P value for treatment by concentration interaction. For multiple means comparison and additional statistical data, see Tables 2a (NO assay) and 2b (MTT assay) for additional statistical analysis. Data shown are mean ± SEM; $n \geq 3$ per treatment group and treatment concentration.

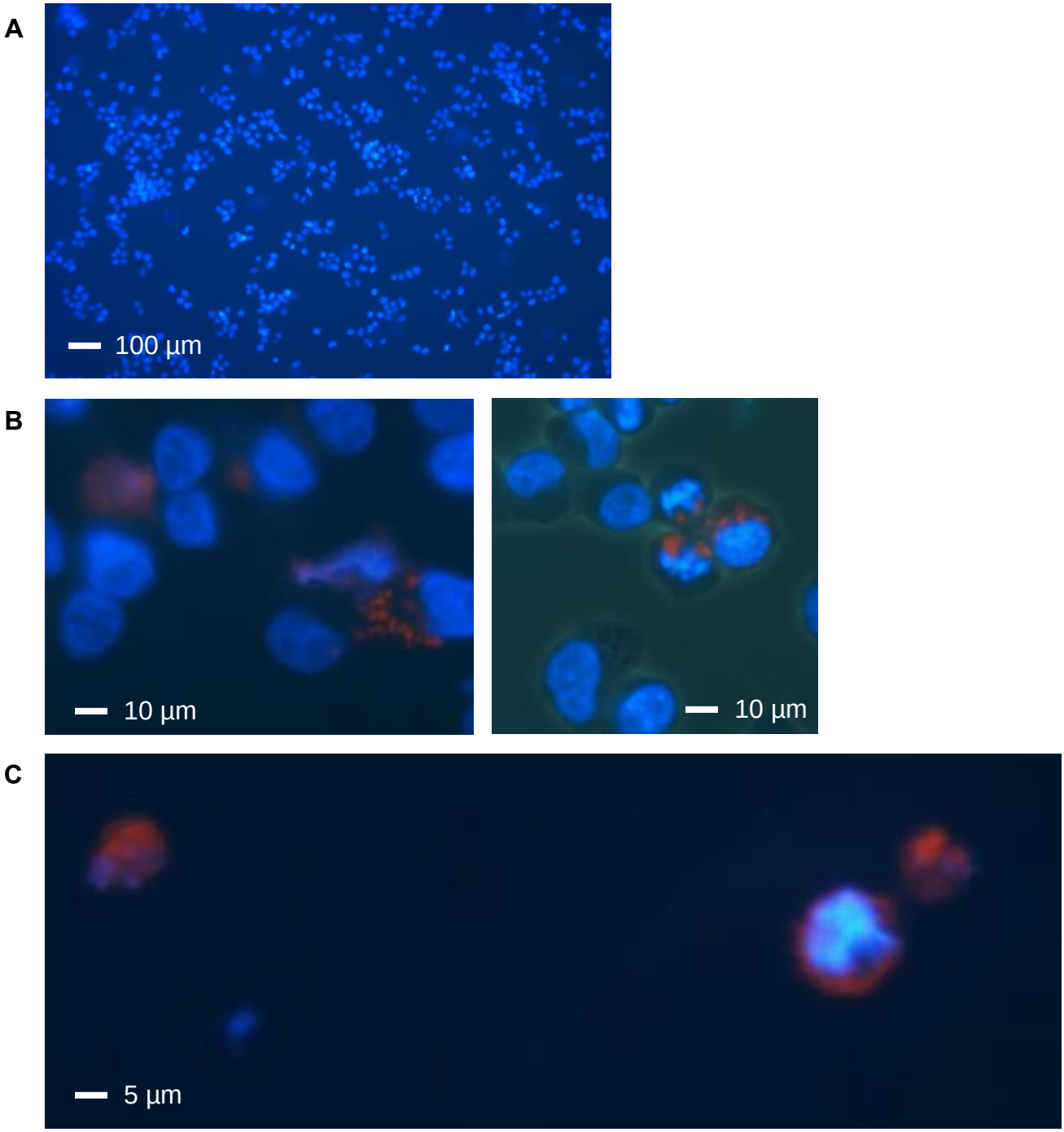

Figure 3. Fluorescence microscopy MQ-NCSU chicken macrophages were treated with 0.1 µM InP/ZnS, 670 nm emission for 5 and24 to visual timing of macrophage entry. Blue color: DAPI nuclear stain; Red color: InP/ZnS QD. A) Untreated, 5 h, 100x magnification; B) 0.1 µM InP/ZnS QD treatment, 5 h, 400x magnification C) 0.1 µM InP/ZnS QD treatment, 24 h post, 400x magnification.

Table 1a.
Statistical analysis of data shown in **Figure 1, Nitric Oxide Production.** Treatment type and treatment concentration effects on the levels of nitric oxide production in chicken macrophages following 24 h treatment with LPS, mIgG, and NP.

LPS Treatment

		Concentration (µg/mL)						
Treatment	P-Conc.	5×10^{-6}	5×10^{-5}	5×10^{-4}	5×10^{-3}	5×10^{-2}	5×10^{-1}	5×10^{0}
LPS	<0.001	Z	Z	Z	Z	Y	X	X

mIgG Treatment

		Concentration (µg/mL)						
Treatment	P-Conc.	0	0.5	1.0	2.5	5.0	10.0	20.0
mIgG	0.298							

IO Treatment

				Concentration (µg/mL)						
Treatment	P-Treat	P-Conc.	P-IXN	0	0.5	1.0	2.5	5	10.0	20.0
	<0.001	<0.001	<0.001							
IO		<0.001		Z b	Z	Z	YZ	Y a	X a	W a
EF-IO		0.539		a				b	b	b

W, X, Y, Z: For each treatment, nitric oxide levels at concentrations without a common letter are different at $P < 0.05$. Letters "Z to U" indicate ascending order of nitric oxide production.

a, b: Treatments without a common letter are different. Letters "b to a" indicate ascending order of nitric oxide production.

Table 1b.
Statistical analysis of data shown in **Figure 1, Cell Viability.** Treatment type and treatment concentration effects on the viability of chicken macrophages following 24 h treatment with LPS, mIgG, and NP.

LPS Treatment

		Concentration (µg/mL)				
Treatment	P-Conc.	5×10^{-4}	5×10^{-3}	5×10^{-2}	5×10^{-1}	5×10^{0}
LPS	<0.001	Z	Z	Y	X	W

mIgG Treatment

		Concentration (µg/mL)						
Treatment	P-Conc.	0	0.5	1.0	2.5	5.0	10.0	20.0
mIgG	0.173							

IO Treatment

				Concentration (µg/mL)						
Treatment	P-Treat	P-Conc.	P-IXN	0	0.5	1.0	2.5	5	10	20
	0.994	0.111	0.016							
IO		<0.016		YZ	Z	YZ	YZ	YZ	YX	X
EF-IO		0.823								

W, X, Y, Z: For each treatment, cell viability at concentrations without a common letter are different at $P < 0.05$. Letters "Z to W" indicate decreasing cell viability.

Table 2a.
Statistical analysis of data shown in **Figure 2, Nitric Oxide Production.** Treatment type and treatment concentration effects on the levels of nitric oxide production in chicken macrophages following 24 h treatment with QD NP.

QD Treatment

				Concentration (μM)						
Treatment	P-Cells	P-Conc.	P-IXN	0	0.015	0.031	0.062	0.125	0.25	0.5
	<0.001	<0.001	<0.001							
Normal Std Without cells		<0.001		Z a	Z b	Z a	Y b	X ab	W a	V b
Normal Std Curve With cells		<0.001		Z a	Z a	Y a	X a	W a	V a	U a
QD-Std Curve Without cells		<0.001		Z b	Z d	Z b	Y d	X c	W b	V c
QD-Std Curve With cells		<0.001		Z b	Z c	Y b	X c	W bc	V b	U a

U, V, W, X, Y, Z: For each treatment, nitric oxide levels at concentrations without a common letter are different at $P < 0.05$. Letters "Z to U" indicate ascending order of nitric oxide production.

a, b, c, d: Treatments without a common letter are different. Letters "d to a" indicate ascending order of nitric oxide production.

Table 2b.
Statistical analysis of data shown in **Figure 2, Cell Viability.** Treatment type and treatment concentration effects on the viability of chicken macrophages following 24 h treatment with QD NP.

QD Treatment

		Concentration (μM)						
Treatment	P-Conc.	0	0.015	0.031	0.062	0.125	0.25	0.5
QD	<0.001	Z	YZ	Y	X	X	X	W

W, X, Y, Z: For each treatment, cell viability at concentrations without a common letter are different at $P < 0.05$. Letters "Z to W" indicate decreasing cell viability.

CHAPTER II

Measurement of innate immune response to InP/ZnS quantum dots in complex dermal tissue

Introduction

Evolving as the precursor to specific immunity, the innate immune system is the first line of defense against pathogens or other foreign invaders and is active in repair of damaged tissue (Abbas et al., 2012). Innate immune defenses are comprised of physical and biochemical barriers; leukocytes including macrophages, dendritic cells, natural killer cells, specificity-limited T and B cells, and mast cells; and soluble proteins. As a first line of defense, the innate immune response is rapid. Toll-like receptors on the surface of immune cells recognize general pathogen markers known as pathogen associated molecular patterns (PAMPs) (Albiger et al., 2007). Upon recognition, pathogens may be eliminated directly as in the case of phagocytosis by neutrophils (heterophils in birds) and macrophages or by activities of the complement system (Abbas et al., 2012). Additionally, the innate immune response may stimulate the adaptive immune system by presentation of antigens to the T lymphocytes of adaptive immunity. Once pathogen recognition is initiated, the process of inflammation follows, including cytokine production and leukocyte recruitment (Abbas et al., 2012). As innate immunity plays a role in recognition of foreign materials, nanoparticles (NP) are a likely target of the innate immune system.

From the introduction of NP for use in targeted therapy in the mid-20th century, the 21st century has seen vast expansion in the use of nanoparticles in medicine. Nanoparticles may be engineered with surface chemistries that enable binding of molecules that allow NP to be directed to specific tissues enabling their use in diagnostic applications such as biomedical imaging or for delivering payloads to cells (Aguilar, 2012; Alivisatos, 1996; Alivisatos, 1996; Bruchez et al., 1998). Despite many new and innovative applications for NP in drug delivery vehicles, bioimaging, and as vaccine carriers (Bilan et al., 2016; Chan et al., 2002; Chan and Nie,

1998; Larson et al., 2003; Pusic et al, 2011; Rosenthal et al., 2011; Yang et al., 2009), numerous in vitro studies have shown that NP may be toxic to living systems due to the release and deposition of heavy metal ions in tissue and their ability to stimulate innate immunity (Li et al., 2003; Nel et al., 2006; Zhang et al., 2015). In vitro studies in several cell types, including human and murine liver cells, also have shown that NP stimulate the production of reactive oxygen species leading to mitochondrial toxicity (Nguyen et al., 2015; Zhang et al., 2015). Quantum dot (QD) nanoparticles, particularly cadmium-core QD, were shown to be toxic to cells in vitro, other formulations of QD, such as indium-core QD, were found to be less toxic than cadmium-core QD in human lung carcinoma and human neuroblastoma cells due to differences in QD chemical structure (Brunetti et al., 2013). Methods to overcome toxicity have focused on altering chemical composition by coating QD cores in shells of elements such as zinc, allowing for further surface modifications that enable water solubility which is critical for biological applications (Lovric et al., 2005).

To more adequately demonstrate the effects of NP on living systems, in vivo studies addressing complex interactions of NP with cells and soluble factors of innate immunity are needed (Brunetti et al., 2013; Dobrovolskaia and McNeil, 2007; Fischer and Chan, 2007). In vivo models provide distinct advantages over in vitro models in that bioactivities of NP can be examined within the complex environment of the whole organism, where cells and soluble factors interact with the NP and each other. Complex physiological responses such as inflammation simply cannot be replicated in single cell in vitro systems. Therefore, even when NP are characterized in cell culture as non-toxic or to lack immunostimulatory effects, introduction of NP into living animals may nevertheless initiate non-anticipated physiological

activities (e.g. complement activation, inflammation) that may be harmful to the animal or may be useful in biomedical manipulations.

Animal models have been systematically developed to explore medical science including pathogenic processes, diagnosis, therapy, nutrition, metabolism, and novel drug development as applied to humans and other animals (Rand, 2008). As the need for in vivo NP studies increases, so increases the need for viable animal models to determine potential NP bioactivities. When considering animal models, ease of housing, small size, and favorable temperament are requirements that improve feasibility of animal studies (Rand, 2008). The chicken meets these criteria and as such has been the route to discovery of many important concepts now accepted in modern immunology including the delineation of bursa (B) and thymus (T)-derived lymphocytes (Davison et al., 2014).

Recently, the growing feather of the chicken has been described as a unique cutaneous test tissue to study the cellular/tissue responses to various test-compounds in a complex tissue (Erf and Ramachandran, 2016; Erf, U.S. Patent No.: 8,216,551). In chickens, the living portion of a growing feather consists of a column of pulp tissue that is surrounded by the feather sheath. The pulp consists mostly of dermis bordered by epidermis. The use of the growing feather (GF) as a skin test-site has many advantages over other skin derivatives: injection and collection of injected GF is minimally invasive and does not require surgery or termination of the animal; intradermal injection is easily achieved; the pulp of each injected GF constitutes a uniform biopsy sample, sufficient for various ex vivo analyses; and, simultaneous injection of multiple GF and collection at various times post-injection, provides opportunity to examine cellular/tissue activities initiated by NP in a complex tissue. Hence, this model offers an improved method for the in vivo study of NP.

In this study, we investigated the in vivo innate immune system response to quantum dots (QD) and mouse IgG protein antigen-conjugated QD (QD-mIgG) in the chicken growing feather model. Initial experiments were conducted to determine the effects of QD dose and QD treatment time on leukocyte infiltration into QD injected dermal GF tissue. Additional experiments compared leukocyte concentrations in peripheral blood and leukocyte infiltration into chicken GF following GF-injection of QD, QD-mIgG, mIgG alone, and mIgG mixed with aluminum hydrogel adjuvant (Alum+mIgG). The goals of this study were to 1) determine the viability of the chicken growing feather as an in vivo model to study the immunostimulatory effects of quantum dots and 2) determine differences in innate immune activity between quantum dots conjugated with protein antigen versus protein antigen mixed with a traditional aluminum hydrogel (alum) adjuvant. This work was supported by NIH-NIBIB R15 EB015187; G. F. Erf, PI.

MATERIALS AND METHODS

Experimental Animals Non-vaccinated male or female Brown Line (BL) or Light Brown Leghorn (LBL) layer-type chicks (all MHC $B^{101/101}$) were reared in floor pens on wood shaving litter in rooms fitted with HEPA filtration at the University of Arkansas Poultry Health Laboratory (Arkansas Experiment Station, University of Arkansas, Fayetteville, AR). Standard light and temperature protocols were followed (Shi and Erf, 2012) with food and water available ad libitum. Animal use was approved by the University of Arkansas Institutional Animal Care and Use Committee (approval #15020).

Quantum Dot Time Course Study Four female BL chickens 13 weeks of age were selected for feather injection with QD test material. The purpose of this initial experiment was to observe the general leukocyte infiltration response to the test materials. Growing feathers of

uniform size (8 mm-10 mm column of pulp with about 5 mm of emerging barbs) were used for dermal injections.

Quantum Dot Dose Response Study Twelve male LBL chickens (3 QD doses, n = 4 chickens per dose) 18 weeks of age were selected for growing feather (GF) injection with QD test material in order to determine the optimum concentration of QD needed to stimulate immune activity without significantly reducing tissue viability. Growing feathers were plucked 18 d prior to GF injections, to have uniform re-generating GF for the cutaneous tests.

Mouse IgG-conjugated Quantum Dot Study Sixteen female LBL chickens (PBS (vehicle), n = 2; mouse IgG antigen, 0.26 mg/mL (mIgG), n = 2; 0.26 mg/mL mIgG mixed with 2% Alum adjuvant (Alum+mIgG), n = 2; 0.5 µM 7 nm InP/ZnS QD (QD), n = 4; or 0.5 µM QD conjugated to 0.26 mg/mL mIgG (QD-mIgG), n = 6) 13 weeks of age were randomly selected for GF injection. Growing feathers were plucked 18 d prior to GF injections, to have uniform re-generating GF for the cutaneous tests.

Test Materials Sterile endotoxin-free Dulbecco's PBS (EF-DPBS, Sigma-Aldrich, St. Louis, MO) was used as the vehicle-only control. Mouse IgG (mIgG, Rockland Immunochemicals Inc., Limerick, PA) was used as the test antigen either alone, conjugated to 7 nm indium phosphide zinc sulfide quantum dots (QD-mIgG) (InP/ZnS QD, Mesolight, Inc., Little Rock, AR) or mixed 1:1 with 2% Hydrogel alum adjuvant (Alum+mIgG) (Invivogen, San Diego, CA). Lyophilized mIgG was reconstituted with sterile water according to the manufacturer's instructions, aliquoted, and stored at -20°C until thawing and diluting just prior to use.

Quantum Dot Time Course Study Two types (InP/ZnS and ZnCuInS) and three sizes (emission peaks of increasing wavelength relative to increasing size; 590, 620, and 670 nm) of

cadmium-free QD were analyzed for their stability once conjugated with mIgG protein antigen. Due to greater stability in solution, InP/ZnS QD with an emission peak at approximately 670 nm were chosen for these studies (courtesy Dr. Zoraida Aguilar). 50 µL InP/ZnS QD were provided by Mesolight (Little Rock, AR) at a concentration of 2 µM and diluted 1:2 in endotoxin-free water prior to injection.

Quantum Dot Dose Response Study QD with a stock concentration of 10 µM (10 nmol in 1 mL) were used. QD were vortexed vigorously then diluted with sterile EF-DPBS.

Mouse IgG-conjugated Quantum Dot Study QD were purchased from Mesolight, functionalized with polyethylene glycol (PEG) and carboxylic acid (COOH) groups with an emission wavelength of 670 nm, photoluminescence (PL) at 664 nm and a quantum yield of approx. 20-30%. Conjugation of mIgG with QD (QD-mIgG) was completed by Dr. Zoraida Aguilar (Zystein, Inc., Springdale, AR) using 4 molecules mIgG per QD for a final working concentration of 0.26 mg/mL mIgG. QD were vortexed vigorously then diluted with sterile EF-DPBS.

Growing Feather Injection Growing feathers, 10 to 13 along both the left and right breasts tracts of each chicken, were plucked 18 d prior to GF injections, to have uniform re-generating GF for the cutaneous tests. On the day of injection, 3 regenerated GF were plucked and processed as untreated controls while the remaining GF were prepared for injection by cutting the emerging barbs and the portion of the sheath above the epidermal cap with scissors as described in Erf and Ramachandran (2016). Feather injections were performed by injecting 10 GF per breast tract with 10 µL of test materials using 0.3 mL syringes with 0.01 mL gradations fitted with a 31 gauge x 8 mm needle (BD, Franklin Lakes, NJ).

Feather Collection and Preparation of Pulp Cell Suspensions Growing feathers were collected at defined time points, placed in a 1.5 mL microcentrifuge tube containing 1 mL ice-cold PBS (Sigma, St. Louis, MO) and maintained on ice until pulp suspension preparation as described in Erf and Ramachandran (2016).

Quantum Dot Time Course Study GF were harvested at 0, 4, 24, and 48 h time points.

Quantum Dot Dose Response Study GF were collected before (0) and 0.25, 1, 2, 3, 5 and 7 d post-GF injection.

Mouse IgG-conjugated Quantum Dot Study GF were harvested before (0) and 0.25, 1, 2, 3, 4, 5 and 7 d post-GF injection.

In each study, GF were prepared for cell population analysis by carefully removing the pulp (epidermal and dermal tissue) with forceps after splitting the outer sheath with a razor blade. The pulp was then placed directly into a 1.5 mL microcentrifuge tube containing 1 mL of the enzymatic digestion solution, 0.1% collagenase (collagenase type IV, Life Technologies, Carlsbad, CA) in HBSS, supplemented with calcium and magnesium (GIBCO, Thermo Fisher Scientific, Waltham, MA). Following incubation in a 40°C water bath for 15 minutes, single cell suspensions were prepared by passing the partially digested pulp tissue through 60 μm nylon mesh with a plastic syringe plunger while repeatedly adding ice-cold PBS to flush the cells through the mesh. Cell suspensions (approximately 12 mL) were centrifuged at 250 x *g* for 9 min at 4°C then washed with 5 mL DPBS+ (DPBS, 1% bovine serum albumin and 0.1% sodium azide; VWR, Radnor, PA) followed by repeat centrifugation of the resuspended cell pellet. Following the final wash, the cell pellets were resuspended thoroughly by vortexing in approximately 400 μL DPBS+, then 50 μL of the cell suspension was added to a round bottom

96 well plate for immunofluorescent (IF) labeling. Fluorescent-labeled anti-chicken leukocyte mouse-monoclonal antibodies were diluted in DPBS+ 1:100 and added to cell suspensions.

Immunofluorescent Staining and Flow Cytometry Fluorescently-labeled (fluorescein isothiocyanate (FITC) and phycoerythrin (PE)) mouse monoclonal antibodies (Southern Biotechnology Associates, Inc., Birmingham, AL) were used to distinguish individual cell populations. Specifically, individual leukocyte subpopulations were identified using a panel of mouse-monoclonal antibodies specific to chicken leukocyte markers, including total leukocytes (CD45-FITC+), all MHC Class II expressing cells (MHCII-FITC+), macrophages (KUL01-FITC+), B cells (Bu-1-FITC+), αβ1 T cells (T cell receptor (TCR) 2-FITC+), αβ2 T cells (TCR3-PE+), γδ T cells (TCR1-PE+), CD4+ lymphocytes (CD4-FITC+), and CD8+ lymphocytes (CD8-PE+). The isotype of all monoclonal antibodies used was IgG1. To confirm fluorescently labeled antibodies are not binding non-specifically, a pool of all cell suspensions was prepared, incubated with a mixture of FITC- and PE-labeled mouse IgG1 isotype control antibodies. The isotype control stained cell suspensions were also used to distinguish between fluorescence-positive and fluorescence-negative populations (Byrne, 2016). Additionally, single fluorescence-stained cells were used to set compensation and correct the fluorescence detection for overlapping fluorescence emission of the fluorophores used. Fluorescence-based cell population analysis was carried out using a BD FACSort flow cytometer equipped with a 488 nm argon laser (BD Immunocytometry Systems, San Jose, CA) as described in Erf and Ramachandran (2016). For each experiment fluorescently-labeled mouse monoclonal antibody specific to chicken CD45 (CD45-FITC+) was used to select all leukocytes before determination of individual cell subpopulations. The percentage of heterophils was determined based on size (FSC) and granularity (SSC) characteristics of leukocytes (CD45+) as described in Seliger et al.

(2012). Data analysis of cell populations was completed using CellQuest (BD, Franklin Lakes, NJ) and/or FlowJo (Ashland, OR) flow cytometry analysis software.

Cell-Dyn Automated Hematological Analysis Leukocyte population analysis was completed at 0, 0.25 and 7 d following GF injection to measure the concentration of heterophils, lymphocytes and monocytes in the peripheral blood circulation. Approximately 1.5 mL whole blood was collected via the wing vein of which 0.5 mL was used for cell population analysis via Cell-Dyn (Abbott Diagnostics, Abbott Park, IL) automated hematology analyzer.

Statistical Analysis The experimental unit was the individual chicken. Sigma Plot 13 Statistical Software (Systat Software, Inc., San Jose, CA) was used to determine significant effects of time, treatment, and treatment by time interactions using two-way repeated measure analysis of variance (RM ANOVA). Following RM ANOVA, the Holm-Sidak method of multiple means comparison was used to determine the main effect(s) of time and treatment when no significant interactions were found. When time and treatment interactions were found, Fisher's LSD was used for multiple means comparisons. For all analyses, differences were considered significant at $P \leq 0.05$.

RESULTS

Leukocyte infiltration measured at 0, 4, 24, and 48 h following GF injection with QD

Following intradermal (i.d.) injection of 1 μM QD into GF, leukocyte (CD45+) levels in the GF dermis (% pulp cells) more than doubled within 4 h to 45.2 ± 2.2% ($P<0.05$), reached a peak level of 61.0 ± 4.6% ($P < 0.05$) at 24 h then decreased to near base-line levels by 48 h (30.0 ± 8.0%) at 48 h (Figure 1). A similar time-course profile was also observed for MHC class II-expressing cells; although levels of MHC class II+ cells were approximately one-half of those for total leukocytes at each time-point (Figure 1). Examination of individual leukocyte populations

present in the pulp cell suspensions showed elevated ($P < 0.05$) heterophil levels at 4 and 24 h (9.7% ± 0.3 and 9.0% ± 0.9, respectively compared to 2.9 ± 0.4% at 0 h), whereas macrophage levels did not increase significantly post-QD injection (Figure 1). Lymphocytes, including B cells and receptor-defined T cells, were also found to infiltrate the pulp post-QD injection. Specifically, B cell levels were elevated ($P < 0.05$) by 24 h and remained elevated at 48 h (1.6 ± 0.3%, 16.3 ± 2.8% and 11.4 ± 5.4% at 0, 24, and 48 h, respectively) (Figure 2). Among the T cell receptor (TCR) defined T cell subsets, levels of T cells with γδ TCR did not change significantly over the 48 h post-QD-injection (Figure 1). Most of the infiltrating T cells were those with αβ TCR ($P < 0.05$), whereby αβ1 TCR+ T cells infiltrated at higher levels than αβ2 TCR+ T cells (e.g., at 24 h levels were 10.9 ± 1.8% and 3.4 ± 0.5%, respectively) (Figure 2). While CD4+ T cell levels did increase post-injection, statistical analysis did not indicate a significant difference in this cell population over the duration of the 48 h time course (Figure 3). Elevated ($P < 0.05$) levels of CD8+ T cells were found over the time course, increasing from 1.5 ± 0.05% at 0 h to 8.0 ± 2.7% at 24 h then returning to baseline level by 48 h (2.0 ± 0.8%) (Figure 3).

Leukocyte infiltration into the dermis of growing feathers in response to injection with low, medium and high doses of quantum dots (QD)

As indicated by a significant dose by time interaction, the infiltration profiles of total leukocyte (CD45+) differed depending on dose of QD injected into GF. Subsequent analysis of the effect of dose at each time-point, revealed the greatest difference between doses at 5 d ($P = 0.003$) with the low QD dose stimulating leukocyte infiltration at a level approximately 2-fold greater than the medium and high QD doses. Significant effect of QD dose was also observed at 1 d ($P = 0.041$), though the medium and high doses stimulated higher infiltration than the low

dose at this early time point. Comparing the effect of time for each individual QD dose, leukocyte levels peaked ($P < 0.001$) with a 4-fold increase at 2 d (46.5 ± 7.8%) at the low dose and remained at an elevated level through the remainder of the time course. The medium and high QD doses also stimulated a 4-fold increase in total leukocytes ($P < 0.001$), though the peak level was reached 1 day earlier in the time course compared to the low dose. Following the peak levels at 1 d, leukocyte levels in the medium and high QD dose injected GF remained elevated at 2 and 3 d before dropping to lower levels on 5 and 7 d. At the conclusion of the time course, leukocyte levels returned to baseline in response to the high QD dose (9.9 ± 0.7%), while levels remained elevated (24.1 ± 7.5%) in response to the medium QD dose (Figure 4, Table 1). It should be noted that at later time points (5 d and 7 d), the high dose resulted in GF with greatly retarded growth and damaged/dry appearance.

For MHC class II+ cells, no differences were found between QD doses while overall cell levels rose (time main effect $P < 0.001$) from 3% (± 1.7%) at pre-injection to peak near 32% (± 1.8%) at 2 d. Levels of MHCII+ cells declined gradually following the peak at 2 d though remained elevated at the conclusion of treatment (19.0 ± 2.1%) (Figure 4, Table 1). Independent of dose, heterophil levels were elevated (time main effect $P < 0.05$) from 0.25-2 d post QD injection and increased nearly 3-fold at 1 d for medium and high doses. Heterophil levels then dropped to near pre-injection level by 3 and 5 d before returning to baseline levels by 7 d. Overall, heterophil infiltration was highest with the high dose of QD (dose main effect $P = 0.046$), followed by the medium and low dose (Figure 4, Table 1). Macrophage levels were relatively unchanged during the early phase post-injection but increased gradually and were significantly elevated (time main effect $P = 0.018$) at 5 d (12.6 ± 2.0%) compared to pre-injection levels (2.0 ± 1.9). Overall, macrophage levels post-QD injection were higher with

injection of the high QD dose (dose main effect P = 0.034) than with the medium and low dose (Figure 4, Table 1).

Statistical analysis of the effect of dose and time on the infiltration of various lymphocyte subpopulation revealed no treatment by time interactions and, with the exception of αβ2 TCR+ T cells (dose main effect P = 0.042), no QD dose effect on lymphocyte infiltration. Independent of QD dose, all lymphocyte sub-populations examined infiltrated the GF pulp following QD injection (Figure 5, Table 2). Elevated levels of B lymphocytes were found at 2 d and 3 d (4.3 ± 1.1% and 8.2 ± 1.0%, respectively) (time main effect P < 0.001), declined at 5 d (3.9 ± 1.0%), then rose sharply at 7 d (16% ± 1.1%) compared to pre-injection levels (0.2 ± 0.9%) (Figure 5, Table 2). Levels of T cells with a γδ T cell receptor (TCR) increased to an initial peak at 1 d (7.8 ± 1.5%) (time main effect P < 0.001) compared to pre-injection level (1.8 ± 1.3%), declined slightly, then increased again reaching a level over 8-fold higher than baseline at 7 d (16.2 ± 1.6%) (Figure 5, Table 2). Quantities of infiltrating T cells with αβ TCR were similar to γδ T cells, though these cells accumulated at a relatively slower rate. Levels of αβ1 TCR+ cells rose steadily (time main effect P < 0.001) peaking at 5 d (12.6 ± 1.1%) then declining to baseline level (0.1 ± 1.0%) at 7 d (Figure 5, Table 2). Following injection with the high QD dose, levels of cells with a αβ2 TCR were significantly elevated (treatment main effect P = 0.042) compared to the low dose. Overall, levels of αβ2 T cells were over 6-fold higher (time main effect P <0.001) than baseline (1.6 ± 1.7%) at 2 d (10.4 ± 1.9%), peaked at 5 d (13.1 ± 1.9%), and while levels declined at 7 d (8.8 ± 2.2%), remained elevated above baseline (Figure 5, Table 2). Levels of CD4+ T cells increased steadily post-injection (time main effect P < 0.001) reaching a plateau at 3 d (14.2 ± 1.0%) and remained elevated through the duration of treatment (Figure 6, Table 3), whereas those of CD8+ T cells increased (time main effect P < 0.001) from a pre-injection level

of 0.8% (± 0.8%) to peak at 1 d (7.5 ± 0.9%) and then declined gradually through the duration of the treatment to remain slightly elevated compared to baseline at 7 d (3.1 ± 0.8%) (Figure 6, Table 3).

Leukocyte infiltration into the dermis of growing feathers in response to injection of quantum dots (QD) with and without antigen-conjugation

Levels (% pulp cells) of immune cell populations infiltrating in response to GF injection of different treatments (PBS, mIgG, Alum+mIgG, QD, QD-mIgG) were measured in the GF dermis (% pulp cells) over a 7 day time course.

Two-way repeated measures ANOVA revealed interactions between time and treatments only for the total (CD45+) leukocyte population. Comparison of leukocyte levels observed with each treatment at individual time-points showed that total leukocytes (CD45+) levels were highest in response to Alum+mIgG, specifically at 2 d, leukocyte levels were approximately 2.5-fold higher (27.2 ± 6.9%) and at 5 d approximately 3.5-fold higher (35.5 ± 2.9%) than the other treatments. Overall time course differences were observed for QD (<0.001), mIgG (P = 0.010), and Alum+mIgG (P = 0.031) (Figure 7, Table 4). For MHC class II+ expressing cells, a treatment main effect (P < 0.001) and a time main effect (P < 0.001) were observed. Overall, levels of MHC class II+ cells were lower in PBS (vehicle) injected GF than those observed with QD, QD-mIgG, Alum+mIgG treatments, but were not different from levels observed when GF were injected with mIgG antigen alone. Alum+mIgG stimulated expression of MHC class II+ molecules on cells in the pulp (13.1 ± 0.9%) to a greater degree than any of the other treatments; QD and QD-mIgG injections were associated with similar levels of MHC class II+ cells (8.3 ± 0.6% and 7.9 ± 0.5%, respectively), but levels for both treatments were lower than those observed with Alum+mIgG, but higher than vehicle or mIgG (3.8 ± 0.9% and 4.6 ± 0.9%,

respectively). Over the time course, levels of MHC class II+ cells increased steadily from 3.2% (± 1.0%) prior to injection level, reached their highest level at 5 d (11.0 ± 1.0%) then dropped slightly to 9.3% (± 1.0%) at the conclusion of the time course (Figure 7, Table 4). For heterophils, no treatment main effect was observed, however there was a time main effect ($P < 0.001$). Heterophils rose over 2-fold to 4.4% (± 0.2%) at 6 h compared to pre-treatment (1.8 ± 0.2%) then decreased to near or below baseline levels through the remainder of the time course (Figure 7, Table 4). Similar to MHC class II+ cells, Alum+mIgG had the greatest effect on macrophage levels (treatment main effect $P = 0.003$) while the other treatments had little effect on macrophage infiltration. Macrophage levels were steady through 5 d (time main effect $P = 0.023$) then rose slightly from 2.7% (± 0.3%) to 3.6% (± 0.3%) at 7 d (Figure 7, Table 4).

All lymphocyte sub-populations examined infiltrated the GF pulp following GF injection of various treatments, with significant main effects of treatment and time (but not time by treatment interactions) found for each of the subpopulations measured. Beginning with B cells, Alum+mIgG, QD, and QD-mIgG each stimulated B cell infiltration nearly 2-fold higher than both mIgG and vehicle alone (treatment main effect $P = 0.004$). Over the time course, B cells increased steadily (time main effect $P < 0.001$) peaking at 4 d (6.4 ± 0.6%) compared to pre-treatment (2.1 ± 0.6%) (Figure 8, Table 5). As with B cell infiltration, Alum+mIgG stimulated infiltration of γδ, αβ1, and αβ2 T cells approximately 2-fold higher than each of the other treatments (treatment main effect $P < 0.05$ for each population). The effect of Alum+mIgG was more pronounced early in the time course for γδ T cells with this population reaching their peak level at 1 d (7.4 ± 0.8%), while Alum+mIgG stimulated peak infiltration of αβ1 and αβ2 T cells later in the time course (6.8 ± 0.9% at 5 d and 9.5 ± 1.0% at 4 d, respectively). As for the overall time effects (time main effect $P < 0.05$ for each population), total γδ T cells reached peak levels

at 1 d (3.4 ± 0.3% versus pre-treatment 1.5 ± 0.3%) while total αβ1 T cells peaked at 4 d (4.1 ± 0.3% versus pre-treatment 1.7 ± 0.3%) and total αβ2 T cells peaked at 5 d (7.0 ± 0.4% versus pre-treatment 3.6 ± 0.3%) (Figure 8, Table 5). Levels of CD4+ T cells increased approximately 2-fold in response to mIgG, QD, and QD-mIgG compared to a 4-fold increase in response to Alum+mIgG (treatment main effect $P < 0.001$). Overall, levels of CD4+ T cells were highest ($P < 0.05$) in GF injected with Alum+mIgG, followed by similar levels in QD, QD-mIgG, and mIgG injected GF, and lowest in PBS-injected GF. Over the time course, levels of CD4+ T cells increased steadily (time main effect $P < 0.001$) from 1.7% (± 0.3%) prior to injection to a peak of 4.6% (± 0.3%) at 4 d and then declined slightly to 3.1% (± 0.3%) at the conclusion of the time course (Figure 9, Table 6). Infiltration of CD8+ lymphocytes also was stimulated to a higher degree (treatment main effect $P = 0.024$) by Alum+mIgG (3.1 ± 0.3%), though just slightly higher than the mIgG (2.2 ± 0.3%), QD (2.9 ± 0.2%), QD-mIgG (2.4 ± 0.1%), versus vehicle (1.6 ± 0.3%). Over the time course, CD8+ T cells increased 2-fold at 4 and 5 d (3.1 ± 0.2%) compared to pre-treatment (1.6 ± 0.2%) (Figure 9, Table 6).

Measurement of peripheral blood leukocyte concentrations after GF injection with PBS (vehicle), mIgG, Alum+mIgG, QD, and QD-mIgG

Using Cell-Dyn automated hematological analysis, heterophil, lymphocyte and monocyte and populations were measured in peripheral whole blood before and at 0.25 and 7 d following GF injection. Based on two-way repeated measures ANOVA no treatment by time interactions were observed for any of the white blood cell populations measured. No main treatment or main time effects were observed for peripheral lymphocyte or monocyte populations. A main time effect was observed for peripheral heterophils ($P < 0.001$), with elevated levels of heterophils at

the 0.25 d time-point (3.2 ± 0.3 K/µL, 8.0 ± 0.3 K/µL, 3.9 ± 0.3 K/ µL at 0, 0.25 and 7 d, respectively). No main treatment effect was observed for heterophils (Figure 10).

DISCUSSION

Due to their unique physical, chemical and optical properties, quantum dot nanoparticles have found many uses in biological applications including bioimaging, drug delivery and vaccine design. While the uses of QD are wide-ranging and benefits apparent, there are risks for toxicity due to their heavy metal make-up. Not only is QD exposure a concern in industrial applications where QD are synthesized or used in manufacturing, the rise in in vivo applications also begs attention to the potential immune effects of the particles (Zhang et al., 2008). There remains a lack of evidence effectively demonstrating this risk (Nel et al., 2006; Hauck et al., 2010; Dobrovolskaia and McNeil, 2007) and thus, more studies are needed to explore the effects of nanoparticles in in vivo models. In this study we utilized the chicken growing feather model to measure the innate cellular/tissue response to quantum dot nanoparticles both as a standalone treatment as well as conjugated to a T-dependent protein antigen, mouse IgG protein. Due to the ability to monitor changes in immune cell infiltration in the same individual animal over time, further evidence is provided that the chicken growing feather injection model is a valuable cutaneous test-site and tool for the study of the innate immune system responses. While antigen-conjugated QD stimulated the innate immune response to a lesser degree compared to alum adjuvant, this study is a first to demonstrate and monitor immunostimulatory activity of QD in a complex tissue in the same individuals without the requirement for euthanasia or invasive procedure to sample the injected tissue.

The chicken has been a source of many important immunological findings and possesses many ideal qualities as a research model (Rand, 2008). The growing feather model allows

temporal, qualitative and quantitative assessment of immune activity initiated by the injection of NP or other test materials into the dermis of the pulp in an individual chicken (Erf and Ramachandran, 2016) while taking advantage of their ease of use as laboratory animal model. Not only is the skin a source of tissue to measure immune activity, the skin is a primary route for NP entry, therefore using the GF cutaneous test-site as a model for NP study is ideal. Other skin models are prevalent in the literature for the study of NP toxicity. Zhang et al. studied penetration of PEGylated QD through perfused porcine skin flaps (Zhang et al., 2008). The downside to these studies is that the animals must be euthanized in order to obtain the tissue and measuring temporal effects of treatment in the same individual are not possible. The GF model does allow repeated measuring and offers an important opportunity to further expand knowledge of the immune effects of NP.

Our initial studies were designed to test the effects of QD on immune cell infiltration over a 48 h time course. Results of this initial time course study indicated the levels of several immune cell populations increased over time in injected GF, infiltrating the dermal tissue in response to QD injections in the GF dermis. Most leukocyte populations reached a maximal level at 24 h then returned to baseline level by 48 h. Heterophils increased more rapidly, reaching a peak level at 4 h. Lymphocyte subpopulations were elevated with B cell infiltration stimulated to a higher degree compared to individual T cell populations; i.e. αβ1 T cells were recruited to a higher degree than both γδ and αβ 2 T cells, and levels of CD4+ and CD8+ T cells were similar to αβ1 T cells. These results indicate that the QD injections are indeed stimulating immune cell activity in the skin.

Once the GF injection method with QD was established, the effects of QD treatment dose were examined. In addition, the dose effects on leukocyte infiltration over a longer time course

were measured. Increasing the QD concentration did stimulate infiltration of immune cells to a higher degree for some of the cell types studied. By testing multiple QD treatment doses, the opportunity for dose by time interactions was introduced. Treatment by time interactions were only seen for total leukocytes. The high and mid doses stimulated total leukocyte infiltration at a faster rate than the low dose. Leukocytes remained at a higher level in response to the low dose through the course of treatment rather than decreasing at a gradual rate back to near baseline level as was observed for the mid and high dose. The crossing over of effects of the treatment doses was seen over the time course reflecting statistical interaction. This presents an interesting finding for further study to determine the effect of the low dose on leukocyte infiltration. Moreover, the tissue damaging effects observed with the higher doses of QD, especially at later time points, further influenced the decision to use a lower dose (0.5 μM) for future studies on adjuvant/immunostimulatory activities of QD (Chapters II and III).

For each cell population analyzed, main time effects were observed over the course of the 7 d treatment. Cell populations started from a baseline level near 0% and many were seen to rise steadily through 3 days. After this initial rise, several populations such as total leukocytes, MHCII+, and heterophils declined. The majority of the other cell types, excluding CD8+ T cells, either declined then rose again or simply kept increasing through the 7 d time course. Additional main treatment dose effects were seen for heterophils, macrophages, and αβ2 T cells and, in each case, the high dose stimulated the increase of these cell populations to a greater degree than the low and medium doses. These results indicate that not only are the QD treatments stimulating influx of innate immune cells, but also that the QD may be beginning to effect adaptive immunity as well by stimulating lymphocyte infiltration.

To investigate the potential adjuvant properties of InP/ZnS QD, GF injections with QD and alum hydrogel along with protein antigen (mIgG) were carried out over a 7 d time course. QD were conjugated with mIgG while alum hydrogel was mixed with mIgG prior to injection. Overall, mIgG alone was observed to stimulate influx of immune cells to a higher degree than PBS alone, however the adjuvants (QD, QD-mIgG, and Alum+mIgG) had a positive effect on immune cell infiltration. Alum mixed with mIgG antigen had a greater effect on the infiltration of innate immune cell populations including total leukocytes, MHCII+ cells, and macrophages than QD conjugated with mIgG This trend continued across the lymphocyte subpopulations, however B cells were more responsive to the QD-NP, both unconjugated and conjugated, than the individual T cell subsets. In addition, peripheral blood concentrations showed a rise in heterophils only, with no effect on lymphocytes or monocytes within hours of intradermal injections, corroborating with flow cytometry levels, although the spikes in heterophil levels were observed with vehicle and other treatments suggesting that the increase in heterophils within 6 h of i.d. injection may be due to inflammation initiated by injection-associated tissue damage. Regarding the overall effect on the innate immune system, QD stimulated the influx of various leukocyte populations to the site of injection, and maintained the presence of leukocytes at similar levels and time as the alum adjuvant and antigen mixture. Future studies on the functional activities (e.g. cytokine production) of infiltrating leukocytes and resident tissue cells will shed more light on possible adjuvant activities of QD. The growing feather injection model will be well suited to address local responses and activities initiated in a complex tissue by QD and other NP.

Many studies have investigated the effects of cadmium-based QD; however, relatively few have focused on other types of QD, including indium-based QD. Interestingly, an increasing

number of studies are investigating both in vitro and in vivo effects of QD. Hauck et al. (2010) studied the effects of PEG-coated cadmium core QD on Sprague-Dawley rats and found that acute and chronic exposure QD following i.v. QD administration did not induce signs of toxicity. The group found that NP are cleared from blood by monocytes and accumulated in the liver and spleen (Hauck et al., 2010). Wang et al. studied the effects of 8 nm QD in both in vitro and in vivo assays utilizing BALB/c mice. In vitro studies investigated the phagocytic capacity of peritoneal macrophages and isolated mouse spleen-derived lymphocytes. Results indicated QD fluorescence was taken up by macrophages at 24 h and at 48 h and QD were not digested or discharged. On the other hand, as expected, little to no uptake of QD by lymphocytes was observed. The observations are in agreement with those observed in chicken macrophages exposed to QD (Chapter I). Wang et al. (2016) went on to perform organ and blood analysis along with flow cytometry to measure lymphocyte subpopulations in the spleens of QD-treated mice including T cells (CD3), B cells (CD19), and natural killer cells (NK, CD49b). Their results indicated that QD had a negative effect on macrophage viability, but actually stimulated lymphocytes in vitro, a phenomenon in agreement with observed T and B lymphocytes recruited into QD injected GF observed here. However, in vivo, the group found no differences in any major blood markers and thus determined the QD had no toxic effects (Wang et al., 2016). Lymphocytes were affected with a decrease in CD3+ T lymphocytes and enhanced release of pro-inflammatory cytokines TNFα and IL-6 in murine spleens. An increase in CD19+ B cells was also seen, and provided further evidence of immune system stimulation (Wang et al., 2016) similar to observations in the avian system. Maysinger et al. studied the ability of cadmium-core PEGylated QD to stimulate astrocyte activation in the brains of live mice – a marker of cellular response to stress and brain injury. Their results showed that immune cell function changes were

transient over a 7 d time course with increasing activity over the first 3 d of exposure followed by a return to baseline by 7. The group reported that PEGylated QD are compartmentalized in lysosomes of glial cells, but not in mitochondria. Maysinger et al. also combined QD treatment with an astrocyte-response reporter for bioimaging of induced responses in live animals in real time, though their results demonstrate quantitative limitations with this sort of imaging (Maysinger et al., 2007).

Few studies have focused on indium-based QD, though initial results indicate these particles may offer a safer alternative to cadmium-based particles. Lin et al. (2015) measured physiological effects of PEGylated InP/ZnS QD in mice following tail vein injections. Their results also found deposition of QD in the liver and spleen, up to 84 d post injection, with no changes in the physical characteristics of the animals during the course of treatment. Lin et al., measured indium in the blood by ICP-MS and found that QD exited the blood quickly (Lin et al., 2015). Brunetti et al. compared cadmium and indium-based QD in vitro and in vivo in a 2013 study in mice. The QD used in this study differed only in their core – surface coatings and external functional groups were identical. In vitro results indicated a higher release of cadmium compared to indium believed to be due to indium's increased stability and resistance to hydrolysis. With regard to oxidative stress, intracellular degradation was believed to be the cause of increased ROS. They used drosophila as the in vivo model and QD-supplemented food as the route of entry. In vivo results indicated systemic toxicity to cadmium-based QD due to the upregulation of heat shock proteins as well as the induction of apoptosis signaled by upregulation of p53. Indium-based QD were not found to cause upregulation of either of these protein families (Brunetti et al., 2013).

The results of the current study and the findings of the other studies investigating the in vivo effects of QD indicate several common themes. A variety of measurements were carried out to determine the effects of QD in vivo including both qualitative physical appearance measurements and quantitative physiological measurements. The results of many studies show that the animals have no physical signs of disease or other adverse effect physiological effects of QD treatments (Lin et al., 2015), though there is evidence of organ deposition or other signs of toxicity. It is plausible that physical measurements such as weight gain/loss, body temperature, etc., are not sensitive enough to determine the effect of QD on the animal, specifically the effects on the immune system. With the lack of obvious signs of toxicity, is possible that the ability to identify the potential for the induction of immunological memory may be missed. Quantitative measurement of heavy metals in the liver and kidneys is a common measurement parameter, though these measurements may not give a true sense of the impact of QD on immunity since in many studies, QD are injected i.v., and are deposited in these organs from the bloodstream. Dermal injection in complex tissue, as in the case of injection in chicken GF, exposes QD to leukocytes in the tissue and to those infiltrating from the blood, allowing for examination of local bioactivity of the NP. Additionally, in many studies where tandem in vitro and in vivo studies are conducted, the results do not fully agree. As seen in the study by Wang et al. (2016), the effect of QD on lymphocytes differed depending on whether the exposure was in culture or measured systemically. These findings reiterate the importance of in vivo studies to more fully understand the actual biological effects that are taking place in the living animal and therefore, should offer more valid evidence when applied to human applications. The effects of QD are influenced by many factors including the response of the individual, whether that is a metabolic and/or immune response and by the particles themselves including physical and chemical

properties. Surface coatings such as PEG and COOH are important for bioactivity, increasing solubility and protecting the metal core from leaching toxic metals to surrounding tissue. Lee et al. found that QD with COOH groups had greater tissue deposition in isolated perfused porcine skin flaps compared to PEGylated QD (Lee et al., 2007). In culture, HEK cells COOH increased pro-inflammatory cytokines IL-1β, IL-6, and IL-8 versus PEG coatings (Ryman-Rasmussen et al., 2007).

The current study addresses some of the limitations of studies in the literature measuring the immunostimulatory effects of QD. This study is one of few studies to investigate specific local immune cell infiltration following treatment. Other in vivo models have been utilized for the study of QD, however many of them require euthanasia of the animal in order to harvest the organs that are likely to contain NP residues. Therefore, repeated sampling is not possible and therefore temporal effects of treatment are impossible to obtain in the same individual. The current study addresses this limitation; using the growing feather "in vivo test tube" of a chicken provides an important window into tissue/cellular activities initiated by QD (Erf, U.S. Patent No.: 8,216,551) similar to the window into systemic activities provided by sampling the blood. Many QD studies to date have focused on the effects of cadmium-based QD. Our study is one of few to investigate the effects of indium-based QD.

Future directions to further characterize the innate immune response to QD include measurement of cytokine profiles to learn more about the type of immune activities being triggered. Measurement of additional cell types including dendritic cells would shed more light on the physiological response to the QD injections as dendritic cells are likely first responders following injection. Additional methods such as lactate dehydrogenase to measure cell

permeability, intracellular esterase activity and apoptosis assays such as Annexin V or caspase activation would help to round out the picture of the effect of QD on innate immunity.

REFERENCES

Abbas, A. K., A. H. Lichtman, and S. Pillai. 2012. Cellular and Molecular Immunology. 7th ed. Elsevier Saunders, Philadelphia, PA.

Albiger, B, S. Dahlberg, B. Henriques-Normark, and S. Normark. 2007. Role of the innate immune system in host defense against bacterial infections: focus on the Toll-like receptors. J. Intern. Med. 261:511-528.

Aguilar, Z. P. 2012. Nanomaterials for Medical Applications. Elsevier, Boston.

Alivisatos, A. P. 1996. Semiconductor clusters, nanocrystals, and quantum dots. Science. 217:933-937.

Alivisatos, A. P. 1996. Perspectives on the physical chemistry of semiconductor nanocrystals. J. Phys. Chem. 100:13226-13239.

Bilan, R., A. Sukhanova, and I. Nabiev. 2016. Quantum dot-based nanotools for bioimaging, diagnostics, and drug delivery. ChemBioChem. 10.1002/cbic.201600357.

Bruchez, M., M. Moronne, P. Gin, S. Weiss, and A. P. Alivisatos. 1998. Semiconductor nanocrystals as fluorescent biological labels. Science. 281:2013-2016.

Brunetti, V., H. Chibli, R. Fiammengo, A. Galeone, M. A. Malvindi, G. Vecchio, R. Cingolani, J. L. Nadeau, and P. P. Pompa. 2013. InP/ZnS as a safer alternative to CdSe/ZnS core/shell quantum dots: in vitro and in vivo toxicity assessment. Nanoscale. 5:307-317.

Byrne, K. A. 2016. Innate immunity in chickens: in vivo responses to different pathogen associated molecular patterns. Theses and Dissertations. 1638.

Chan, W. C. W., D. J. Maxwell, X. Gao, R. E. Bailey, M. Han, and S. Nie. 2002. Luminescent quantum dots for multiplexed biological detection and imaging. Curr. Opin. Biotechnol. 13:40-46.

Chan, W. C. W., and S. Nie. 1998. Quantum dot bioconjugates for ultrasensitive nonisotopic detection. Science. 281:2016-2018.

Davison, F., B. Kaspers, and K. A. Schat. 2014. Avian Immunology. 2nd ed. Elsevier, San Diego, CA.

Dobrovolskaia, M. A, and S. E. McNeil. 2007. Immunological properties of engineered nanomaterials. Nat. Nanotech. 2:469-478.

Erf, G. F., Inventor. U.S. Patent No.: 8,216,551. Date of Patent: Jul. 10, 2012. In vivo system to monitor tissue responses in birds.

Erf, G. F., and I. R. Ramachandran. 2016. The growing feather as a dermal test site: comparison of leukocyte profiles during the response to Mycobacterium butyricum in growing feathers, wattles, and wing webs. Poult. Sci. 95:1–12.

Fischer, H. C., and W. C. W. Chan. 2007. Nanotoxicity: the growing need for in vivo study. Curr. Opin. Biotech. 18:656-571.

Hauck, T. S., R. E. Anderson, H. C. Fischer, S. Newbigging, and W. C. W. Chan. 2010. In vivo quantum dot toxicity assessment. Small. 6:138-144.

Larson, D. R., W. R. Zipfel, R. M. Williams, S. W. Clark, M. P. Bruchez, F. W. Wise, and W. W. Webb. 2003. Water-soluble quantum dots for multiphoton fluorescence imaging in vivo. Science. 300:1434-1436.

Lee, H. A., M. Imran, N. A. Monteiro-Riviere, V. L. Colvin, W. W. Yu, and J. E. Riviere. 2007. Biodistribution of quantum dot nanoparticles in perfused skin: evidence of coating dependency on periodicity in arterial extraction. Nano Lett. 7:2865-2870.

Li, N., C. Sioutas, A. Cho, D. Schmitz, C. Misra, J. Sempf, M. Wang, T. Oberley, J. Froines, and A. Nel. 2003. Ultrafine particulate pollutants induce oxidative stress and mitochondrial damage. Environ. Health Perspect. 111:455-460.

Lin, G., Q. Ouyang, R. Hu, Z. Ding, J. Tian, F. Yin, G. Xu, Q. Chen, X. Wang, and K. T. Yong. 2015. In vivo toxicity assessment of non-cadmium quantum dots in BALB/c mice. Nanomedicine: NBM. 5:341-350.

Lovric, J., S. J. Cho, F. M. Winnik, and D. Maysinger. 2005. Unmodified cadmium telluride quantum dots induce reactive oxygen species formation leading to multiple organelle damage and cell death. Chemistry & Biology. 12:1227-1234.

Maysinger, D., M. Behrendt, M. Lalancette- Hebert, and J. Kriz. 2007. Real-time imaging of astrocyte response to quantum dots: in vivo screening model system for biocompatibility of nanoparticles. Nano Lett. 7:2513-2520.

Nel, A., T. Xia, L. Madler, and N. Li. 2006. Toxic potential of materials at the nanolevel. Science. 311:622-627.

Nguyen, K., P. Rippstein, A. F. Tayabali, and W. G. Willmore. 2015. Mitochondrial toxicity of cadmium telluride quantum dot nanoparticles in mammalian hepatocytes. Toxicol. Sci. 146:31-42.

Pusic, K., H. Xu, A. Stridiron, Z. Aguilar, A. Wang, and G. Hui. 2011. Blood stage merozoite surface protein conjugated to nanoparticles induce potent parasite inhibitory antibodies. Vaccine. 29:8898-8908.

Rand, M. S. 2008. Selection of biomedical animal models. In: Sourcebook of Models for Biomedical Research. P. M. Conn, ed. Humana Press Inc. Totowa, NJ.

Rosenthal, S. J., J. C. Chang, O. Kovtun, J. R. McBride, and I. D. Tomlinson. 2011. Biocompatible quantum dots for biological applications. Chemistry & Biology. 18:10-24.

Ryman-Rasmussen, J. P., J. E. Riviere, and N. A. Monteiro-Riviere. 2007. Surface coatings determine cytotoxicity and irritation potential of quantum dot nanoparticles in epidermal keratinocytes. J. Invest. Derm. 127:143-153.

Seliger, C., B. Schaerer, M. Kohn, H. Pendl, S. Weigend, B. Kaspers, and S. Härtle. 2012. A rapid high-precision flow cytometry based technique for total white blood cell counting in chickens. Vet. Immunol. Immunopathol. 145:865-99.

Shi, F., and G. F. Erf. 2012. IFN-γ, IL-21, and IL-10 co-expression in evolving autoimmune vitiligo lesions of Smyth line chickens. J. Invest. Derm. 132:642-649.

Wang, X., J. Tian, K. T. Yong, X. Zhu, M. C. M. Lin, W. Jang, J. Li, Q. Huang, and G. Lin. 2016. Immunotoxicity assessment of CdSe/ZnS quantum dots in macrophages, lymphocytes and BALB/c mice. J. Nanobiotechnol. 14:10.

Yang, L., X-H. Peng, A. Y. Wang, X. Wang, Z. Cao, C. Ni, P. Karna, X. Zhang, W. C. Wood, X. Gao, S. Nie, and H. Mao. 2009. Receptor-targeted nanoparticles for in vivo imaging of breast cancer. Clin. Cancer Res. 15:4722-4732.

Zhang, L. W., W. W. Yu, V. L. Colvin, and N. A. Monteiro-Riviere. 2008. Biological interactions of quantum dot nanoparticles in skin and in human epidermal keratinocytes. Tox. App. Pharmacol. 228:200-211.

Zhang, T., Y. Hu, M. Tang, L. Kong, J. Ying, T. Wu, Y. Xue, and Y. Pu. 2015. Liver toxicity of cadmium telluride quantum dots (CdTe QD) due to oxidative stress in vitro and in vivo. Int. J. Mol. Sci. 16:23279-23299.

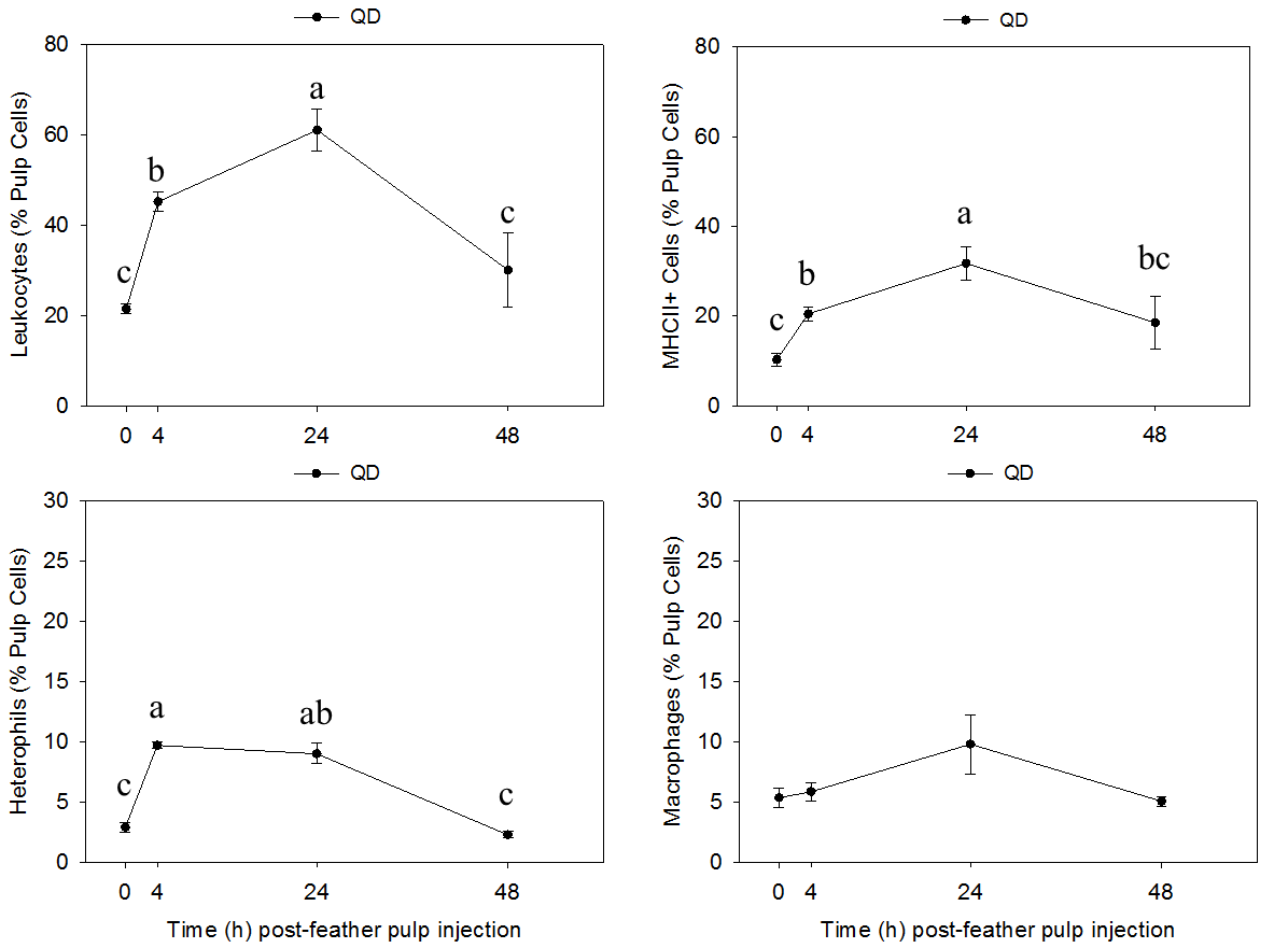

Figure 1. Infiltration of total leukocytes, MHCII+ cells, heterophils and macrophages into the dermis of growing feathers at 0, 4, 24, and 48 h after injection with quantum dots (QD). Growing feathers (GF) of 3 chickens were injected with 10 µL of 2 µM InP/ZnS QD; 3 GF per chicken. One GF collected at 0 (before injection), 4, 24 and 48 h post-injection from each chicken was used for preparation of individual pulp cell suspensions. A panel of chicken-specific fluorescence-conjugated mouse monoclonal antibodies was used to identify leukocytes (CD45+), MHC class II+ cells and macrophages (KUL01) in the pulp cell suspensions. The percentage of heterophils was determined based on size (FSC) and granularity (SSC) characteristics of leukocytes (CD45+). Two-color cell population analysis was carried out by flow cytometry and data for individual leukocyte populations were expressed as the percentage of total pulp cells (% pulp cells). Data shown are mean ± SEM; n = 3 per time point.

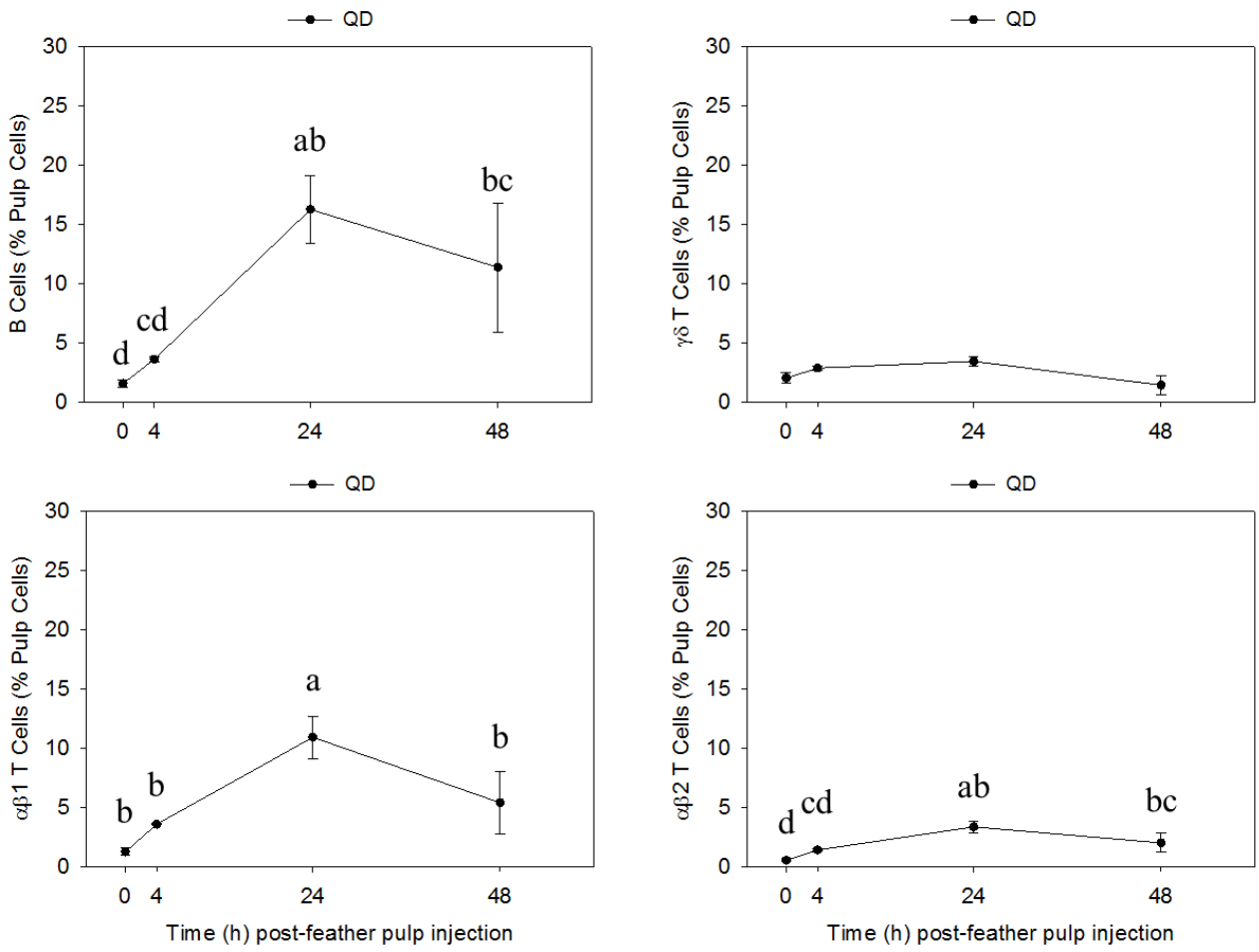

Figure 2. Infiltration of B and T cell populations into the dermis of growing feathers at 0, 4, 24, and 48 h after injection with quantum dots (QD). Growing feathers (GF) of 3 chickens were injected with 10 µL of 2 µM InP/ZnS QD; 3 GF per chicken. One GF collected at 0 (before injection), 4, 24 and 48 h post-injection from each chicken was used for preparation of individual pulp cell suspensions. A panel of chicken-specific fluorescence-conjugated mouse monoclonal antibodies was used to identify B cells (Bu-1) and T cell receptor (TCR)-defined T cell populations (γδ TCR+ T cells, αβ1 TCR+ T cells, and αβ2 TCR+ T cells) in the pulp cell suspensions. Two-color cell population analysis was carried out by flow cytometry and data for individual leukocyte populations were expressed as the percentage of total pulp cells (% pulp cells). Data shown are mean ± SEM; n = 3 per time point.

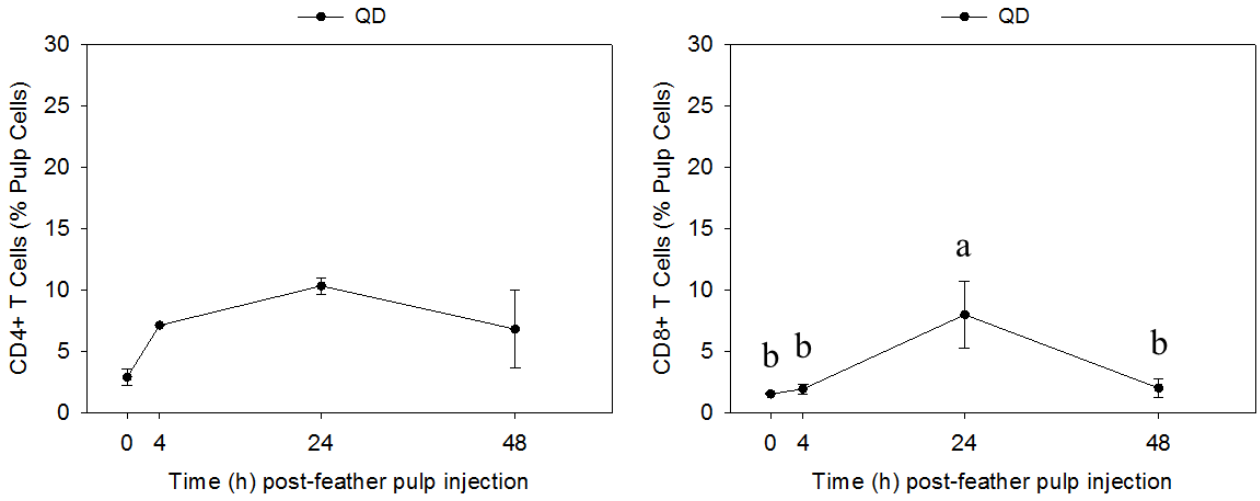

Figure 3. Infiltration of CD4+ and CD8+ T lymphocytes into the dermis of growing feathers at 0, 4, 24, and 48 h after injection with quantum dots (QD). Growing feathers (GF) of 3 chickens were injected with 10 µL of 2 µM InP/ZnS QD; 3 GF per chicken. One GF collected at 0 (before injection), 4, 24 and 48 h post-injection from each chicken was used for preparation of individual pulp cell suspensions. A panel of chicken-specific fluorescence-conjugated mouse monoclonal antibodies was used to identify CD4+ T cells and CD8+ T cells in the pulp cell suspensions. Two-color cell population analysis was carried out by flow cytometry and data for individual leukocyte populations were expressed as the percentage of total pulp cells (% pulp cells). Data shown are mean ± SEM; n = 3 per time point.

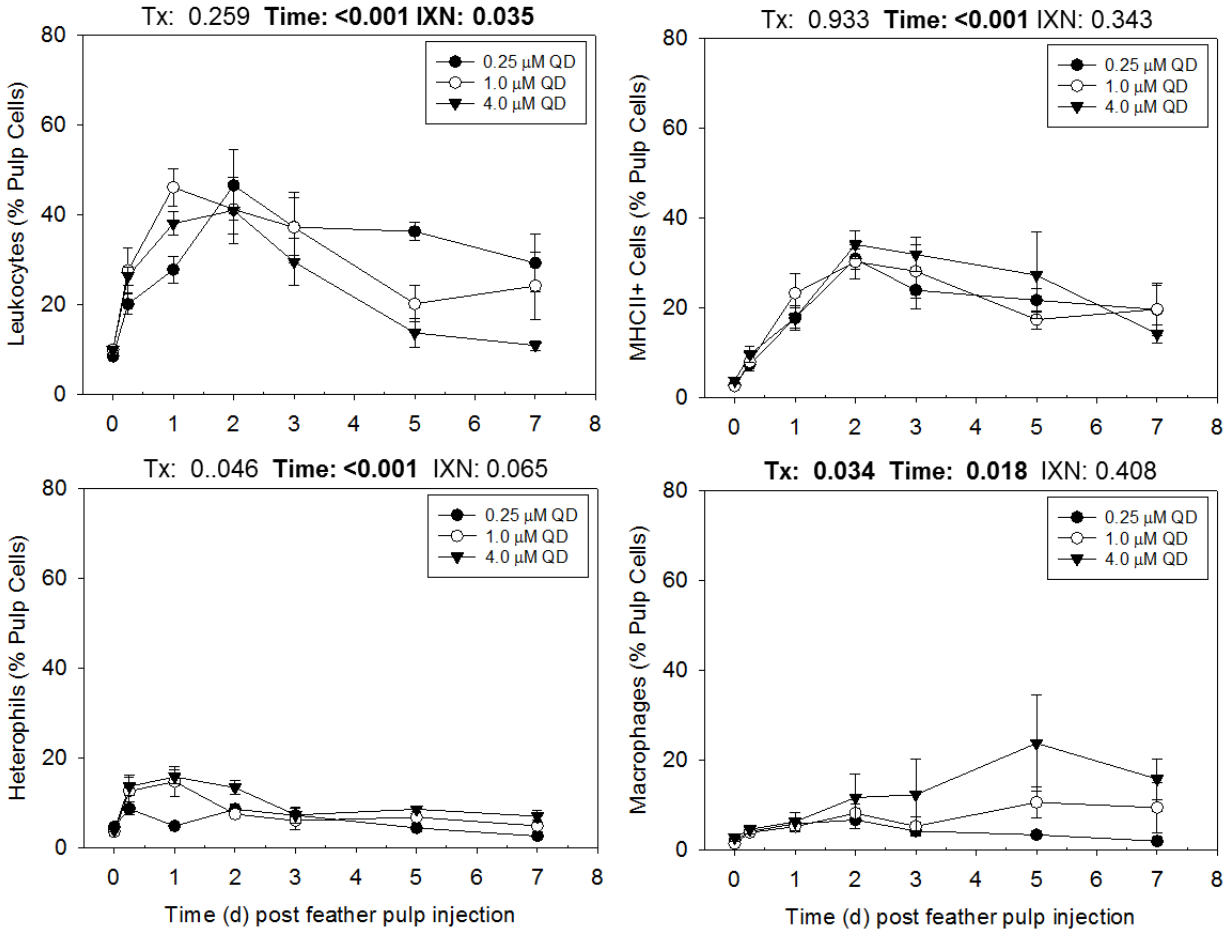

Figure 4. Infiltration of total leukocytes, MHCII+ cells, heterophils and macrophages into the dermis of growing feathers after injection with different dosages of quantum dots (QD). Growing feathers (GF) of 12 chickens were injected with 10 µL of either 0.25, 1.0, or 4.0 µM InP/ZnS QD; 20 GF per chicken; 4 chickens per dosage. One GF collected at 0 (before injection), 0.25, 1, 2, 3, 5, and 7 d post-injection from each chicken was used for preparation of individual pulp cell suspensions. A panel of chicken-specific fluorescence-conjugated mouse monoclonal antibodies was used to identify leukocytes (CD45+), MHC class II+ cells and macrophages (KUL01) in the pulp cell suspensions by two-color direct immunofluorescent staining. The percentage of heterophils was determined based on size (FSC) and granularity (SSC) characteristics of leukocytes (CD45+). Cell population analysis was carried out by flow cytometry and data for individual leukocyte populations were expressed as the percentage of total pulp cells (% pulp cells). Results based on 2-way repeated measures ANOVA are indicated above each graph; Tx = P value for treatment effect; Time = P value for time effect; IXN = P value for treatment by time interaction. For multiple means comparison and additional statistical data, see Table 1. Data shown are mean ± SEM; n = 4 per dose and time point.

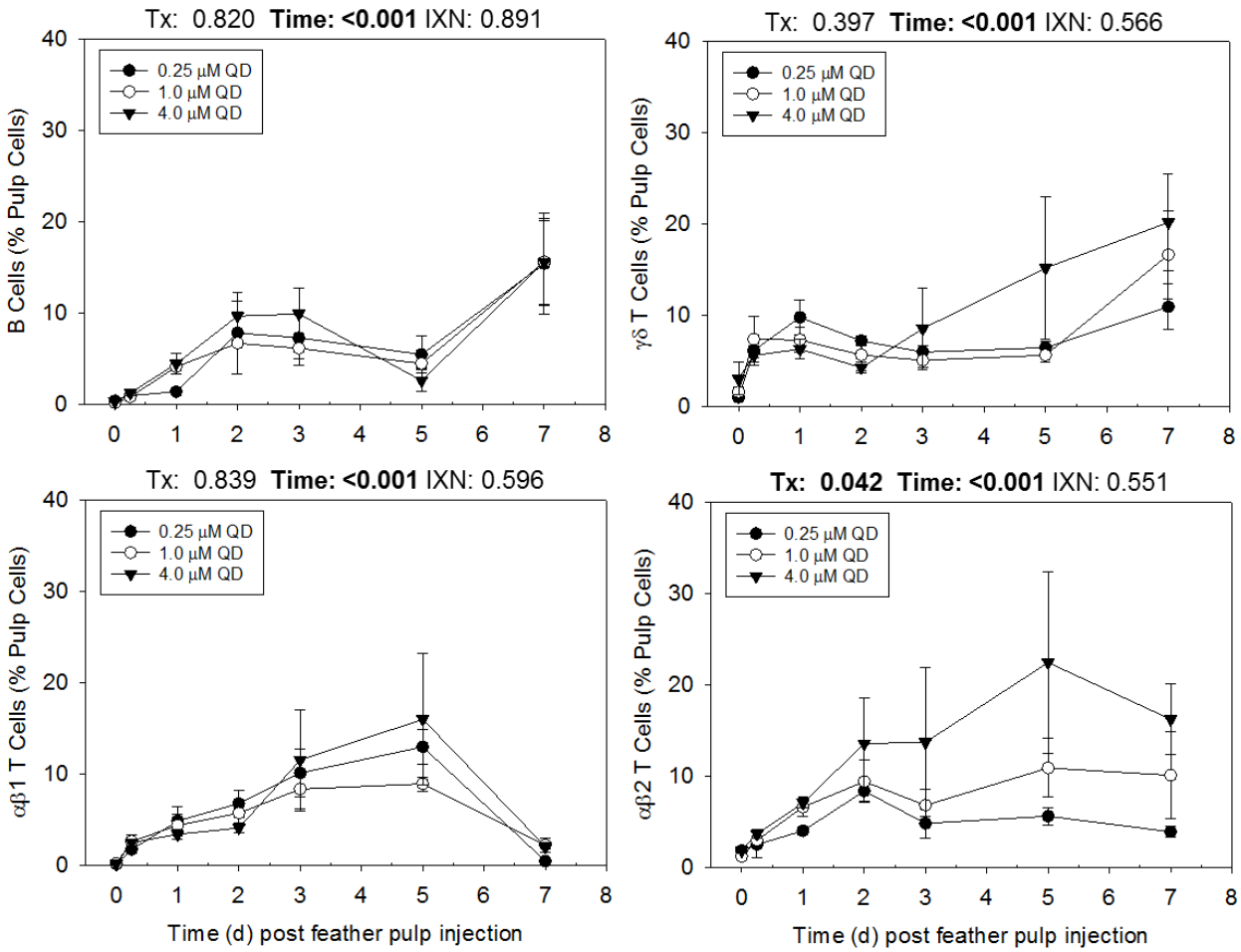

Figure 5. Infiltration of B and T cell subpopulations into the dermis of growing feathers after injection with different dosages of quantum dots (QD). Growing feathers (GF) of 12 chickens were injected with 10 µL of either 0.25, 1.0, or 4.0 µM InP/ZnS QD; 20 GF per chicken; 4 chickens per dosage. One GF collected at 0 (before injection), 0.25, 1, 2, 3, 5, and 7 d post-injection from each chicken was used for preparation of individual pulp cell suspensions. A panel of chicken-specific fluorescence-conjugated mouse monoclonal antibodies was used to identify B cells (Bu-1) and T cell receptor (TCR)-defined T cell populations (γδ TCR+ T cells, αβ1 TCR+ T cells, and αβ2 TCR+ T cells) in the pulp cell suspensions by two-color direct immunofluorescent staining. Cell population analysis was carried out by flow cytometry and data for individual leukocyte populations were expressed as the percentage of total pulp cells (% pulp cells). Results based on 2-way repeated measures ANOVA are indicated above each graph; Tx = P value for treatment effect; Time = P value for time effect; IXN = P value for treatment by time interaction. For multiple means comparison and additional statistical data, see Table 2. Data shown are mean ± SEM; n = 4 per dose and time point.

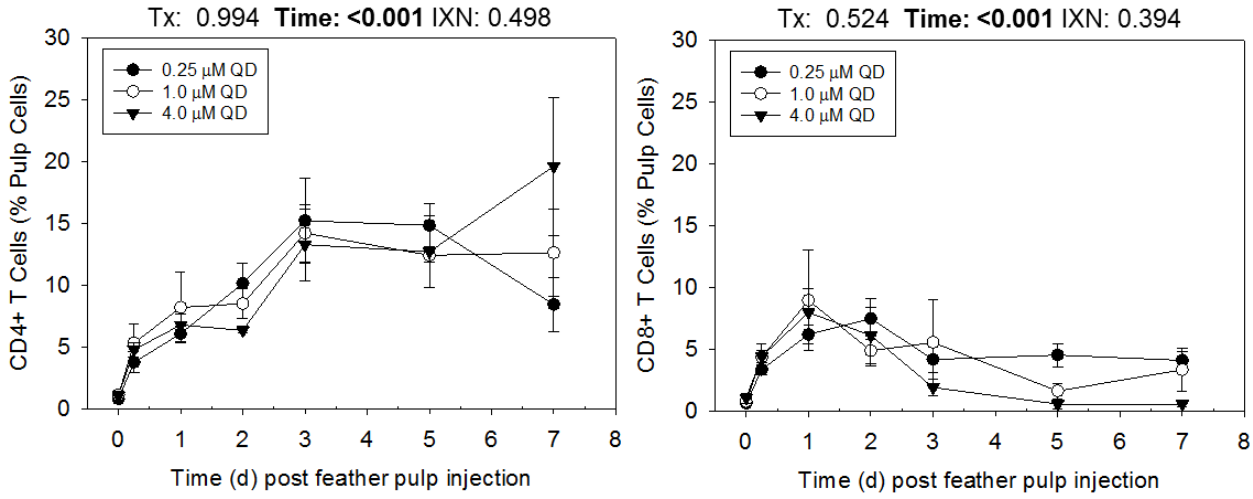

Figure 6. Infiltration of CD4+ and CD8+ T lymphocytes into the dermis of growing feathers after injection with different dosages of quantum dots (QD). Growing feathers (GF) of 12 chickens were injected with 10 µL of either 0.25, 1.0, or 4.0 µM InP/ZnS QD; 20 GF per chicken; 4 chickens per dosage. One GF collected at 0 (before injection), 0.25, 1, 2, 3, 5, and 7 d post-injection from each chicken was used for preparation of individual pulp cell suspensions. A panel of chicken-specific fluorescence-conjugated mouse monoclonal antibodies was used to CD4+ T cells and CD8+ T cells in the pulp cell suspensions by two-color direct immunofluorescent staining. Cell population analysis was carried out by flow cytometry and data for individual leukocyte populations were expressed as the percentage of total pulp cells (% pulp cells). Results based on 2-way repeated measures ANOVA are indicated above each graph; Tx = P value for treatment effect; Time = P value for time effect; IXN = P value for treatment by time interaction. For multiple means comparison and additional statistical data, see Table 3. Data shown are mean ± SEM; n = 4 per dose and time point.

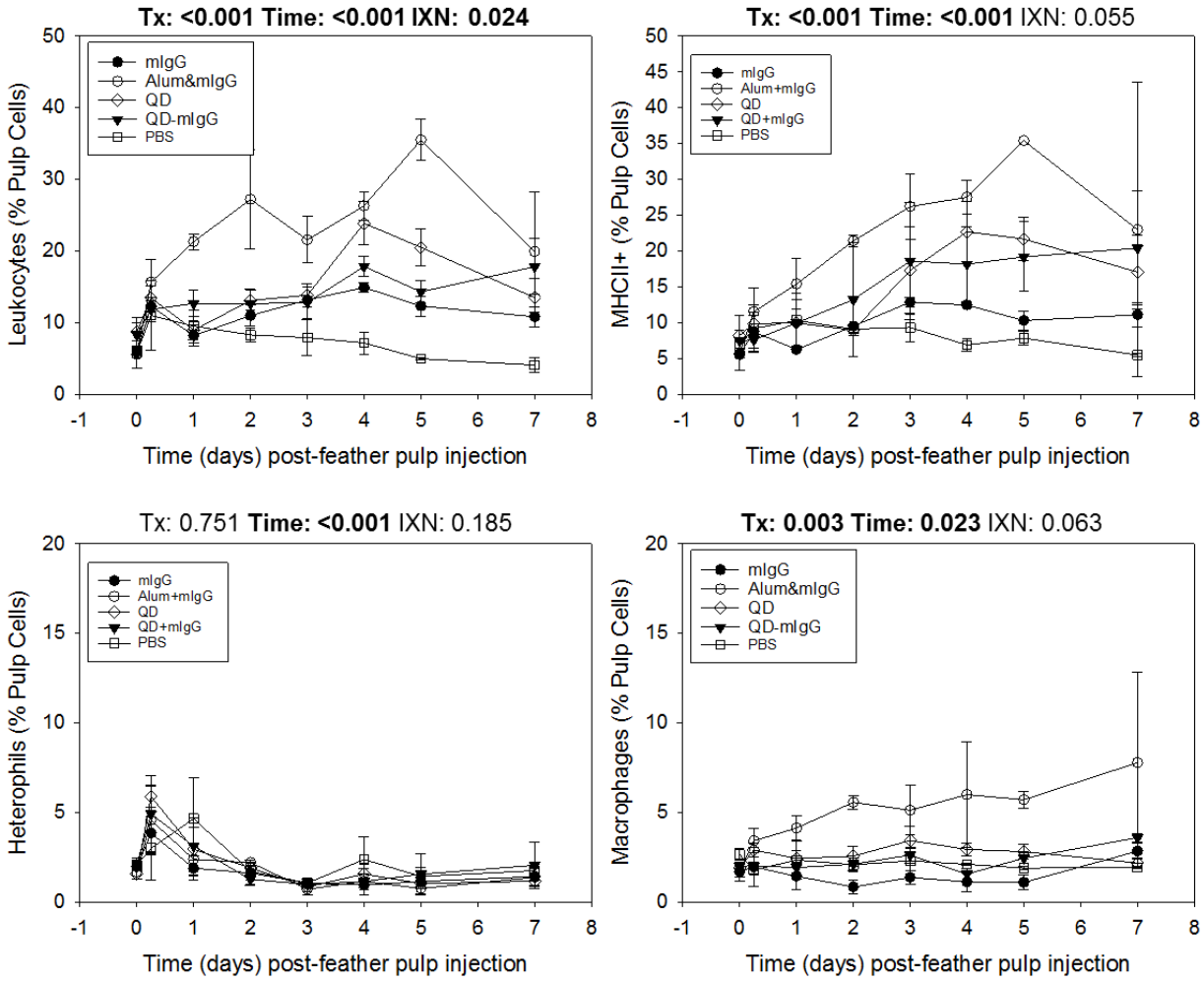

Figure 7. Infiltration of total leukocytes, MHCII+ cells, heterophils and macrophages into the dermis of growing feathers after injection of quantum dots (QD) with and without antigen-conjugation. Growing feathers (GF) of 16 chickens were injected with 10 µL of either PBS (vehicle; n = 2), mouse IgG antigen (0.26 mg/mL mIgG; n = 2), 0.26 mg/mL mIgG mixed with 15% Alum adjuvant (Alum+mIgG; n = 2), 0.5 µM 7 nm InP/ZnS QD (QD, n = 4), or 0.5 µM QD conjugated to 0.26 mg/mL mIgG (QD-mIgG; n = 6); 20 GF per chicken. One GF collected at 0 (before injection), 0.25, 1, 2, 3, 4, 5, and 7 d post-injection from each chicken was used for preparation of individual pulp cell suspensions. A panel of chicken-specific fluorescence-conjugated mouse monoclonal antibodies was used to identify leukocytes (CD45+), MHC class II+ cells and macrophages (KUL01) in the pulp cell suspensions by two- to three-color direct immunofluorescent staining. The percentage of heterophils was determined based on size (FSC) and granularity (SSC) characteristics of leukocytes (CD45+). Cell population analysis was carried out by flow cytometry and data for individual leukocyte populations were expressed as the percentage of total pulp cells (% pulp cells). Results based on 2-way repeated measures ANOVA are indicated above each graph; Tx = P value for treatment effect; Time = P value for time effect; IXN = P value for treatment by time interaction. For multiple means comparison and additional statistical data, see Table 4. Data shown are mean ± SEM.

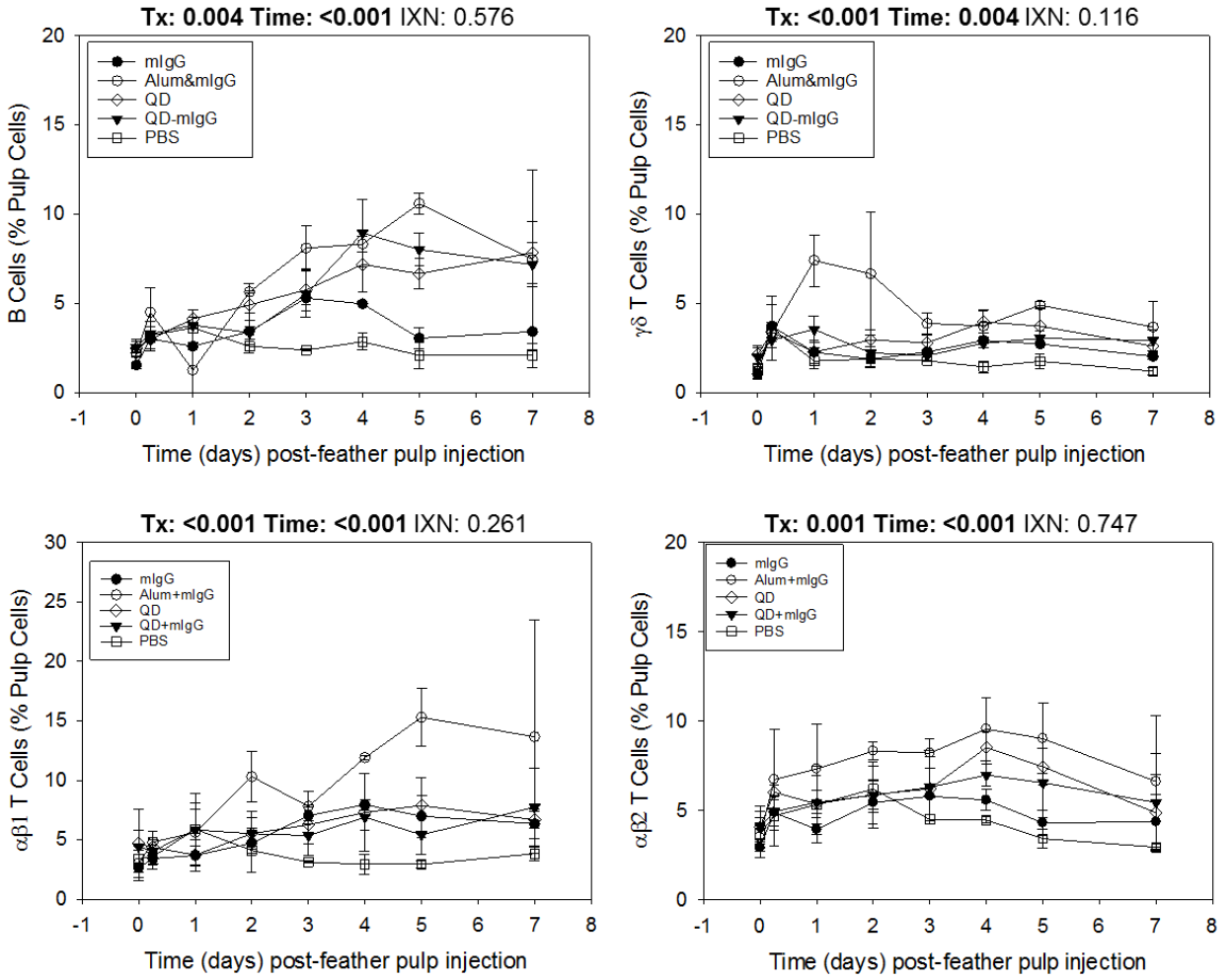

Figure 8. Infiltration of B and T lymphocyte subpopulations into the dermis of growing feathers after injection of quantum dots (QD) with and without antigen-conjugation. Growing feathers (GF) of 16 chickens were injected with 10 µL of either PBS (vehicle; n = 2), mouse IgG antigen (0.26 mg/mL mIgG; n = 2), 0.26 mg/mL mIgG mixed with 15% Alum adjuvant (Alum+mIgG; n = 2), 0.5 µM 7 nm InP/ZnS QD (QD, n = 4), or 0.5 µM QD conjugated to 0.26 mg/mL mIgG (QD-mIgG; n = 6); 20 GF per chicken. One GF collected at 0 (before injection), 0.25, 1, 2, 3, 4, 5, and 7 d post-injection from each chicken was used for preparation of individual pulp cell suspensions. A panel of chicken-specific fluorescence-conjugated mouse monoclonal antibodies was used to identify B cells (Bu-1) and T cell receptor (TCR)-defined T cell populations (γδ TCR+ T cells, αβ1 TCR+ T cells, and αβ2 TCR+ T cells) in the pulp cell suspensions by two- to three-color direct immunofluorescent staining. Cell population analysis was carried out by flow cytometry and data for individual leukocyte populations were expressed as the percentage of total pulp cells (% pulp cells). Results based on 2-way repeated measures ANOVA are indicated above each graph; Tx = P value for treatment effect; Time = P value for time effect; IXN = P value for treatment by time interaction. For multiple means comparison and additional statistical data, see Table 5. Data shown are mean ± SEM.

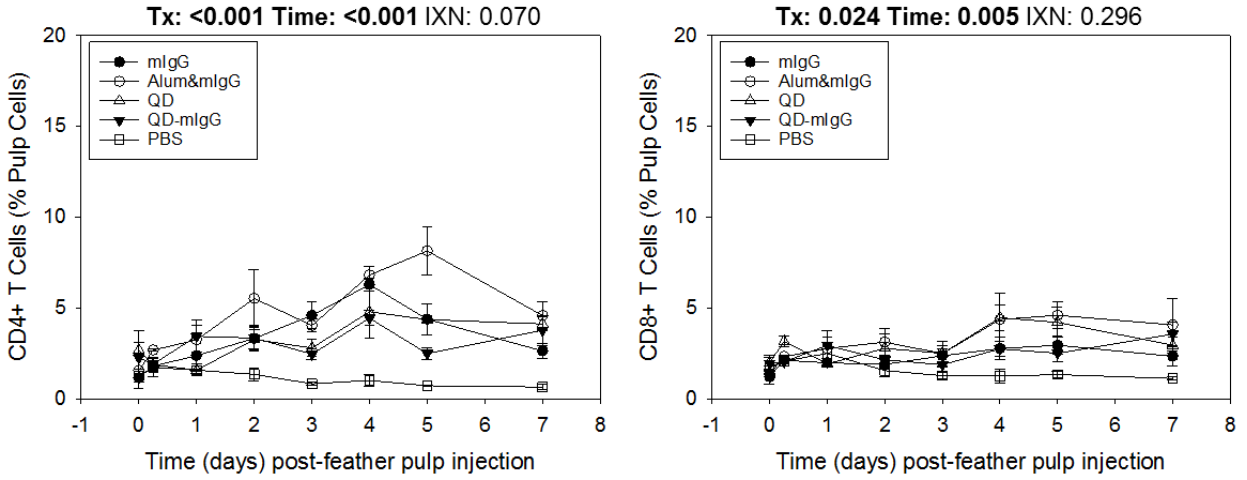

Figure 9. Infiltration of CD4+ and CD8+ T lymphocytes into the dermis of growing feathers after injection of quantum dots (QD) with and without antigen-conjugation. Growing feathers (GF) of 16 chickens were injected with 10 µL of either PBS (vehicle; n = 2), mouse IgG antigen (0.26 mg/mL mIgG; n = 2), 0.26 mg/mL mIgG mixed with 15% Alum adjuvant (Alum+mIgG; n = 2), 0.5 µM 7 nm InP/ZnS QD (QD, n = 4), or 0.5 µM QD conjugated to 0.26 mg/mL mIgG (QD-mIgG; n = 6); 20 GF per chicken. One GF collected at 0 (before injection), 0.25, 1, 2, 3, 4, 5, and 7 d post-injection from each chicken was used for preparation of individual pulp cell suspensions. A panel of chicken-specific fluorescence-conjugated mouse monoclonal antibodies was used to identify CD4+ T cells and CD8+ T cells in the pulp cell suspensions by two- to three-color direct immunofluorescent staining. Cell population analysis was carried out by flow cytometry and data for individual leukocyte populations were expressed as the percentage of total pulp cells (% pulp cells). Results based on 2-way repeated measures ANOVA are indicated above each graph; Tx = P value for treatment effect; Time = P value for time effect; IXN = P value for treatment by time interaction. For multiple means comparison and additional statistical data, see Table 6. Data shown are mean ± SEM.

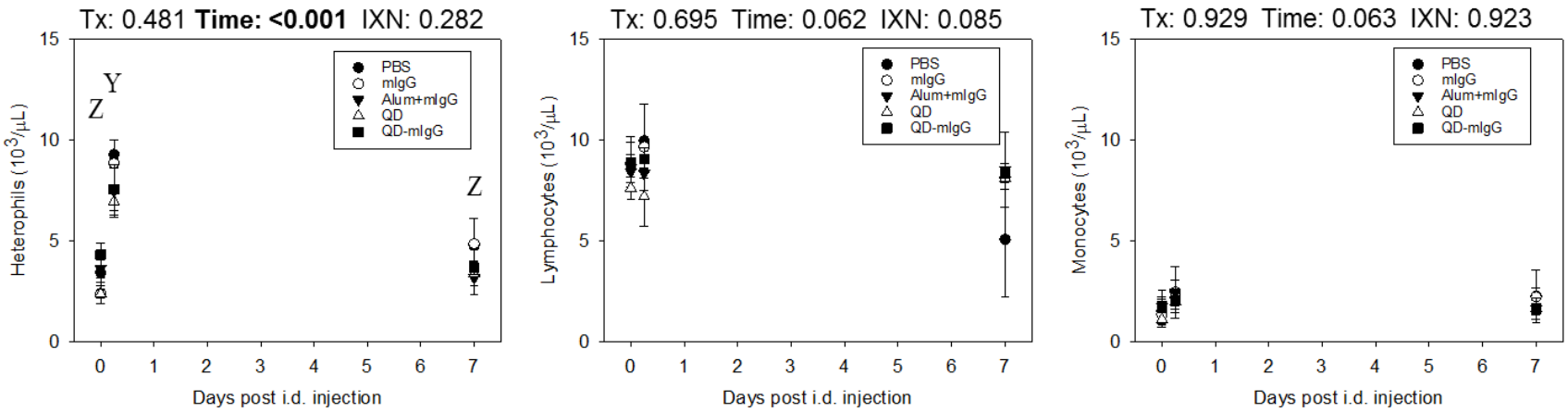

Figure 10. Measurement of peripheral blood leukocyte concentrations after GF injection with PBS (vehicle), mIgG, Alum+mIgG, QD, and QD-mIgG Growing feathers (GF) of 16 chickens were injected at 0 (before), 0.25 and 7 d with 10 µL of either PBS (vehicle; n = 2), mouse IgG antigen (0.26 mg/mL mIgG; n = 2), 0.26 mg/mL mIgG mixed with 15% Alum adjuvant (Alum+mIgG; n = 2), 0.5 µM 7 nm InP/ZnS QD (QD, n = 4), or 0.5 µM QD conjugated to 0.26 mg/mL mIgG (QD-mIgG; n = 6); 20 GF per chicken. Peripheral whole blood was collected via the wing vein at each time point. Heterophil, monocyte and lymphocyte populations were determined via Cell-Dyn automated hematology analyzer. Results based on 2-way repeated measures ANOVA are indicated above each graph; Tx = P value for treatment effect; Time = P value for time effect; IXN = P value for treatment by time interaction. Data shown are mean ± SEM.

Table 1.
Statistical analysis of data shown in **Figure 4.** Time and treatment effects on the levels of infiltrating leukocytes, MHCII+ cells, heterophils and macrophages (% pulp cells) in QD-injected GF.

Leukocytes

Treatment	P-Treat	P-Time	P-IXN	0 d	0.25 d	1 d	2 d	3 d	5 d	7 d
	0.259	<0.001	0.035							
0.25 µM		<0.001		Z	Y	X b	W	X	X a	X
1.0 µM		0.041		Z	WXY	V a	VW	VWX	YZ b	XYZ
4.0 µM		<0.001		Z	XY	WX ab	W	WX	Z b	YZ

MHCII+ Cells

Treatment	P-Treat	P-Time	P-IXN	0 d	0.25 d	1 d	2 d	3 d	5 d	7 d
	0.933	<0.001	0.343	Z	Z	Y	X	X	XY	Y
0.25 µM										
1.0 µM										
4.0 µM										

Heterophils

Treatment	P-Treat	P-Time	P-IXN	0 d	0.25 d	1 d	2 d	3 d	5 d	7 d
	0.046	<0.001	0.065	Z	X	X	XY	YZ	YZ	Z
0.25 µM	b									
1.0 µM	ab									
4.0 µM	a									

Macrophages

Treatment	P-Treat	P-Time	P-IXN	0 d	0.25 d	1 d	2 d	3 d	5 d	7 d
	0.034	0.018	0.408	Z	Z	Z	Z	Z	Y	Z
0.25 µM	b									
1.0 µM	ab									
4.0 µM	a									

V, W, X, Y, Z: For each cell population, levels at time-points without a common letter are different at $P < 0.05$. Letters "Z to V" indicate ascending order of GF infiltration levels. a, b: Treatments without a common letter are different. Letters "b to a" indicate ascending order of GF infiltration levels.

Table 2.
Statistical analysis of data shown in **Figure 5.** Time and treatment effects on the levels of infiltrating B and T lymphocyte subpopulations (% pulp cells) in QD-injected GF.

B cells

Treatment	P-Treat	P-Time	P-IXN	0 d	0.25 d	1 d	2 d	3 d	5 d	7 d
	0.820	<0.001	0.891	Z	Z	YZ	Y	Y	YZ	X
0.25 µM										
1.0 µM										
4.0 µM										

γδ T cells

Treatment	P-Treat	P-Time	P-IXN	0 d	0.25 d	1 d	2 d	3 d	5 d	7 d
	0.397	<0.001	0.566	Z	YZ	YZ	YZ	YZ	Y	X
0.25 µM										
1.0 µM										
4.0 µM										

αβ1 T cells

Treatment	P-Treat	P-Time	P-IXN	0 d	0.25 d	1 d	2 d	3 d	5 d	7 d
	0.839	<0.001	0.596	Z	YZ	YZ	XY	WX	W	YZ
0.25 µM										
1.0 µM										
4.0 µM										

αβ2 T cells

Treatment	P-Treat	P-Time	P-IXN	0 d	0.25 d	1 d	2 d	3 d	5 d	7 d
	0.042	<0.001	0.551	Z	YZ	XYZ	XY	XZ	X	XYZ
0.25 µM	b									
1.0 µM	ab									
4.0 µM	a									

W, X, Y, Z: For each cell population, levels at time-points without a common letter are different at $P < 0.05$. Letters "Z to W" indicate ascending order of GF infiltration levels. a, b: Treatments without a common letter are different. Letters "b to a" indicate ascending order of GF infiltration levels.

Table 3.
Statistical analysis of data shown in **Figure 6.** Time and treatment effects on the levels of infiltrating CD4+ and CD8+ T lymphocyte populations (% pulp cells) in QD-injected GF.

CD4+ T cells

Treatment	P-Treat	P-Time	P-IXN	0 d	0.25 d	1 d	2 d	3 d	5 d	7 d
	0.994	<0.001	0.498	Z	YZ	Y	Y	X	X	X
0.25 µM										
1.0 µM										
4.0 µM										

CD8+ T cells

Treatment	P-Treat	P-Time	P-IXN	0 d	0.25 d	1 d	2 d	3 d	5 d	7 d
	0.524	<0.001	0.394	Z	WXY	W	WX	XY	YZ	XZ
0.25 µM										
1.0 µM										
4.0 µM										

W, X, Y, Z: For each cell population, levels at time-points without a common letter are different at $P < 0.05$. Letters "Z to W" indicate ascending order of GF infiltration levels.

a, b: Treatments without a common letter are different. Letters "b to a" indicate ascending order of GF infiltration levels.

Table 4.
Statistical analysis of data shown in **Figure 7.** Time and treatment effects on the levels of infiltrating leukocyte, MHCII+ cells, heterophils and macrophages (% pulp cells) in QD-injected GF.

Leukocytes

Treatment	P-Treat	P-Time	P-IXN	0 h	0.25 d	1 d	2 d	3 d	4 d	5 d	7 d
	<0.001	<0.001	0.024								
PBS		0.280				b	b		c	d	
mIgG		0.010		Z	WX	YZ b	XY b	WX	W bc	WX cd	XY
Alum+mIgG		0.031		Z	YZ	Y a	XY a	Y	XY a	X a	Y
QD		<0.001		Z	Z	Z b	Z b	Z	Y a	Y b	Z
QD+mIgG		0.099				b	b		b	c	

MHCII+ Cells

Treatment	P-Treat	P-Time	P-IXN	0 h	0.25 d	1 d	2 d	3 d	4 d	5 d	7 d
	<0.001	<0.001	0.055	Z	Z	YZ	XYZ	XY	X	X	XY
PBS	c										
mIgG	c										
Alum+mIgG	a										
QD	b										
QD+mIgG	b										

Heterophils

Treatment	P-Treat	P-Time	P-IXN	0 h	0.25 d	1 d	2 d	3 d	4 d	5 d	7 d
	0.751	<0.001	0.185	Z	X	Y	Z	Z	Z	Z	Z
PBS											
mIgG											
Alum+mIgG											
QD											
QD+mIgG											

Table 4 (Cont.)

Macrophages

Treatment	P-Treat	P-Time	P-IXN	0 h	0.25 d	1 d	2 d	3 d	4 d	5 d	7 d
	0.003	0.023	0.063	Z	YZ	YZ	YZ	YZ	YZ	YZ	Y
PBS	b										
mIgG	b										
Alum+mIgG	a										
QD	b										
QD+mIgG	b										

W, X, Y, Z: For each cell population, levels at time-points without a common letter are different at $P < 0.05$. Letters "Z to W" indicate ascending order of GF infiltration levels.

a, b, c, d: Treatments without a common letter are different. Letters "d to a" indicate ascending order of GF infiltration levels.

Table 5.
Statistical analysis of data shown in **Figure 8.** Time and treatment effects on the levels of infiltrating B and T lymphocyte subpopulations (% pulp cells) in QD-injected GF.

B cells

Treatment	P-Treat	P-Time	P-IXN	0 h	0.25 d	1 d	2 d	3 d	4 d	5 d	7 d
	0.004	<0.001	0.576	Z	YZ	XYZ	XYZ	XY	X	XY	XY
PBS	c										
mIgG	bc										
Alum+mIgG	a										
QD	ab										
QD+mIgG	ab										

γδ T cells

Treatment	P-Treat	P-Time	P-IXN	0 h	0.25 d	1 d	2 d	3 d	4 d	5 d	7 d
	<0.001	0.004	0.116	Z	Y	Y	Y	YZ	YZ	Y	YZ
PBS	c										
mIgG	bc										
Alum+mIgG	a										
QD	b										
QD+mIgG	bc										

αβ1 T cells

Treatment	P-Treat	P-Time	P-IXN	0 h	0.25 d	1 d	2 d	3 d	4 d	5 d	7 d
	<0.001	<0.001	0.261	Z	Z	YZ	YZ	YZ	Y	Y	YZ
PBS	c										
mIgG	b										
Alum+mIgG	a										
QD	b										
QD+mIgG	b										

Table 5 (Cont.)

αβ2 T cells

Treatment	P-Treat	P-Time	P-IXN	0 h	0.25 d	1 d	2 d	3 d	4 d	5 d	7 d
	0.001	<0.001	0.747	Z	XYZ	XYZ	XY	XY	X	XY	YZ
PBS	c										
mIgG	bc										
Alum+mIgG	a										
QD	ab										
QD+mIgG	bc										

X, Y, Z: For each cell population, levels at time-points without a common letter are different at $P < 0.05$. Letters "Z to X" indicate ascending order of GF infiltration levels.

a, b, c: Treatments without a common letter are different. Letters "c to a" indicate ascending order of GF infiltration levels.

Table 6.
Statistical analysis of data shown in **Figure 9.** Time and treatment effects on the levels of infiltrating CD4+ and CD8+ T lymphocytes (% pulp cells) in QD-injected GF.

CD4+ T cells

Treatment	P-Treat	P-Time	P-IXN	0 h	0.25 d	1 d	2 d	3 d	4 d	5 d	7 d
	<0.001	<0.001	0.070	Z	Z	ZY	XYZ	XYZ	X	XY	XYZ
PBS	c										
mIgG	b										
Alum+mIgG	a										
QD	b										
QD+mIgG	b										

CD8+ T cells

Treatment	P-Treat	P-Time	P-IXN	0 h	0.25 d	1 d	2 d	3 d	4 d	5 d	7 d
	0.024	0.005	0.296	Z	YZ	YZ	YZ	YZ	Y	Y	YZ
PBS	b										
mIgG	ab										
Alum+mIgG	ab										
QD	a										
QD+mIgG	ab										

X, Y, Z: For each cell population, levels at time-points without a common letter are different at $P < 0.05$. Letters "Z to X" indicate ascending order of GF infiltration levels.

a, b, c: Treatments without a common letter are different. Letters "c to a" indicate ascending order of GF infiltration levels.

CHAPTER III

Primary and memory cellular and humoral immune responses to intramuscular mouse IgG protein antigen-conjugated InP/ZnS quantum dot immunizations as a platform for vaccine development

Introduction

Since Edward Jenner's first manipulation of the immune system to illicit protection from smallpox in 1798, vaccination has become the most effective means for preventing infection (Abbas et al., 2012). Vaccination involves manipulating the immune system by intentionally introducing a pathogen in a form that does not cause disease, but triggers an immune response in the individual such that long term protection is gained. Successful vaccination results when the individual becomes protected against future encounters with the pathogen. In order to understand vaccination, one must understand how both the innate and adaptive immune systems work together to produce the long term protection.

The innate and adaptive arms of the immune system work together to protect the organism from infection. While the innate immune system is the body's non-specific, first line of defense to antigenic foreign materials and pathogens, the adaptive immune system prepares the body for repeated exposures to specific pathogens through both humoral and cell mediated immunity. The humoral response is characterized by B lymphocytes that produce antigen-specific antibodies capable of microbe neutralization, neutralization, and complement mediated lysis. Cell mediated immunity is carried out by T lymphocytes that either directly (e.g. cytotoxic T cells) or indirectly (T helper cells that activate other leukocytes) participate in the elimination of intra- and extra-cellular pathogens (Abbas et al., 2012). The innate and adaptive immune systems work together when antigen presenting cells (APCs) of the innate immune system (especially dendritic cells) engulf microbes, process them using intracellular machinery and express the antigenic microbial fragments on their surface in conjunction with major histocompatibility complex (MHC) proteins to T lymphocytes. Cytokines released by APCs signal and activate other cells of the immune system further strengthening the immune response

(Abbas et al., 2012). Following presentation of the antigen to T helper lymphocytes, the antigen-specific lymphocytes undergo clonal expansion, and differentiate into effector T helper cells. Activated T helper cells help in the activation, clonal expansion, and differentiation of antigen-specific B cells (i.e. become antibody-producing plasma cells), antigen-specific cytotoxic T cells (i.e. become target cell killers), and provide stimuli to innate leukocytes to become more effective in eliminating infections. In addition, during T helper cell dependent immune responses, large numbers of antigen-specific "memory" lymphocytes are produced that are ready to mount a faster and stronger immune response should the antigen be encountered again.

The basic principle of vaccination is to administer a "harmless" form of a pathogen, which may be a live attenuated or inactivated microbe, a protein or protein subunit in order to trigger the innate and adaptive immune systems to mount a protective response to the vaccine antigen. Sometimes the antigenic material in the vaccine is designed to be safer, but is not strong enough to stimulate an adequate immune response. In this case, other substances, known as adjuvants, are added to the vaccine antigen which improve the immunoreactivity of the vaccine (Coffman et al., 2010). Adjuvants, such as aluminum salts or water/oil emulsions, may serve as delivery systems that hold the antigen at the site of injection with or without immunostimulatory properties that activate cells of innate immunity (Awate et al., 2013; van Aalst et al., 2017). While knowledge of adjuvant properties is growing with increased research, much is still largely misunderstood regarding their mechanism of action. Recent research has shed more light on mechanisms of adjuvant action, including the sustained release or depot effect, cytokine and chemokine stimulating properties, effects on leukocyte recruitment, improvement in APC function (e.g. increasing antigen uptake, APC maturation, increasing MHC II molecule expression, migration to draining lymph nodes), and activation of inflammasomes (Schijns and

Lavelle, 2011). Aluminum salts, known simply as alum, are believed to produce the depot effect by strong electrostatic interactions between alum and antigen (Corradin and del Giudice, 2005). This effect enhances the function of APCs by increasing antigen uptake, however studies have shown that the depot effect is not required for adjuvant activity and in fact, alum adjuvants can create a local inflammatory response that induces recruitment of innate immune cells (Kool et al., 2012).

While alum is perhaps the most widely used adjuvant, nanoparticles (NP) have recently been shown to have adjuvant properties and have been used in vaccine applications (Aguilar, 2012; Bilan et al., 2016; Poland, 2012; Yang et al., 2016; Zhao et al., 2014). Nanoparticles have been shown to induce long-lasting antibody titers requiring less antigen and potentially fewer administrations (Dobrovolskaia and McNeil, 2007). Pusic et al. (2011) have used both quantum dot (QD) and iron oxide (IO) NP to boost immune responsiveness to a recombinant blood stage malaria vaccine in mice. Their results showed that < 15 nm QD were able to stimulate significantly higher antibody titers compared to conventional oil-water adjuvants like Freund's Complete Adjuvant (CFA) and Montanide ISA51, and that the antibodies produced were highly inhibitory against parasite growth. Due to toxicity concerns with cadmium-based QD, Pusic et al. (2013) turned their focus to the safer and more inexpensive iron oxide NP vaccine strategy. Their results showed that IO-conjugated recombinant malaria vaccine induced antibody titers similar to the traditional adjuvants; however, the antibodies produced were again much more inhibitory against parasite growth (Pusic et al., 2013). While NP have been shown to be promising alternatives to conventional adjuvants, NP toxicity is a great concern and must be investigated further (Nel et al., 2006; Soenen et al., 2011). Toxicity has primarily been attributed to the production of reactive oxygen species (ROS) and deposition in tissue of heavy metals such

as cadmium (Hauck et al., 2010; Nel et al., 2006; Wang et al., 2016). To realize the full potential of NP for vaccine applications, shortcomings such as the lack of comprehensive evaluation methods, inconsistency in the size and shape of NP, and the presence of contaminants in NP preparations (Dobrovolskaia et al., 2009) must be addressed with better in vivo models (Fischer and Chan, 2007).

Recently Erf and Ramachandran demonstrated the viability of the chicken growing feather (GF) dermal injection model as a cutaneous test-site to examine tissue/cellular immune response in the same individual over time (Erf, U.S. Patent No.: 8,216,551; Erf and Ramachandran, 2016). The GF injection model has presented several distinct advantages over traditional in vivo models, one of the most important being that no euthanasia or surgery is required to obtain injected dermal tissue samples, allowing for minimally invasive repeated sampling in the same individual over time. The GF dermal tissue is essentially an "in vivo test tube" that is easily removed from the living animal for ex vivo analysis of in vivo activities with no negative impact on the physiology of the animal (Erf and Ramachandran, 2016).

In response to the growing need for in vivo models for the study of the biological effects of NP, we proposed to use the GF dermal injection model to compare the immune response to mouse IgG protein antigen when conjugated with QD NP with the immune response to mouse IgG protein antigen mixed with traditional alum adjuvant. Our objectives were to 1) measure immune cell infiltration into the GF following GF injection with mIgG during both primary and memory effector immune responses; and 2) measure the humoral immune response following primary and secondary antigen administration by sampling the peripheral blood to assess antibody production. The goals of this study were to validate the GF dermal injection model for in vivo study of NP vaccine preparations and to further characterize the adjuvant properties of

QD NP as compared to traditional alum adjuvant. This work was supported by NIH-NIBIB R15 EB015187; G. F. Erf, PI.

MATERIALS AND METHODS

Experimental Animals Non-vaccinated male and female Light Brown Leghorn (LBL) layer-type chickens were reared in floor pens on wood shaving litter in rooms fitted with HEPA filtration of intake air at the University of Arkansas Poultry Health Laboratory (Arkansas Experiment Station, University of Arkansas, Fayetteville, AR). Twenty-six male LBL chickens were randomly assigned to 2 treatment groups of 13 (Groups 1 and 2). Group 1 chickens underwent primary intramuscular (i.m.) immunization in the breast muscle at 7 weeks of age followed by GF injection 10 days post primary immunization. Group 2 chickens also received primary i.m. immunization at 7 weeks, followed by secondary i.m. immunization at 11 weeks of age, and GF injection 5 days post-secondary immunization. A third group of 13 female LBL chickens (Group 3) received both primary and secondary (i.m.) immunizations, but did not receive GF injections. Standard light and temperature protocols were followed (Shi and Erf, 2012) with food and water available ad libitum. Animal use was approved by the University of Arkansas Institutional Animal Care and Use Committee (approval #15020).

Test Materials Endotoxin-free Dulbecco's PBS (EF-DPBS, Sigma-Aldrich, St. Louis, MO) was used as the vehicle-only control. Mouse IgG (mIgG, Rockland Immunochemicals Inc., Limerick, PA) served as the test antigen either alone (mIgG, 0.26 mg/mL, final concentration), conjugated to 7 nm InP/ZnS QD (QD-mIgG), or mixed 1:1 with 2% Hydrogel alum adjuvant (Alum+mIgG). Conjugation of mIgG with QD was completed by Dr. Zoraida Aguilar (Zystein, Inc., Springdale, AR) using 4 molecules mIgG per QD for a final working concentration of 0.26 mg/mL mIgG in 0.5 μM QD. No further dilution was required for the in vivo use of mIgG-QD.

Immunizations were 0.1 mL of the following test materials with the number of birds immunized in each group at each time point given in parentheses: PBS (2), mIgG (2) (0.26 mg/mL), Alum+mIgG (3) (1:1, 0.26 mg/mL mIgG) or QD-mIgG (6) (0.26 mg/mL mIgG in 0.5 μM QD). Groups 1 and 2 received GF injections of 0.01 mL mIgG test antigen (1 mg/mL) 10 days after primary i.m. immunization and 5 days after secondary i.m. immunization. Group 3 did not receive GF injections.

Measurement of Primary & Memory Leukocyte Infiltration by Immunofluorescent Staining of Pulp Cell Suspensions and Cell Population Analysis by Flow Cytometry A panel of chicken-specific fluorescently-labeled (fluorescein isothiocyanate (FITC) and phycoerythrin (PE), and spectral red (SPRD)) mouse monoclonal antibodies (Southern Biotechnology Associates, Inc., Birmingham, AL) were used to distinguish individual cell populations including total leukocytes (CD45-SPRD+), MHC class II expressing cells (MHCII-FITC+), macrophages (KUL01-PE+), B cells (Bu-1-FITC+), IgG+ B cells (Bu-1-FITC+, IgG-PE+), IgM+ B cells (Bu-1-FITC+, IgM-PE+) and T cell receptor (TCR)-defined T cell populations including γδ T cells (TCR1-FITC+), γδ T cells expressing CD8 (TCR1-FITC+, CD8-PE+), αβ1 TCR+ T cells (TCR2-FITC+), αβ2 TCR+ T cells (TCR3-FITC+), as well as CD4+ (CD4-PE+) and CD8+ (CD8-PE+) T cells in the pulp cell suspensions by two- or three-color direct immunofluorescent staining. The isotype of all mouse monoclonal antibodies used was IgG1. A pool of all cell suspensions was prepared and incubated with FITC, PE and SPRD labeled mouse IgG1 isotype controls to confirm fluorescently labeled antibodies were not binding non-specifically and to distinguish between fluorescence positive and negative populations (Byrne, 2016). Fluorescence-based cell population analysis was carried out using a BD FACSort flow cytometer according to compensation and acquisition procedures as described in Erf and Ramachandran

(2016). The percentage of heterophils was determined based on size (FSC) and granularity (SSC) characteristics of leukocytes (CD45-SPRD+) as described in Seliger et al. (2012). Cell populations were measured in the GF dermis (% pulp cells) by flow cytometry at 0 (before injection), and 0.25, 1, 2, 3, 4, 5, and 7 d post-injection during the primary and memory effector phases of the immune response. Data analysis of cell populations was completed using FlowJo (Ashland, OR) flow cytometry analysis software. The proportions of various leukocyte populations present in the pulp cell suspension were expressed as a percentage of total pulp cells.

Measurement of the Humoral Immune Response To measure the production of antibodies specific to the mouse IgG test antigen (chicken anti-mouse IgG and IgM isotypes), approximately 1 mL of whole blood was collected from the wing vein of each bird before (0) and 3, 5, 7, 10, 14, 21, and 28 days post-primary and secondary i.m. immunizations using heparinized syringes (3 mL with 25 x 1 gauge needles). Whole blood was centrifuged at 1000 x *g* at 4°C for 5 minutes. The plasma fraction was divided equally between two 0.5 mL microcentrifuge tubes and stored at -80°C until antibody analysis via enzyme-linked immunosorbent assay (ELISA).

***Enzyme Linked Immunosorbent* Assay** The concentration of IgG and IgM antibodies specific for mouse IgG test antigen was measured by ELISA following primary and secondary i.m. immunization with test materials. Reactions were carried out at room temperature unless otherwise noted. Ninety-six-well ELISA plates were coated with 100 µL mouse IgG (Rockland Immunochemicals Inc., Limerick, PA) at a concentration of 5 µg/mL diluted in coating buffer (0.05 M sodium carbonate-bicarbonate buffer, pH 9.6) for at least 24 h at 4°C. Wells were washed 5 times with wash buffer (TBS-T: 50 mM Tris HCl, 0.14 M NaCl, 0.05% Tween-20, pH 8.0) after coating then incubated with 200 µL blocking solution per well (50 mM Tris HCl, 0.14

M NaCl, 1% BSA) for at least 1 h at 4°C. After blocking, wells were washed 5 times with TBS-T as before. Mouse IgG-specific chicken IgG (Invitrogen, Thermo Fisher Scientific, Waltham, MA) was used as the standard and added in duplicate for each assay plate. Mouse IgG-specific chicken IgG was used as the standard for IgG and IgM measurement since there is currently no chicken anti-mouse IgM antibody commercially available. IgG standard concentrations ranged from 0.15 to 78 ng/mL and were prepared using doubling dilutions in dilution buffer (TBS-T plus 1% BSA). Samples were prepared in dilution buffer at dilutions ranging from 1:200 to 1:320,000. Samples and standards, 100 μL per well, were added in duplicate on separate plates for concurrent measurement of mouse IgG-specific IgG and IgM antibodies and incubated at room temperature for 1 hour. Assay controls included measurement of non-specific binding and background color. Non-specific binding was measured by adding detection antibody to wells incubated with dilution buffer alone. Background color was determined by adding all components except the HRP enzyme. Following sample and standard incubations, wells were washed 5 times, then either goat anti-chicken IgG or goat anti-chicken IgM horseradish peroxidase-conjugated secondary detection antibodies (1:10,000 dilution) (Bethyl Laboratories Inc., Montgomery, TX) were added to each well, 100 μL per well, and the plates incubated at room temperature for 1 h. Following detection antibody incubation, wells were washed 5 times, then 100 μL TMB substrate (3,3',5,5'-tetramethylbenzidine, TMB One Component HRP Microwell Substrate, Bethyl Laboratories, Inc., Montgomery, TX) was added to each well and plates incubated for 10-15 minutes at room temperature. At full color development, the enzymatic reaction was stopped by adding 100 μL 2 M sulfuric acid. Quantitation of absorbance at 450 nm was performed using a Bio-Tek ELx800 microplate reader controlled by Gen5 software (Bio-Tek Instruments, Winooski, VT). Data analysis was completed using Gen5

software including calculation of the standard curve using a 4-parameter logistic equation to define the relationship between known concentrations of mIgG-specific chicken antibodies and corresponding optical absorbance measurements. This standard curve equation was then used to determine plasma concentrations of chicken IgM and IgG antibodies specific for mouse IgG antigen.

Statistical Analysis The experimental unit was the individual chicken. Sigma Plot 13 Statistical Software (Systat Software, Inc., San Jose, CA) was used to determine significant effects of time, treatment, and treatment by time interactions using two-way repeated measure analysis of variance (RM ANOVA). Following RM ANOVA, the Holm-Sidak method of multiple means comparison was used to determine the main effect(s) of time and treatment when no significant interactions were found. When time and treatment interactions were found, one-way RM ANOVA followed by Fisher's LSD multiple means comparison was performed for each treatment separately to determine the effects of time; for treatment comparisons, ANOVA was carried out at each time-point followed by Fisher's LSD multiple means comparison. For all analyses, differences were considered significant at $P \leq 0.05$.

RESULTS

Leukocyte infiltration in response to injection of mouse IgG into the dermis of growing feathers in unsensitized chickens and chickens sensitized with either mouse IgG conjugated to quantum dots or mouse IgG mixed with alum adjuvant

Two groups of 13 chickens each were injected intramuscularly (i.m.) with PBS as vehicle alone (unsensitized) or immunized i.m. with 0.1 mL of 0.26 mg/mL mIgG (mIgG), 0.26 mg/mL mIgG mixed with 2% Alum adjuvant (Alum+mIgG), or 0.26 mg/mL mIgG conjugated to 0.5 μM QD (QD-mIgG) followed by GF injection with mIgG antigen (10 μL of 1 mg/mL per GF) during

the primary (day 10) and memory (day 5) effector phases of the immune response. Infiltrating immune cells were measured for 7 d in the antigen-injected GF pulp (% pulp cells) during each phase of the immune responses.

For MHC class II-expressing cells, no main time effect was observed in unsensitized chickens. In sensitized chickens only time main effects were observed ($P < 0.001$) during both the primary and memory effector responses. When mIgG was injected into GF during the primary effector response, levels of MHC class II+ cells increased steadily from 0 d (5.2 ± 1.3%) to a maximum of 2-fold greater than baseline at 2 d (13.3 ± 1.3%) before steadily decreasing to just below baseline level (4.7 ± 1.3%) at the conclusion of the time course. During the memory effector response, MHC class II+ cells increased more quickly compared to the primary response, peaking at 1 d at a level nearly 3-fold higher (16.0 ± 1.1%) than baseline (5.4 ± 1.1%) before gradually returned to near pre-treatment levels at 7 d (Figure 1, Table 1). Overall, levels of MHCII+ cells in mIgG-injected GF were highest in QD-mIgG, followed by Alum+mIgG, and lowest with mIgG immunization treatments (main effect $P = 0.034$).

In unsensitized chickens a time main effect ($P < 0.001$) was observed for heterophils consisting of a sharp, nearly 4-fold, increase from 0 d (2.6 ± 0.35%) to 0.25 d (7.9 ± 1.1%) followed by a return to baseline levels at 2 d (1.6 ± 0.1%) through the remainder of the time course. Similarly, in sensitized chickens during the primary effector response, heterophil levels more than doubled from 0 d (2.8 ± 0.3%) to 0.25 d (6.2 ± 0.3%), then decreased to baseline level where they remained for the duration of the time course (time main effect $P < 0.001$). Due to treatment by time interactions during the memory effector response, each treatment and time point were analyzed individually. Heterophil levels followed a similar pattern for each treatment with nearly 2-fold higher levels at baseline compared to levels seen at 7 d, declining from

baseline through 3 d before spiking intermittently at 4 d (Figure 1, Table 1). Overall, QD-mIgG treated birds had the highest level of infiltrating heterophils at 0 d during the memory effector response (Figure 1, Table 1).

In unsensitized chickens a time main effect ($P = 0.004$) was observed for macrophages consisting of nearly 2-fold elevated levels at 0.25 and 1 d. In sensitized birds, a time main effect was also observed ($P = 0.001$) during the primary effector response. Macrophages more than doubled from 0 d (3.0 ± 0.7%) to 0.25 d (6.1 ± 0.7 %), remained elevated through 2 d (5.3 ± 0.7%), then returned to baseline. Due to treatment by time interactions during the memory effector response, each treatment and time point were analyzed individually. Macrophage levels were elevated nearly 3-fold at 1 d compared to baseline in Alum+mIgG and QD-mIgG immunized birds, decreased thereafter and then rose again at 4 d (Figure 1, Table 1).

All lymphocyte sub-populations examined infiltrated the GF pulp following mIgG antigen injection with significant main effects of treatment and time found for each of the subpopulations measured. In unsensitized chickens no time main effect was observed for B cells. A time main effect was observed ($P < 0.001$) during the primary effector response with B cell levels doubling through 2 d (10.4 ± 0.6%) then decreasing gradually over the time course to baseline level at 7 d. Due to treatment by time interactions during the memory effector response, each treatment and time point were analyzed individually. Similar to macrophages, B cells were higher in Alum+mIgG and QD-mIgG immunized birds compared to mIgG alone reaching their highest level early in the time course, by 1 d, and were also elevated again at 4 d (Figure 2, Table 2).

In addition to identifying B cells based on the expression of pan B cell surface molecule Bu-1, B cells were also phenotyped based on presence of IgG or IgM surface receptors. No main

effect of time was observed for IgG expressing cells in unsensitized birds. No treatment by time interactions were observed for IgG+ B cells in sensitized birds. Treatment main effects were observed during the primary ($P = 0.015$) and memory ($P = 0.005$) effector responses for IgG+ B cells. GF-infiltrating B cells in Alum+mIgG and QD-mIgG immunized chickens, included nearly 2 and 3-fold more Bu-1+IgG+ cells compared to B cells in mIgG immunized chickens during the primary and memory responses, respectively. A time main effect ($P = 0.001$) was observed for IgG expressing cells only during the memory effector phase with levels peaking at 4 d nearly 2-fold higher than baseline. For IgM expressing B cells, a main time effect ($P = 0.025$) was observed in GF of unsensitized chickens characterized by a gradual increase in Bu-1+ IgM+ B cells through 5 d. No treatment by time interactions were observed for IgM+ B cells in sensitized chickens. Main effects of time were observed during the primary ($P < 0.001$) and memory ($P < 0.001$) effector responses in sensitized birds. Expression profiles were similar for each phase with cells increasing through 2 d and 3 d to levels over 2-fold higher than baseline, then gradually returning to baseline by 7 d (Figure 2, Table 2).

There was no main time effect for γδ T cells in unsensitized chickens. No treatment by time interactions occurred in sensitized chickens during the primary or memory responses. There also was no time main effect during the primary response; however, there was a time main effect ($P < 0.001$) during the memory response for γδ T cells in sensitized chickens. The trend in infiltrating γδ T cells was similar during both phases with an increase in cells at 1 d and followed by a decrease by 2 d. Through the remainder of the time course, γδ T cells overall were slightly elevated during the primary phase and returned to near baseline after 3 d during both the primary and memory phases. There was a time main effect ($P < 0.001$) for γδ T cells in response to QD-

mIgG immunization during the memory effector phase with pronounced increase at 1 d and again at 4 d (Figure 3, Table 3).

For αβ T cells, a time main effect was observed in GF of in unsensitized chickens ($P < 0.05$) increasing to 22.4 ± 2.3% at 1 d then declining gradually to 13.3 ± 1.3% at 7 d. No treatment by time interaction was observed for this population in sensitized birds. Main time effects were observed for αβ T cells during both primary ($P < 0.001$) and memory ($P < 0.001$) effector phases. During the primary effector phase, αβ T cells increased nearly 2-fold 1 d following injection then declined gradually over the remainder of the time course back to baseline level. During the memory effector phase, the increase in αβ T cells was highest 1 d in all immunized chickens with Alum+mIgG- and QD-mIgG-immunizations stimulating greater levels of αβ T cells overall compared to mIgG immunization. Following the peak of αβ T cells at 1 d (29.3 ± 1.2%), levels declined gradually to reach baseline by 7d (13.7 ± 1.2) (Figure 3, Table 3).

No time main effect was observed in unsensitized chickens for CD4+ T cells. A main time effect of time was observed ($P = 0.009$) during the primary effector response with CD4+ T cells peaking at 2 d (7.1 ± 0.7%) then gradually returning to baseline at 7 d (4.2 ± 0.7%). Based on treatment by time interactions during the memory effector response, the treatments had different effects on CD4+ T cells infiltration over time. Levels of CD4+ T cells were higher in birds immunized with mIgG alone at 1 d and 3 compared to Alum+mIgG and QD-mIgG immunizations with the biggest difference of nearly 3-fold higher occurring at 3 d (Figure 4, Table 4).

For CD8+ T cells, a main effect of time was observed in unsensitized chickens with elevated levels at 0.25 d and again at 4 d. No treatment by time interaction was observed for

CD8+ T cells in sensitized chickens. Time main effects were observed for CD8+ T cells during both primary ($P < 0.001$) and memory ($P < 0.001$) effector phases, with the highest levels of infiltration early in the time course, rising nearly 2-fold by 1 d then declining gradually to baseline level at 7 d (Figure 4, Table 4).

Antibody response in unsensitized chickens and chickens sensitized with mouse IgG conjugated to quantum dots or mouse IgG mixed with alum adjuvant

IgM Antibody Response

The various formulations of mIgG immunizations resulted in different antigen-specific IgM antibody production profiles following primary and secondary immunizations (time x treatment interactions $P <0.001$ and $P <0.018$, respectively) (Table 5). Following the first administration of mIgG antigen, IgM levels were elevated slightly at 5 d and 7 d (0.8 ± 0.1 µg/mL) before returning to baseline by 14 d. Following Alum+mIgG primary immunization, IgM levels were elevated at 7 d (2.1 ± 0.5 µg/mL) and 10 d (2.6 ± 0.7 µg/mL) returning to baseline levels at14 d and onwards (Figure 5). Similarly, following primary immunization with QD-mIgG IgM levels were elevated at 5 d, reaching peak levels on 7 d (5.7 ± 0.9 µg/mL) and 10 d (6.5 ± 1.0 µg/mL) and gradually returning to near baseline levels on day 21 and 28 post-immunization. Comparison of immunization treatments revealed treatment differences in IgM levels on 5, 7, 10, and 14 d post immunization with highest levels ($P < 0.05$) observed in QD-mIgG, followed by Alum+ mIgG, and lowest in mIgG immunized chickens (Figure 5, Table 5).

The antigen-specific IgM response profiles following a second immunization with the various mIgG formulation were nearly identical to that observed during the primary response, except that IgM levels for all three treatments were similarly high (2-2.7 µg/mL) on day 5. While in mIgG immunized chickens IgM levels started to drop again by 7 d, those of Alum+mIgG and

QD-mIgG immunized chickens increased further reaching peak levels on 7 d (2.3 and 5.4 µg/mL, respectively) and decreased gradually to near baseline levels by 28 days. Overall, the IgM levels were highest ($P < 0.05$) in QD-mIgG-, intermediate in Alum+mIgG-, and lowest in mIgG-immunized chickens (Figure 5, Table 5).

IgG Antibody Response

The various formulations of mIgG immunizations resulted in different antigen-specific IgG antibody productions profiles following primary and secondary immunizations (time x treatment interactions $P < 0.001$ and $P < 0.003$, respectively) (Table 5). Following the first administration of mIgG antigen, IgG levels were elevated at 10 d (14.9 ± 0.1 µg/mL) and 14 d (11.4 ± 4.6 µg/mL) before returning to baseline by 21 d. Following Alum+mIgG primary immunization, IgG levels were elevated at 10 d (126.3 ± 38.7 µg/mL) and 14 d (78.0 ± 20.0 µg/mL) before returning to baseline levels at 21 d and onwards (Figure 5). Following primary immunization with QD-mIgG, IgG levels were elevated at 7 d (64.5 ± 12.2), reached peak levels on 10 d (186.7 ± 41.1 µg/mL) then gradually returned to near baseline levels on day 28 post-immunization. Comparison of immunization treatments revealed treatment differences in IgG levels on 5, 7, 14, 21 and 28 d post immunization with highest levels ($P < 0.05$) observed in QD-mIgG, followed by Alum+ mIgG, and lowest in mIgG immunized chickens (Figure 5, Table 5).

Following the second administration of mIgG immunizations, IgG levels rose more quickly and reached higher, sustained levels compared to those observed during the primary response. Following the second administration of mIgG antigen, IgG levels were elevated at 5 d, peaked at 7 d (54.5 ± 7.7 µg/mL), then gradually returned to near baseline by 21 d. Following Alum+mIgG secondary immunization, IgG levels began to rise sharply at 5 d, peaked at 7 d (350.4 ± 93.1 µg/mL) and gradually decreased thereafter, but were still elevated (119.0 ± 35.6) at

28 d compared to baseline. During the first 7 d following secondary administration of QD-mIgG, the IgG response was similar to that following secondary Alum+mIgG. However, in QD-mIgG immunized chickens, IgG levels continued to rise rather than decline after 7 d, reaching a peak level at 14 d (417.4 ± 76.6 µg/mL) and remaining at high levels (278.9 ± 66.5 µg/mL) at 28 d. Overall, the IgG levels were highest ($P < 0.05$) in QD-mIgG-, intermediate in Alum+mIgG-, and lowest in mIgG-immunized chickens (Figure 5, Table 5).

DISCUSSION

The chicken GF dermal injection method presented a unique opportunity to utilize an "in vivo test tube" to study immune responses to antigen in complex tissue with repeated sampling in the same individual (Erf and Ramachandran, 2016). To our knowledge this is one of the first in vivo studies to assess and monitor the tissue/cellular immune responses to antigen in animals immunized with antigen conjugated to InP/ZnS QD along with monitoring the humoral response as a model for potential QD vaccine applications.

Our results confirm the infiltration of leukocytes in mIgG-protein antigen injected GF of unsensitized chickens and of chickens sensitized with mIgG alone, mIgG conjugated with QD, or mIgG mixed with alum during both primary and memory immune effector responses. In unsensitized chickens, many cells types were observed to rise at 6 h after GF mIgG injection which may be indicative of the innate immune response to tissue injury. While time effect differences were revealed for most of the cell populations analyzed, immunization differences were seen for fewer of the infiltrating cell populations. In several cases the QD-mIgG and Alum+mIgG immunizations did stimulate the leukocyte infiltration to a greater degree than mIgG alone. For MHCII+ cells no differences between treatments were found during the primary response, however, QD-mIgG immunization stimulated higher levels of MHCII+ cells

in antigen-injected GF than mIgG alone. This finding is consistent with the fact that particulate adjuvants play a role in antigen presentation, thereby increasing the recruitment of MHCII+ cells including monocytes/macrophages and B cells. Considering that dendritic cells (DC) are key MHCII+ antigen presenting cells, they too may have been part of the increased levels of MHCII+ cells when antigen was injected into GF although no marker was available to identify these cells specifically.

An initial influx of heterophils was found following GF injection of antigen in unsensitized chickens and in chickens during the primary effector phase. However, surprisingly, this influx was not seen during the memory effector phase at the early time point. Heterophils are a first-response cell that will invade the site of tissue damage as a part of the innate immune response. The lower heterophil infiltration during adaptive memory responses is an interesting observation and supports the protective role of adaptive immunity in eliminating the antigen before inflammatory processes are initiated. Additional study is warranted based on the results seen during the memory effector response to determine whether factors other than antibodies are inhibiting heterophil infiltration.

Levels of lymphocyte populations including total B cells, γδ T cells, and αβ T cells, each were higher during the memory response compared to the primary response. QD-mIgG and Alum+mIgG immunizations stimulated greater infiltration of these cell types in mIgG injected GF compared to mIgG antigen immunization. Despite time effect differences, CD4+ T helper cell levels increased only slightly during the primary or memory phases. Cytotoxic (CD8+) T cells were more responsive during the primary effector phase compared to the memory phase with only a small difference seen between treatments during the primary phase.

The production of antibodies specific for mIgG antigen during the primary and memory humoral responses was characterized by significantly higher plasma IgM antibody concentrations following QD-mIgG immunization compared to mIgG alone and Alum+mIgG. QD-mIgG was found to stimulate IgG antibody production to a slightly higher degree than Alum+mIgG during the primary phase. However, during the memory phase, QD-mIgG and Alum+mIgG stimulated a much higher IgG antibody immune response beginning earlier in the treatment. In response to QD-mIgG immunization, IgG levels kept climbing at 7 d whereas the levels tapered off in response to Alum+mIgG. At the conclusion of the time course, mIgG antigen-specific IgG levels remained higher in QD-mIgG immunized chickens than those of Alum+mIgG immunized chickens.

Results from the cellular and humoral immune responses, specifically lymphocyte infiltration into GF and mIgG antigen-specific antibody production during the primary and memory responses, provide evidence that T cell help influenced a memory response phenotype. Contributing evidence of T cell help from the cellular immune response include the changes in B cells, specifically higher IgM+ B cells during the primary phase and higher IgG+ B cells during the memory phase. Additionally, levels of αβ T cells with helper function increased in GF during the memory phase. The changes in mIgG antigen-specific antibody production, from largely IgM during the primary response to IgG during the secondary response indicated that T cell help contributed to B cell activation and antibody isotype switching. Considering that the antigen used was a protein antigen that can easily be removed with the help of antibodies, cells like T helper cells and cytotoxic T cells that are typically important in the elimination of intracellular antigen are not expected to play key roles during the effector responses at the site of antigen-injection.

This work helps to solidify the growing feather as a unique, minimally invasive, and effective window into immune system responses to antigen in a complex tissue, similar to the window into systemic activities provided by sampling the blood and other tissue fluids. While minipigs and other large animals may offer better models of the human immune response (Gerdts et al., 2015; Ploemen et al., 2014), these animals must be euthanized in most cases in order to realize study results. Our studies have shown that GF may be collected for 7 days post-injection, providing multiple samples from the same animal over this time course, without euthanasia or invasive procedures. In addition, recent studies focusing on dermal vaccines have shown superiority over the more common subcutaneous injection route (Yasuda et al., 2016). Tozuka et al., demonstrated via injection site excision that intradermal vaccination facilitated antigen delivery to draining lymph nodes better than subcutaneous injection (Tozuka et al., 2016).

In this study we have shown that immune system responses to nanoparticle-conjugated antigens may indeed be monitored in the chicken, both at the local tissue level using the GF cutaneous test-site to monitor cellular responses as well as in the systemic circulation by measuring the concentration and quality of antigen-specific antibodies. It appears that the unique properties QD NP alter immune function in vivo, stimulating humoral immunity greater than traditional adjuvants or antigen alone.

Additional studies should accelerate the use of QD into areas such as vaccine delivery, targeted drug delivery, and other innovative biological applications. As antigen size can impact antigen presentation efficiency, questions remain whether QD are targeted to lysosomes and investigation is warranted to determine the mechanism used by QD to enhance adaptive immune responses. Dendritic cells were not measured in this study though being that DCs are a primary APC, this cell type is an important one for further study with regards to temporal activities

following GF injection. As the advantages of the GF model and antigen-NP immunization were realized in this study, future work in these areas is guaranteed to have a positive impact on the field of vaccinology.

REFERENCES

Abbas, A. K., A. H. Lichtman, and S. Pillai. 2012. Cellular and Molecular Immunology. 7th ed. Elsevier Saunders, Philadelphia, PA.

Aguilar, Z. P. 2012. Nanomaterials for Medical Applications. Elsevier, Boston.

Awate, S., Babiuk, L. A., and Mutwiri, G. Mechanisms of action of adjuvants. 2013. Front. Immunol. 4:1-10.

Bilan, R., A. Sukhanova, and I. Nabiev. 2016. Quantum dot-based nanotools for bioimaging, diagnostics, and drug delivery. ChemBioChem. 10.1002/cbic.201600357.

Byrne, K. A. 2016. Innate immunity in chickens: in vivo responses to different pathogen associated molecular patterns. Theses and Dissertations. 1638.

Coffman, R. L., Sher, A., and Seder, R. A. 2010. Vaccine adjuvants: putting innate immunity to work. Immunity. 33:492-503.

Corradin, G., and G. del Giudice. 2005. Novel adjuvants for vaccines. Curr. Med. Chem. – Anti-Inflammatory & Anti-Allergy Agents. 4:000-000.

Dobrovolskaia, M. A., D. R. Germolec, and J. L. Weaver. 2009. Evaluation of nanoparticle immunotoxicity. Nat. Nanotech. 4:411-414.

Dobrovolskaia, M. A, and S. E. McNeil. 2007. Immunological properties of engineered nanomaterials. Nat. Nanotech. 2:469-478.

Erf, G. F., Inventor. U.S. Patent No.: 8,216,551. Date of Patent: Jul. 10, 2012. In vivo system to monitor tissue responses in birds.

Erf, G. F., and I. R. Ramachandran. 2016. The growing feather as a dermal test site: comparison of leukocyte profiles during the response to Mycobacterium butyricum in growing feathers, wattles, and wing webs. Poult. Sci. 95:1–12.

Fischer, H. C., and W. C. W. Chan. 2007. Nanotoxicity: the growing need for in vivo study. Curr. Opin. Biotech. 18:656-571.

Gerdts, V., H. L. Wilson, F. Meurens, S. van Drunen Little – van den Hurk, D. Wilson, S. Walker, C. Wheler, H. Townsend, and A. A. Potter. 2015. Large animal models for vaccine development and testing. ILAR J. 56:53-62.

Hauck, T. S., R. E. Anderson, H. C. Fischer, S. Newbigging, and W. C. W. Chan. 2010. In vivo quantum dot toxicity assessment. Small. 6:138-144.

Kool, M., K. Fierens, and B. N. Lambrecht. 2012. Alum adjuvant: some of the tricks of the oldest adjuvant. J. Med. Microbiol. 61:927-934.

Nel, A., T. Xia, L. Madler, and N. Li. 2006. Toxic potential of materials at the nanolevel. Science. 311:622-627.

Ploemen, I. H. J., H. J. H. B. Hirschberg, H. Kraan, A. Zeltner, S. van Kuijk, D. P. K. Lankveld, M. Royals, G. F. A. Kersten, and J. P. Amorij. 2014. Minipigs as an animal model for dermal vaccine delivery. Comp. Med. 64:50-54.

Poland, G. 2012. Nanovaccinology: the next generation of vaccines meets 21st century materials science and engineering. Vaccine. 30:6609-6611.

Pusic, K., Z. Aguilar, J. McLoughlin, S. Kobuch, H. Xu, M. Tsang, A. Wang, and G. Hui. 2013. Iron oxide nanoparticles as a clinically acceptable delivery platform for a recombinant blood-stage human malaria vaccine. FASEB J. 27:1153-1166.

Pusic, K., H. Xu, A. Stridiron, Z. Aguilar, A. Wang, and G. Hui. 2011. Blood stage merozoite surface protein conjugated to nanoparticles induce potent parasite inhibitory antibodies. Vaccine. 29:8898-8908.

Seliger, C., B. Schaerer, M. Kohn, H. Pendl, S. Weigend, B. Kaspers, and S. Härtle. 2012. A rapid high-precision flow cytometry based technique for total white blood cell counting in chickens. Vet. Immunol. Immunopathol. 145:865-99.

Schijns, V. E. J. C., and E. C. Lavelle. 2011. Trends in vaccine adjuvants. Expert Rev. Vaccines. 10:539-550.

Shi, F., and G. F. Erf. 2012. IFN-γ, IL-21, and IL-10 co-expression in evolving autoimmune vitiligo lesions of Smyth line chickens. J. Invest. Derm. 132:642-649.

Soenen, S. J., P. Rivera-Gil, J.-M. Montenegrob, W. J. Parak, S. C. De Smedt, and K. Braeckmans. 2011. Cellular toxicity of inorganic nanoparticles: common aspects and guidelines for improved nanotoxicity evaluation. Nano Today. 6:446-465.

Tozuka, M., T. Oka, N. Jounai, G. Egawa, K. J. Ishii, K. Kabashima, and F. Takeshita. 2016. Efficient antigen delivery to the draining lymph nodes is a key component in the immunogenic pathway of the intradermal vaccine. J. Dermatol. Sci. 82:38-45.

van Aalst, S., I. S. Ludwig, P. J. S. van Kooten, R. van der Zee, W. van Eden, and F. Broere. 2017. Dynamics of APC recruitment at the site of injection following injection of vaccine adjuvants. Vaccine. 35:1622-1629.

Wang, X., J. Tian, K. T. Yong, X. Zhu, M. C. M. Lin, W. Jang, J. Li, Q. Huang, and G. Lin. 2016. Immunotoxicity assessment of CdSe/ZnS quantum dots in macrophages, lymphocytes and BALB/c mice. J. Nanobiotechnol. 14:10.

Yang, L., W. Li, M. Kirberger, W. Liao, and J. Ren. 2016. Design of nanomaterial based systems for novel vaccine development. Biomater. Sci. 4:785-802.

Yasuda, T., T. Ura, M. Taniguchi, and H. Yoshida. 2016. Intradermal delivery of antigens enhances specific IgG and diminishes IgE production: potential use for vaccination and allergy immunotherapy. PLoS ONE. 11:e0167952.

Zhao, L., A. Seth, N. Wibowo, C. X. Zhao, N. Mitter, C. Yu, and A. P. J. Middelberg. 2014. Nanoparticle vaccines. Vaccine. 32:327-337.

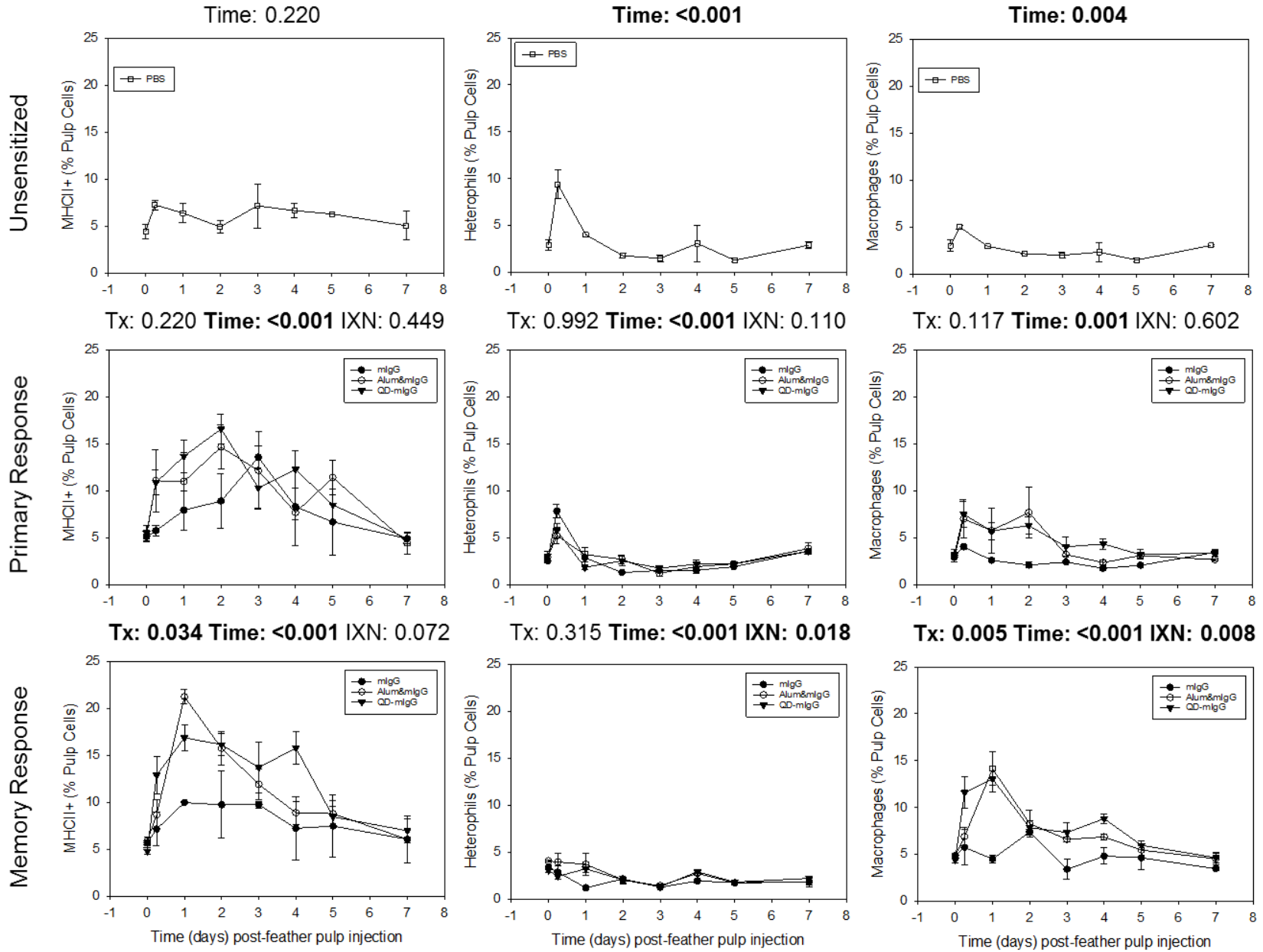
Unsensitized
Primary Response
Memory Response
Time: 0.220
Time: <0.001
Time: 0.004
Tx: 0.220 Time: <0.001 IXN: 0.449
Tx: 0.992 Time: <0.001 IXN: 0.110
Tx: 0.117 Time: 0.001 IXN: 0.602
Tx: 0.034 Time: <0.001 IXN: 0.072
Tx: 0.315 Time: <0.001 IXN: 0.018
Tx: 0.005 Time: <0.001 IXN: 0.008
MHCII+ (% Pulp Cells)
Heterophils (% Pulp Cells)
Macrophages (% Pulp Cells)
PBS
mIgG
Alum&mIgG
QD-mIgG
Time (days) post-feather pulp injection

Figure 1. Infiltration of MHCII+ cells, heterophils and macrophages in response to injection of mouse IgG into the dermis of growing feathers in unsensitized chickens and chickens sensitized with quantum dots (QD) with and without antigen-conjugation. Two groups of 13 chickens each were injected intramuscularly (i.m.) on day 0 and boosted 28 d following the initial injection with PBS as vehicle alone (n = 2, unsensitized) or sensitized with 0.26 mg/mL mIgG (n = 2), 0.26 mg/mL mIgG mixed with 2% Alum adjuvant (n = 3), or 0.5 µM QD conjugated with 0.26 mg/mL mIgG (n = 6). To measure the primary effector immune response (Group 1), GF were injected 10 d following the initial immunization with 10 µL 0.26 mg/mL mIgG antigen. To measure the memory effector immune response (Group 2), GF were injected 5 d following the second immunization with 10 µL 0.26 mg/mL mIgG. One GF collected at 0 (before injection), 0.25, 1, 2, 3, 4, 5, and 7 d post-injection from each chicken was used for preparation of individual pulp cell suspensions. A panel of chicken-specific fluorescence-conjugated mouse monoclonal antibodies was used to identify MHC class II+ cells and macrophages (KUL01). The percentage of heterophils was determined based on size (FSC) and granularity (SSC) characteristics of leukocytes (CD45+). These cell populations were measured in the GF dermis (% pulp cells) by two- to three-color direct immunofluorescent staining flow cytometry during each phase of the immune response. Results based on 2-way repeated measures ANOVA are indicated above each graph; Tx = P value for treatment effect; Time = P value for time effect; IXN = P value for treatment by time interaction. For multiple means comparison and additional statistical data, see Table 1. Data shown are mean ± SEM.

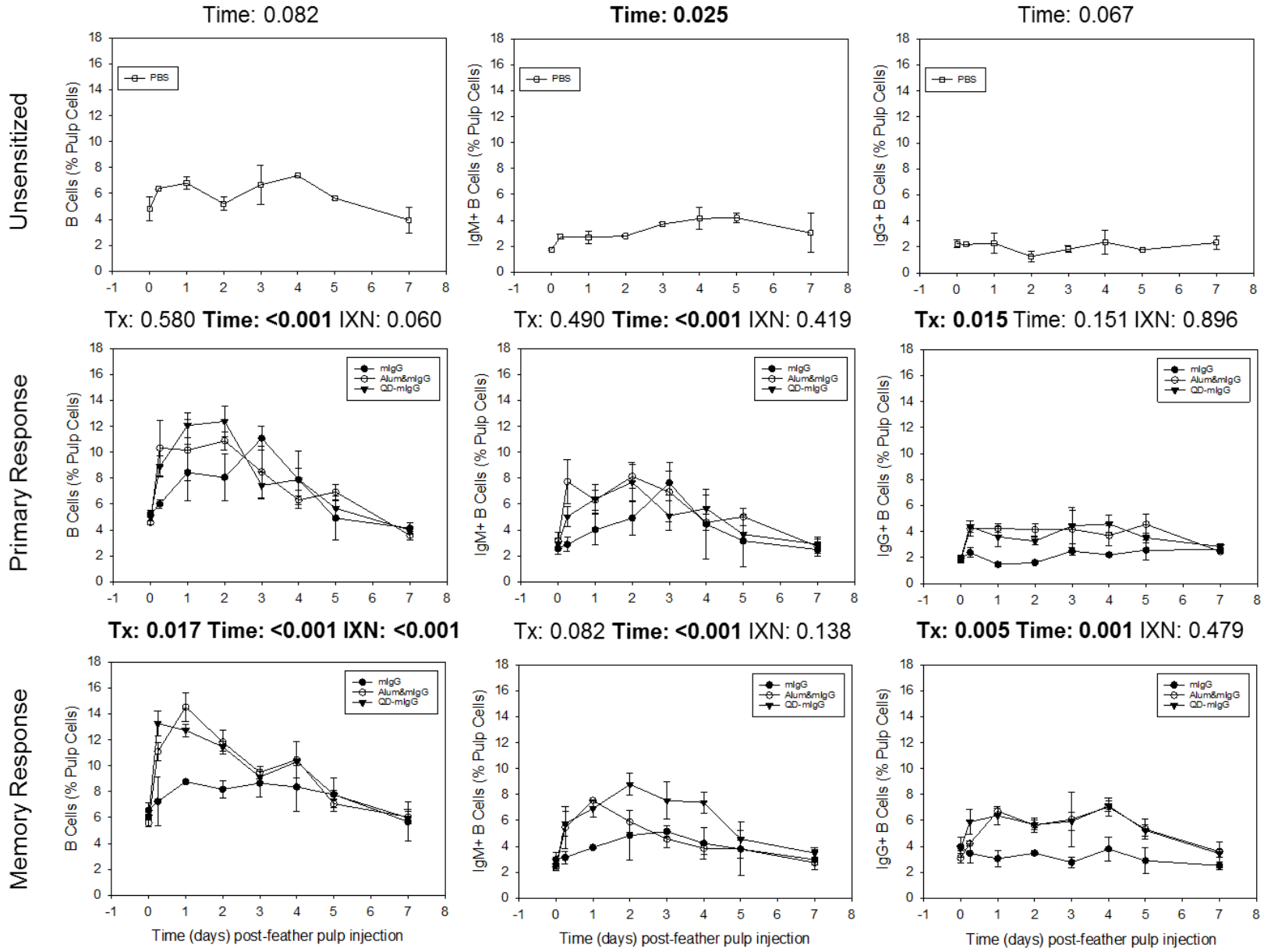
Unsensitized
Primary Response
Memory Response
Time: 0.082
Time: 0.025
Time: 0.067
Tx: 0.580 Time: <0.001 IXN: 0.060
Tx: 0.490 Time: <0.001 IXN: 0.419
Tx: 0.015 Time: 0.151 IXN: 0.896
Tx: 0.017 Time: <0.001 IXN: <0.001
Tx: 0.082 Time: <0.001 IXN: 0.138
Tx: 0.005 Time: 0.001 IXN: 0.479
B Cells (% Pulp Cells)
IgM+ B Cells (% Pulp Cells)
IgG+ B Cells (% Pulp Cells)
PBS
mIgG
Alum&mIgG
QD-mIgG
Time (days) post-feather pulp injection

Figure 2. Infiltration of B lymphocytes in response to injection of mouse IgG into the dermis of growing feathers in unsensitized chickens and chickens sensitized with quantum dots (QD) with and without antigen-conjugation. Two groups of 13 chickens each were injected intramuscularly (i.m.) on day 0 and boosted 28 d following the initial injection with PBS as vehicle alone (n = 2, unsensitized) or sensitized with 0.26 mg/mL mIgG (n = 2), 0.26 mg/mL mIgG mixed with 2% Alum adjuvant (n = 3), or 0.5 μM QD conjugated with 0.26 mg/mL mIgG (n = 6). To measure the primary effector immune response (Group 1), GF were injected 10 d following the initial immunization with 10 μL 0.26 mg/mL mIgG antigen. To measure the memory effector immune response (Group 2), GF were injected 5 d following the second immunization with 10 μL 0.26 mg/mL mIgG. One GF collected at 0 (before injection), 0.25, 1, 2, 3, 4, 5, and 7 d post-injection from each chicken was used for preparation of individual pulp cell suspensions. A panel of chicken-specific fluorescence-conjugated mouse monoclonal antibodies was used to identify total B cells (Bu-1), IgG+ B cells and IgM+ B cells. These cell populations were measured in the GF dermis (% pulp cells) by two- to three-color direct immunofluorescent staining flow cytometry during each phase of the immune response. Results based on 2-way repeated measures ANOVA are indicated above each graph; Tx = P value for treatment effect; Time = P value for time effect; IXN = P value for treatment by time interaction. For multiple means comparison and additional statistical data, see Table 2. Data shown are mean ± SEM.

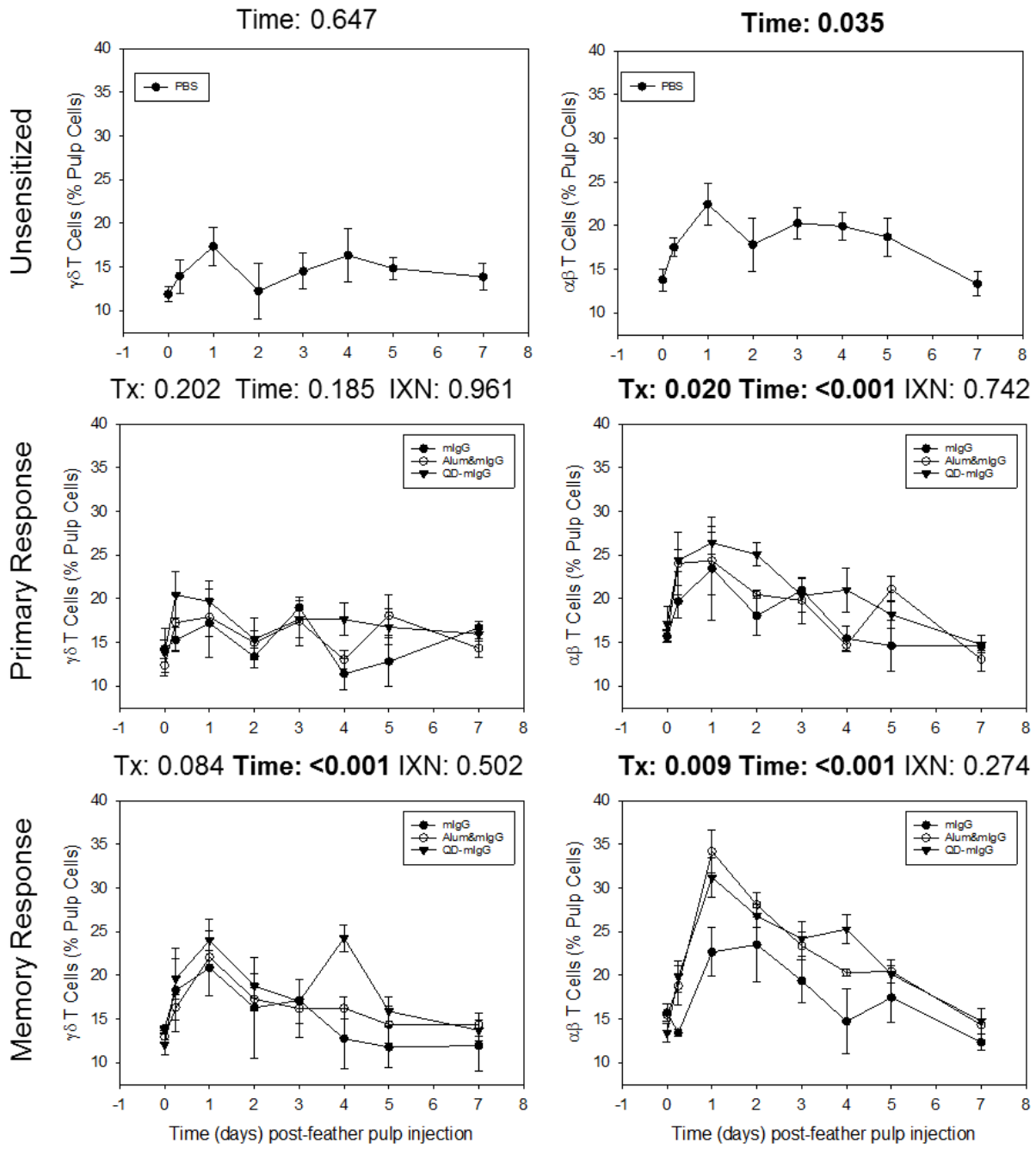
Unsensitized
Primary Response
Memory Response
Time: 0.647
Time: 0.035
Tx: 0.202 Time: 0.185 IXN: 0.961
Tx: 0.020 Time: <0.001 IXN: 0.742
Tx: 0.084 Time: <0.001 IXN: 0.502
Tx: 0.009 Time: <0.001 IXN: 0.274
PBS
mIgG
Alum&mIgG
QD-mIgG
γδ T Cells (% Pulp Cells)
αβ T Cells (% Pulp Cells)
Time (days) post-feather pulp injection

Figure 3. Infiltration of γδ and αβ T lymphocyte subpopulations in response to injection of mouse IgG into the dermis of growing feathers in unsensitized chickens and chickens sensitized with quantum dots (QD) with and without antigen-conjugation. Two groups of 13 chickens each were injected intramuscularly (i.m.) on day 0 and boosted 28 d following the initial injection with PBS as vehicle alone (n = 2, unsensitized) or sensitized with 0.26 mg/mL mIgG (n = 2), 0.26 mg/mL mIgG mixed with 2% Alum adjuvant (n = 3), or 0.5 µM QD conjugated with 0.26 mg/mL mIgG (n = 6). To measure the primary effector immune response (Group 1), GF were injected 10 d following the initial immunization with 10 µL 0.26 mg/mL mIgG antigen. To measure the memory effector immune response (Group 2), GF were injected 5 d following the second immunization with 10 µL 0.26 mg/mL mIgG. One GF collected at 0 (before injection), 0.25, 1, 2, 3, 4, 5, and 7 d post-injection from each chicken was used for preparation of individual pulp cell suspensions. A panel of chicken-specific fluorescence-conjugated mouse monoclonal antibodies was used to identify γδ T cell receptor (TCR)-defined and αβ T cell receptor (TCR)-defined T cell populations. These cell populations were measured in the GF dermis (% pulp cells) by two- to three-color direct immunofluorescent staining flow cytometry during each phase of the immune response. Results based on 2-way repeated measures ANOVA are indicated above each graph; Tx = P value for treatment effect; Time = P value for time effect; IXN = P value for treatment by time interaction. For multiple means comparison and additional statistical data, see Table 3. Data shown are mean ± SEM.

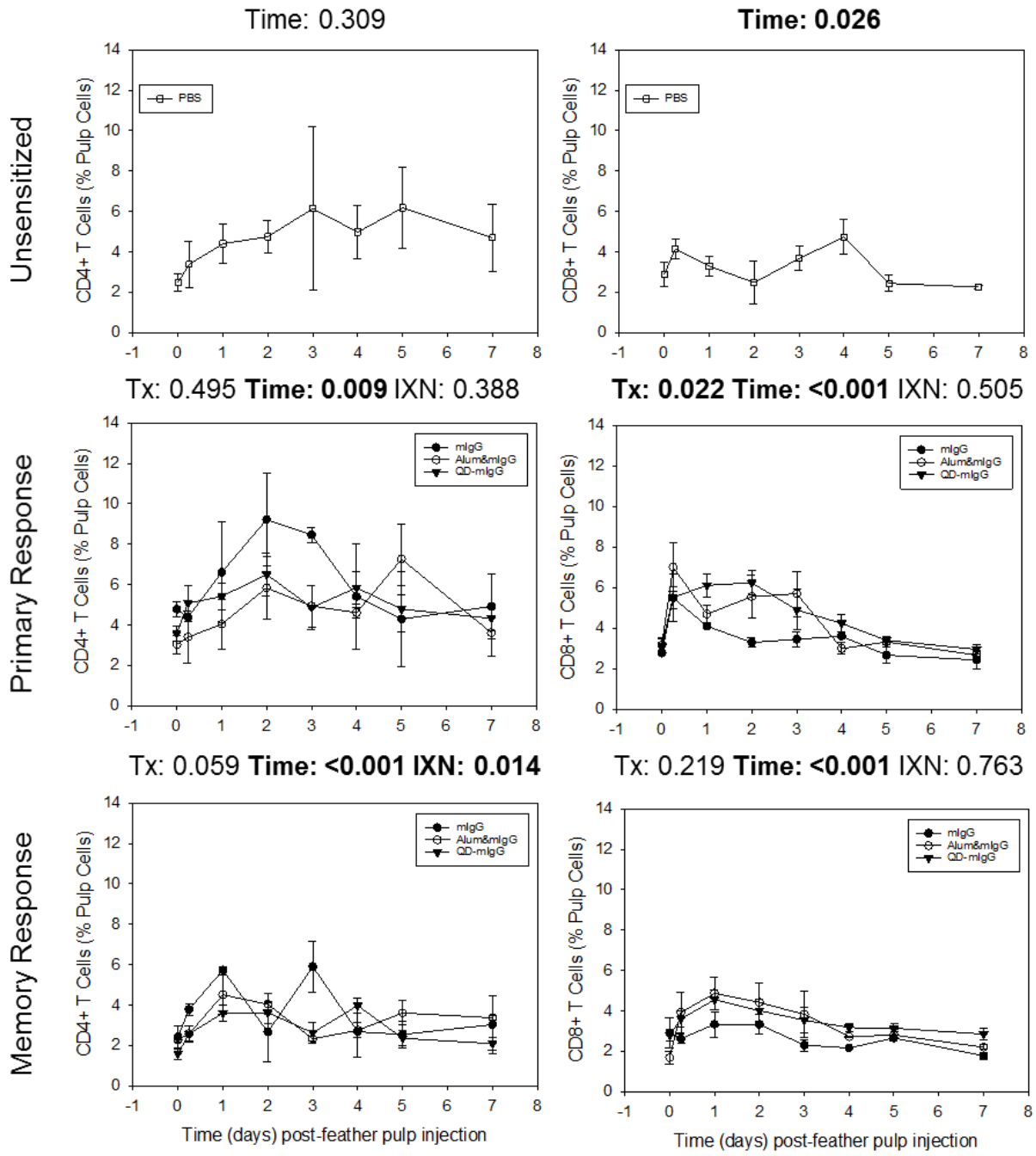
Unsensitized
Primary Response
Memory Response
Time: 0.309
Time: 0.026
Tx: 0.495 Time: 0.009 IXN: 0.388
Tx: 0.022 Time: <0.001 IXN: 0.505
Tx: 0.059 Time: <0.001 IXN: 0.014
Tx: 0.219 Time: <0.001 IXN: 0.763
CD4+ T Cells (% Pulp Cells)
CD8+ T Cells (% Pulp Cells)
PBS
mIgG
Alum&mIgG
QD-mIgG
Time (days) post-feather pulp injection

Figure 4. Infiltration of CD4+ and CD8+ T lymphocytes in response to injection of mouse IgG into the dermis of growing feathers in unsensitized chickens and chickens sensitized with quantum dots (QD) with and without antigen-conjugation. Two groups of 13 chickens each were injected intramuscularly (i.m.) on day 0 and boosted 28 d following the initial injection with PBS as vehicle alone (n = 2, unsensitized) or sensitized with 0.26 mg/mL mIgG (n = 2), 0.26 mg/mL mIgG mixed with 2% Alum adjuvant (n = 3), or 0.5 µM QD conjugated with 0.26 mg/mL mIgG (n = 6). To measure the primary effector immune response (Group 1), GF were injected 10 d following the initial immunization with 10 µL 0.26 mg/mL mIgG antigen. To measure the memory effector immune response (Group 2), GF were injected 5 d following the second immunization with 10 µL 0.26 mg/mL mIgG. One GF collected at 0 (before injection), 0.25, 1, 2, 3, 4, 5, and 7 d post-injection from each chicken was used for preparation of individual pulp cell suspensions. A panel of chicken-specific fluorescence-conjugated mouse monoclonal antibodies was used to identify CD4+ T cells and CD8+ T cells. These cell populations were measured in the GF dermis (% pulp cells) by two- to three-color direct immunofluorescent staining flow cytometry during each phase of the immune response. Results based on 2-way repeated measures ANOVA are indicated above each graph; Tx = P value for treatment effect; Time = P value for time effect; IXN = P value for treatment by time interaction. For multiple means comparison and additional statistical data, see Table 4. Data shown are mean ± SEM.

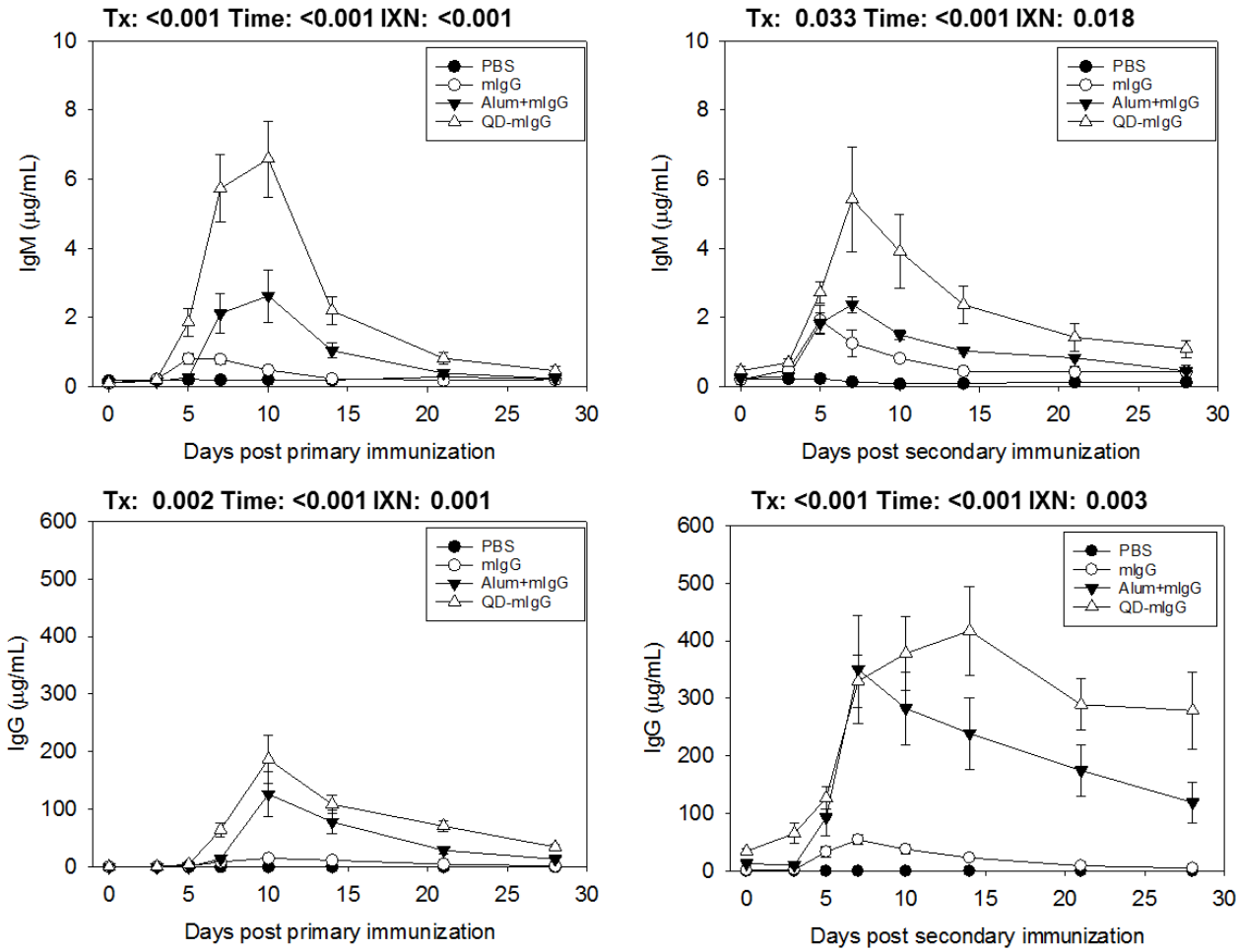

Figure 5. Antibody response to injection of mouse IgG into the dermis of growing feathers in unsensitized chickens and chickens sensitized with quantum dots (QD) with and without antigen-conjugation. Three groups of 13 chickens each were injected intramuscularly (i.m.) on day 0, boosted 28 d following the initial injection with PBS as vehicle alone (n = 2 per group, unsensitized) or sensitized with 0.26 mg/mL mIgG (n = 2 per group), 0.26 mg/mL mIgG mixed with 2% Alum adjuvant (n = 3 per group), or 0.5 µM QD conjugated with 0.26 mg/mL mIgG (n = 6 per group). Antibodies specific to the mouse IgG test antigen (chicken anti-mouse IgG and IgM isotypes) were measured via enzyme-linked immunosorbent assay (ELISA) using plasma samples collected before (0) and 3, 5, 7, 10, 14, 21, and 28 days post-primary and secondary i.m. immunizations. Mouse IgG-specific chicken IgG was used as the standard for IgG and IgM measurement since there is currently no chicken anti-mouse IgM antibody commercially available. Data analysis was completed using Gen5 software including calculation of the standard curve using a 4-parameter logistic equation to define the relationship between known concentrations of mIgG-specific chicken antibodies and corresponding optical absorbance measurements. The standard curve equation was used to determine plasma concentrations of chicken IgM and IgG antibodies specific for mouse IgG antigen. Results based on 2-way repeated measures ANOVA are indicated above each graph; Tx = P value for treatment effect; Time = P value for time effect; IXN = P value for treatment by time interaction. For multiple means comparison and additional statistical data, see Table 5. Data shown are mean ± SEM.

Table 1.
Statistical analysis of data shown in **Figure 1.** Time and treatment effects on the levels of infiltrating MHCII+ cells, heterophils and macrophages (% pulp cells) in QD-injected GF.

MHCII+ Cells - Unsensitized

Immunization	P-Treat	P-Time	P-IXN	0 d	0.25 d	1 d	2 d	3 d	4 d	5 d	7 d
PBS (vehicle)		0.220									

MHCII+ Cells – Primary effector response

Immunization	P-Treat	P-Time	P-IXN	0 d	0.25 d	1 d	2 d	3 d	4 d	5 d	7 d
	0.220	<0.001	0.449	Z	Y	XY	X	XY	Y	Y	Z
mIgG											
Alum+mIgG											
QD-mIgG											

MHCII+ Cells – Memory effector response

Immunization	P-Treat	P-Time	P-IXN	0 d	0.25 d	1 d	2 d	3 d	4 d	5 d	7 d
	0.034	<0.001	0.072	Z	XY	V	VW	WX	XY	YZ	Z
mIgG	b										
Alum+mIgG	ab										
QD-mIgG	a										

Heterophils - Unsensitized

Immunization	P-Treat	P-Time	P-IXN	0 d	0.25 d	1 d	2 d	3 d	4 d	5 d	7 d
PBS (vehicle)		<0.001		YZ	X	Y	Z	Z	YZ	Z	YZ

Heterophils – Primary effector response

Immunization	P-Treat	P-Time	P-IXN	0 d	0.25 d	1 d	2 d	3 d	4 d	5 d	7 d
	0.992	<0.001	0.110	WX	V	XY	XYZ	Z	YZ	XYZ	W
mIgG											
Alum+mIgG											
QD-mIgG											

Table 1 (Cont.)

Heterophils – Memory effector response

Immunization	P-Treat	P-Time	P-IXN	0 d	0.25 d	1 d	2 d	3 d	4 d	5 d	7 d
	0.315	<0.001	0.018								
mIgG		0.046		X ab	XY	Z	YXZ	Z	YZ	YZ	YZ
Alum+mIgG		0.002		X b	XY	XY	Z	Z	XYZ	Z	Z
QD-mIgG		<0.001		VW a	WXY	V	YZ	Z	VWX	YZ	XY

Macrophages - Unsensitized

Immunization	P-Treat	P-Time	P-IXN	0 d	0.25 d	1 d	2 d	3 d	4 d	5 d	7 d
PBS (vehicle)		0.004		Z	X	XY	Z	YZ	YZ	Z	Z

Macrophages – Primary effector response

Immunization	P-Treat	P-Time	P-IXN	0 d	0.25 d	1 d	2 d	3 d	4 d	5 d	7 d
	0.117	0.001	0.602	YZ	W	WXY	WX	YZ	Z	Z	YZ
mIgG											
Alum+mIgG											
QD-mIgG											

Macrophages – Memory effector response

Immunization	P-Treat	P-Time	P-IXN	0 d	0.25 d	1 d	2 d	3 d	4 d	5 d	7 d
	0.005	<0.001	0.008								
mIgG		0.146				b			b		
Alum+mIgG		<0.001		Z	YZ	X a	Y	YZ	YZ b	Z	Z
QD-mIgG		<0.001		Z	VW	V a	XY	XYZ	X a	YZ	Z

V, W, X, Y, Z: For each cell population, levels at time-points without a common letter are different at $P < 0.05$. Letters "Z to V" indicate ascending order of GF infiltration levels.

a, b: Treatments without a common letter are different. Letters "b to a" indicate ascending order of GF infiltration levels.

Table 2.
Statistical analysis of data shown in **Figure 2.** Time and treatment effects on the levels of infiltrating B lymphocyte populations (% pulp cells) in QD-injected GF.

B cells - Unsensitized

Immunization	P-Treat	P-Time	P-IXN	0 d	0.25 d	1 d	2 d	3 d	4 d	5 d	7 d
PBS (vehicle)		0.082									

B cells – Primary effector response

Immunization	P-Treat	P-Time	P-IXN	0 d	0.25 d	1 d	2 d	3 d	4 d	5 d	7 d
	0.580	<0.001	0.060	YZ	VW	UV	U	UVW	WX	XY	Z
mIgG											
Alum+mIgG											
QD-mIgG											

B Cells – Memory effector response

Immunization	P-Treat	P-Time	P-IXN	0 d	0.25 d	1 d	2 d	3 d	4 d	5 d	7 d
	0.017	<0.001	<0.001								
mIgG		0.713			b	b	b				
Alum+mIgG		<0.001		Z	Y ab	X a	Y a	Y	Y	Z	Z
QD-mIgG		<0.001		Z	V a	V a	W a	X	WX	Y	Z

IgG+ B Cells - Unsensitized

Immunization	P-Treat	P-Time	P-IXN	0 d	0.25 d	1 d	2 d	3 d	4 d	5 d	7 d
PBS (vehicle)		0.067									

IgG+ B Cells – Primary effector response

Immunization	P-Treat	P-Time	P-IXN	0 d	0.25 d	1 d	2 d	3 d	4 d	5 d	7 d
	0.015	0.151	0.896								
mIgG	b										
Alum+mIgG	a										
QD-mIgG	a										

Table 2 (Cont.)

IgG+ B Cells – Memory effector response

Immunization	P-Treat	P-Time	P-IXN	0 d	0.25 d	1 d	2 d	3 d	4 d	5 d	7 d
	0.005	0.001	0.479	YZ	XY	WX	WX	WXY	W	XY	Z
mIgG	b										
Alum+mIgG	a										
QD-mIgG	a										

IgM+ B Cells - Unsensitized

Immunization	P-Treat	P-Time	P-IXN	0 d	0.25 d	1 d	2 d	3 d	4 d	5 d	7 d
PBS (vehicle)		0.025		Z	Z	YZ	Z	Z	XY	X	XYZ

IgM+ B Cells – Primary effector response

Immunization	P-Treat	P-Time	P-IXN	0 d	0.25 d	1 d	2 d	3 d	4 d	5 d	7 d
	0.490	<0.001	0.419	YZ	VWX	VWX	V	VW	WXY	XYZ	Z
mIgG											
Alum+mIgG											
QD-mIgG											

IgM+ B Cells – Memory effector response

Immunization	P-Treat	P-Time	P-IXN	0 d	0.25 d	1 d	2 d	3 d	4 d	5 d	7 d
	0.082	<0.001	0.138	Z	XY	WX	W	WX	WXY	YZ	Z
mIgG											
Alum+mIgG											
QD-mIgG											

U, V, W, X, Y, Z: For each cell population, levels at time-points without a common letter are different at $P < 0.05$. Letters "Z to U" indicate ascending order of GF infiltration levels.

a, b: Treatments without a common letter are different. Letters "b to a" indicate ascending order of GF infiltration levels.

Table 3.
Statistical analysis of data shown in **Figure 3.** Time and treatment effects on the levels of infiltrating γδ and αβ T lymphocyte subpopulations (% pulp cells) in QD-injected GF.

γδ T Cells - Unsensitized

Immunization	P-Treat	P-Time	P-IXN	0 d	0.25 d	1 d	2 d	3 d	4 d	5 d	7 d
PBS (vehicle)		0.647									

γδ T Cells – Primary effector response

Immunization	P-Treat	P-Time	P-IXN	0 d	0.25 d	1 d	2 d	3 d	4 d	5 d	7 d
	0.202	0.185	0.961								
mIgG											
Alum+mIgG											
QD-mIgG											

γδ T Cells – Memory effector response

Immunization	P-Treat	P-Time	P-IXN	0 d	0.25 d	1 d	2 d	3 d	4 d	5 d	7 d
	0.084	<0.001	0.502	Z	X	W	XY	XYZ	XY	YZ	Z
mIgG											
Alum+mIgG											
QD-mIgG											

αβ T Cells - Unsensitized

Immunization	P-Treat	P-Time	P-IXN	0 d	0.25 d	1 d	2 d	3 d	4 d	5 d	7 d
PBS (vehicle)		0.035		Z	YZ	Y	YZ	Y	Y	YZ	Z

αβ T Cells – Primary effector response

Immunization	P-Treat	P-Time	P-IXN	0 d	0.25 d	1 d	2 d	3 d	4 d	5 d	7 d
	0.020	<0.001	0.742	Z	W	W	WX	WXY	YZ	XYZ	Z
mIgG	b										
Alum+mIgG	ab										
QD-mIgG	a										

Table 3 (Cont.)

αβ T Cells – Memory effector response

Immunization	P-Treat	P-Time	P-IXN	0 d	0.25 d	1 d	2 d	3 d	4 d	5 d	7 d
	0.009	<0.001	0.274	YZ	XY	V	V	W	WX	WX	Z
mIgG	b										
Alum+mIgG	a										
QD-mIgG	a										

V, W, X, Y, Z: For each cell population, levels at time-points without a common letter are different at $P < 0.05$. Letters "Z to V" indicate ascending order of GF infiltration levels.

a, b: Treatments without a common letter are different. Letters "b to a" indicate ascending order of GF infiltration levels.

Table 4.
Statistical analysis of data shown in **Figure 4.** Time and treatment effects on the levels of infiltrating CD4+ and CD8+ T lymphocytes (% pulp cells) in QD-injected GF.

CD4+ T Cells - Unsensitized

Immunization	P-Treat	P-Time	P-IXN	0 d	0.25 d	1 d	2 d	3 d	4 d	5 d	7 d
PBS (vehicle)		0.309									

CD4+ T Cells – Primary effector response

Immunization	P-Treat	P-Time	P-IXN	0 d	0.25 d	1 d	2 d	3 d	4 d	5 d	7 d
	0.495	0.009	0.388	Z	Z	YZ	X	XY	YZ	XYZ	Z
mIgG											
Alum+mIgG											
QD-mIgG											

CD4+ T Cells – Memory effector response

Immunization	P-Treat	P-Time	P-IXN	0 d	0.25 d	1 d	2 d	3 d	4 d	5 d	7 d
	0.059	<0.001	0.014								
mIgG		0.196						a			
Alum+mIgG		0.063						b			
QD-mIgG		0.002		Z	YZ	XY	XY	YZ b	X	Z	Z

CD8+ T Cells - Unsensitized

Immunization	P-Treat	P-Time	P-IXN	0 d	0.25 d	1 d	2 d	3 d	4 d	5 d	7 d
PBS (vehicle)		0.026		YZ	XY	XY	YZ	YZ	X	YZ	Z

CD8+ T Cells – Primary effector response

Immunization	P-Treat	P-Time	P-IXN	0 d	0.25 d	1 d	2 d	3 d	4 d	5 d	7 d
	0.022	<0.001	0.505	Z	W	WX	WX	XY	YZ	Z	Z
mIgG	b										
Alum+mIgG	a										
QD-mIgG	a										

Table 4 (Cont.)

CD8+ T Cells – Memory effector response

Immunization	P-Treat	P-Time	P-IXN	0 d	0.25 d	1 d	2 d	3 d	4 d	5 d	7 d
	0.219	<0.001	0.763	YZ	VWX	V	VW	WXY	XYZ	XYZ	Z
mIgG											
Alum+mIgG											
QD-mIgG											

V, W, X, Y, Z: For each cell population, levels at time-points without a common letter are different at $P < 0.05$. Letters "Z to V" indicate ascending order of GF infiltration levels.

a, b: Treatments without a common letter are different. Letters "b to a" indicate ascending order of GF infiltration levels.

Table 5.
Statistical analysis of data shown in **Figure 5.** Time and treatment effects on the plasma levels of mouse-IgG specific IgM and IgG antibodies.

IgM – Primary response

Immunization	P-Treat	P-Time	P-IXN	0 d	3 d	5 d	7 d	10 d	14 d	21 d	28 d
	<0.001	<0.001	<0.001								
mIgG		<0.001		Z	Z	X ab	X b	Y b	Z b	Z	Z
Alum+mIgG		<0.001		Z	Z	Z b	Y b	Y b	Z b	Z	Z
QD-mIgG		<0.001		Z	Z	Y a	X a	X a	Y a	YZ	YZ

IgM – Memory response

Immunization	P-Treat	P-Time	P-IXN	0 d	3 d	5 d	7 d	10 d	14 d	21 d	28 d
	0.033	<0.001	0.018								
mIgG		0.004		Z	YZ	X	XY	YZ	YZ	YZ	YZ
Alum+mIgG		<0.001		Z	YZ	UV	U	VW	WX	XY	XYZ
QD-mIgG		<0.001		Z	Z	WX	V	W	XY	YZ	YZ

IgG – Primary response

Immunization	P-Treat	P-Time	P-IXN	0 d	3 d	5 d	7 d	10 d	14 d	21 d	28 d
	0.002	<0.001	0.001								
mIgG		<0.001		Z	Z	Z ab	XY b	W	WX b	YZ b	Z b
Alum+mIgG		<0.001		Z	Z	Z b	Z b	X	Y ab	YZ b	Z b
QD-mIgG		<0.001		Z	Z	Z a	XY a	W	X a	XY a	YZ a

IgG – Memory response

Immunization	P-Treat	P-Time	P-IXN	0 d	3 d	5 d	7 d	10 d	14 d	21 d	28 d
	<0.001	<0.001	0.003								
mIgG		<0.001		Z b	Z b	X	Y b	YX b	XY b	YZ b	YZ
Alum+mIgG		<0.001		Z b	Z b	Y	W a	WX ab	X ab	XY ab	Y
QD-mIgG		<0.001		Z a	Z a	Y	X a	X a	WX a	X a	X

Table 5 (Cont.)

U, V, W, X, Y, Z: Antibody levels at time-points without a common letter are different at $P < 0.05$. Letters "Z to U" indicate ascending order of antibody levels.

a, b: Treatments without a common letter are different. Letters "b to a" indicate ascending order of antibody levels.

Conclusion

The data presented in this dissertation support the suitability and effectiveness of both cultured chicken macrophages and the chicken growing feather as a dermal test-site to measure the bioactivity of nanoparticles. Results of in vitro studies with MQ-NCSU chicken macrophages (Chapter I) indicated effects of QD and IO NP preparations detectable by NO production in culture medium, though these results were likely complicated by possible endotoxin contamination in IO NP and high background optical absorbance with increasing doses of QD. While QD did not appreciably stimulate nitric oxide production, QD treatment resulted in greatly reduced cell viability with increasing dose. Results of fluorescence microscopy studies indicated QD gained entry into chicken macrophages within 45 minutes and the appearance of QD in the cells changed from defined red dots to more evenly dispersed red color inside the cell and around the nucleus following 24 h incubation. Ultimately, in vitro studies provided valuable information regarding optimal QD concentrations for use in the in vivo studies performed in Chapters II and III. In vivo studies were performed to measure both the innate (Chapter II) and adaptive (Chapter III) immune responses to mIgG protein antigen without and with conjugation to QD using the chicken GF injection model as the cutaneous test-site to monitor leukocyte infiltration in response to intradermal injection. Results from the innate studies (Chapter II) indicated that intradermal injection of QD as well as mIgG-antigen conjugated with QD stimulated infiltration of immune cells into the pulp dermis following GF injection greater than mIgG alone. However, immune cell infiltration over the time course was higher following injection with Alum+mIgG compared to QD, QD-mIgG, and mIgG, indicating that while QD does stimulate immune activity, the level of stimulation during primary exposure is not greater than that of alum adjuvant. Results from the adaptive immune studies (Chapter III) indicated levels of infiltrating monocytes/macrophages and B and T lymphocytes were higher in

antigen injected GF following immunization with Alum+mIgG and QD-mIgG compared to mIgG alone. Overall, QD-mIgG immunization resulted in a local effector response to antigen at least as high or higher than Alum+mIgG immunization; this response to antigen was greater following secondary immunization compared to primary immunization both for Alum+mIgG and QD-mIgG. In addition IgM+ B cells were higher in antigen injected GF during the primary response while higher levels of IgG+ B cells infiltrated GF during the memory the response. Regarding the humoral adaptive immune response following primary and secondary immunization, QD-mIgG immunization stimulated higher antigen-specific IgM and IgG antibodies compared to Alum+mIgG and mIgG. Comparing overall antigen-specific IgM and IgG levels during the primary and memory responses following QD-mIgG immunization, the IgM isotype made up a higher proportion of antigen-specific antibodies during the primary response, while antigen-specific IgG isotype antibodies far exceeded those of IgM during the memory response. Taken together, data from both the cellular and humoral responses were indicative of T cell help in B cell activation and antibody isotype switching, as well as memory development. Interestingly, independent of vaccination treatment, heterophil infiltration into antigen-injected GF was lower during the adaptive memory effector response compared to the innate immune response when antigen was injected in unsensitized chickens; this finding warrants further study to determine whether factors other than rapid removal of antigen with the aid of antigen-specific antibodies are inhibiting heterophil infiltration. To our knowledge, this is one of few studies using both in vitro and in vivo models to assess and monitor the tissue/cellular immune activities to QD in a complex dermal tissue and to simultaneously examine adaptive humoral and cellular immune responses to antigen in animals immunized with antigen conjugated to QD. Particular advantages of the GF model include the ability to monitor

temporal, qualitative, and quantitative changes in complex tissue with minimally-invasive procedures. Additional studies investigating the effects of QD on dendritic cell infiltration in GF should provide additional information on the effects of QD on antigen presenting cells while the measurement of cytokine profiles in the GF would help to advance our understanding of the immunostimulatory properties of QD. New knowledge gained from these studies should further advance the field of NP research and the use of QD in biomedical applications.

UNIVERSITY OF ARKANSAS

Office of Research Compliance

MEMORANDUM

TO: Gisela Erf

FROM: Craig N. Coon, Chairman

DATE: Jan 12, 2015

SUBJECT: IACUC Approval

Expiration Date: Jan 11, 2018

The Institutional Animal Care and Use Committee (IACUC) has APPROVED your Protocol: 15020 Monitoring nanoparticle biology in vivo in the avian model

You may begin immediately.

In granting its approval, the IACUC has approved only the information provided. Should there be any further changes to the protocol during the research, please notify the IACUC in writing (via the Modification form) prior to initiating the changes. If the study period is expected to extend beyond Jan 11, 2018 you must submit a newly drafted protocol prior to that date to avoid any interruption. By policy the IACUC cannot approve a study for more than 3 years at a time.

The IACUC appreciates your cooperation in complying with University and Federal guidelines involving animal subjects.

CNC/aem

cc: Animal Welfare Veterinarian

Administration Building 210 • 1 University of Arkansas • Fayetteville, AR 72701-1201 • 479-575-4572
Fax: 479-575-3846 • http://vpred.uark.edu/199